INVESTIGATION OF THE EFFECT OF HOLE EDGE MARGIN ON FATIGUE LIFE OF COLD EXPANDED HOLES WITH EXISTING CRACKS IN 2024-T351 ALUMINUM ALLOY

by

Evan Michael Ross

A thesis submitted to the faculty of
The University of Utah
in partial fulfillment of the requirements for the degree of

Master of Science

Department of Mechanical Engineering

The University of Utah

August 2019

The University of Utah Graduate School

STATEMENT OF THESIS APPROVAL

The thesis of **Evan Michael Ross**

has been approved by the following supervisory committee members:

Kenneth Monson	, Chair	**May 6, 2019** Date Approved
Ashley Spear	, Member	**May 6, 2019** Date Approved
Owen Kingstedt	, Member	**May 6, 2019** Date Approved

and by **Bruce Gale** , Chair of

the Department of **Mechanical Engineering**

and by David B. Kieda, Dean of The Graduate School.

ABSTRACT

Damage tolerance analysis is used by the United States Air Force to maintain the airworthiness of its aircraft through inspection, fatigue crack growth prediction, and residual strength analysis. Cold expansion is commonly used to impart compressive residual stress around fastener holes to slow the rate of fatigue crack propagation and reduce the frequency of inspections. Previous research has shown that the fatigue life benefit of cold expansion is dependent upon hole edge margin and applied loading, resulting in unconservative predictions of fatigue life in some cases.

Spectrum loading fatigue experiments were performed on cold-expanded 2024-T351 aluminum alloy specimens with holes at varying short edge margins, which were precracked prior to cold expansion. These tests used a fighter aircraft wing root bending spectrum with 33,000 pounds per square inch maximum stress. Results of fatigue testing were compared various fatigue crack growth prediction tools used by the United States Air Force to evaluate the conservatism of the prediction methods.

Results were consistent with previous research and showed that cold expansion increased fatigue life by a factor between 3.44 to 8.22 based on edge margin. This research also found that crack growth analysis using a 0.005 inch initial flaw size did not conservatively predict the growth of cracks at cold-expanded holes with edge margins of 1.30.

This work is dedicated to my lovely bride, Alexandra.

TABLE OF CONTENTS

LIST OF TABLES

Tables

ACKNOWLEDGMENTS

This research would not have been possible without the contributions of many people. Thank you.

I am grateful for my family, friends, coaches, and teachers for helping me become the person I am today. You each have a part in this work. Especially, I would like to thank my parents for never letting me believe there was something I was not capable of achieving.

This research would not have been possible without access to a laboratory with appropriate equipment and expertise. I appreciate my supervisor, Bryce Jolley, for allowing me to spend time in the lab testing. I am also thankful for coworkers who were willing to provide assistance, advice, and expertise whenever it was needed.

Jake Warner, thank you for the extraordinary effort you demonstrated in helping me in every step of this research. This was only possible with your help. I am also thankful for the research that you and Dallen Andrew performed previously to lay the groundwork for this thesis.

I am thankful to FTI Inc. for permission to use their copywritten figures in this paper.

Finally, Ally, thank you for your unwavering love and support during every step of this journey. Thank you for your loving patience and encouragement during the late nights and long days. When I met challenges, you were there to help me overcome them,

and when I had successes, you were there to celebrate with me. I am thankful that I can celebrate this with you.

1 INTRODUCTION

1.1 Brief History of Fatigue Failures

Fatigue failure has been an area of research since 1838 when Wilhelm Albert published a paper on the failure of mine hoist chains, which were subjected to cyclic loading [1]. This was the first of many great advancements in the field. The arrival of airplanes and their requirement for low weight structures introduced new challenges and areas of research in the realm of fatigue. In 1952, the de Haviland Comet became the world's first pressurized passenger jet. Its triumph was short lived as it experienced multiple catastrophic failures in the following years caused by fatigue cracks emanating from its cabin windows [2]. The cabin windows were designed in a square shape, which produced stress concentrations at their corners, making them susceptible to fatigue. This served as a catalyst for improving aircraft design and maintenance practices.

The most common stress concentrations on aircraft, fastener holes, were the origin of damage that caused a C-130A firefighting aircraft to crash in 2002 [3]. Fatigue cracks at multiple fastener holes on the root of the wing joined to form a 12 inch crack, resulting in failure. During an upward maneuver, the wing separated from the fuselage and the entire crew was killed. It was determined that poor maintenance practices contributed to this disaster.

These examples show the progress that has been made in understanding fatigue, while highlighting the importance of continuing research and applying that understanding

to aircraft maintenance practices.

1.2 Designing for Fatigue

1.2.1 Safe-Life Approach

Over time, different methods of accounting for time-based degradation, including fatigue, have been developed. Before inspection techniques had developed sufficiently, the damage sustained by components was not considered at all [4]. One such method, safe-life, was used extensively by the United States Air Force (USAF) until the mid-1970s [5]. With this approach, the service life of the component is estimated from previous testing along with the expected service conditions. Once the estimated life is reached, the component is replaced regardless of the amount of damage it has sustained, maintaining safe operation. Due to the variable nature of fatigue, this results in highly variable levels of conservatism. Three possible outcomes exist for a component using the using a safe-life approach. First, the actual life of the component is estimated accurately, and it is replaced in proper timing. This rarely occurs. The actual life of the component may also be underestimated, and it is replaced sooner than necessary. This is the best outcome in terms of safety, but replacing undamaged components is wasteful of time and money. Alternatively, the actual life of the component may be overestimated, and it may fail in service. A case study on the ineffectiveness of safe-life methodologies is the F-111 aircraft [6]. The F-111 is a swept wing aircraft with a single pivot for each wing. After only approximately 100 flight hours of its 6,000 flight-hour safe-life, a wing pivot fractured causing the aircraft to crash. It was determined that an undetected quench crack in the structure was the root cause of the failure. Failures occurred on other F-111 aircraft

in the same location. Based on these failures, it was determined that safe-life methodologies were insufficient for protecting USAF pilots and aircraft.

1.2.2 Damage Tolerance Design

As an alternative to previous design approaches, methods were developed that consider accumulating damage to a component over time. The method currently used by the USAF is damage tolerance design. Damage tolerance, as the name suggests, designs aircraft structures which can continue operation with some known level of damage [7]. Damage tolerance uses fracture mechanics to calculate the critical amount of damage a component can tolerate for given loading conditions. Inspection is then used to measure the amount of damage currently in the component. Fatigue crack growth data and loading conditions are used to calculate the time required for the current damage to progress to the critical level. Finally, all of this information is used to determine how frequently a structure should be inspected to assure safe operation. This process results in safe, efficient aircraft maintenance and operation. Figure 1.1 shows an illustration of damage tolerance points of interest over the life of a structure. Each component of damage tolerance will be discussed in further detail.

1.2.2.1 Residual Strength

Residual strength is the maximum far-field stress that a component can sustain with a given amount of damage. Linear elastic fracture mechanics (LEFM) can be used to calculate the largest crack in a given location that will not result in failure under the component's expected loading conditions. LEFM was pioneered by Griffith starting in

1920 with his work on the rupture of glass spheres and tubes [8]. This work was built upon by Irwin and Williams to produce the basis for LEFM we use today [9] [10]. Equation (1.1) is a principal equation of LEFM that relates far-field stress and crack length to the stress intensity at the tip of the crack [11].

$$K = \sigma\sqrt{\pi a}\beta \tag{1.1}$$

where K is stress intensity factor, σ is the applied far-field stress, a is crack length, and β is a geometric correction factor. Equation (1.1) can be used to calculate the critical crack size, which results in fracture if the far-field stress, geometry, and critical value of K, K_{IC}, are each known. Commonly, software is used to quickly apply LEFM to complex geometries, but the foundations remain the same. Use of fracture mechanics to accurately predict failure is a major advantage of damage tolerance designs.

1.2.2.2 Nondestructive Inspection

Nondestructive inspection (NDI) is the process of inspecting a component without affecting its performance capabilities. NDI identifies the current amount and location of damage in a component. This is done using a variety of techniques, but most relevant to this research, bolt hole eddy current inspection is often used to inspect aircraft fastener holes. This technique uses a rotating probe with electromagnetic coils to detect small changes in the conductivity of the material, corresponding to discontinuities. Each NDI technique has limitations for the smallest flaw it can detect, which is very significant for damage tolerant design. This limit is known as the minimum detectable flaw size and is defined as the smallest flaw which the given NDI technique will detect 90% of the time with 95% confidence. If no flaw is detected on a component, the only conservative

assumption is that a flaw of the minimum detectable size exists. For USAF analysis, the minimum detectable flaw size for bolt hole eddy current inspection is 0.05 inches [12].

1.2.2.3 Crack Growth

Once the present level of component damage is known through NDI techniques, the remaining life of the component is calculated. Typically, testing is performed in accordance with ASTM E 647 to generate data that relate cyclic stress intensity factor, ΔK, to fatigue crack growth rate (da/dN) [13]. The cyclic stress intensity factor is calculated using (1.2) [11].

$$\Delta K = K_{max} - K_{min} \tag{1.2}$$

where K_{max} and K_{min} are the stress intensity factors calculated using (1.1) for the maximum and minimum stress of each fatigue loading cycle, respectively. These da/dN versus ΔK data are used to calculate the amount of crack growth caused by each cycle of fatigue loading and predict the number of cycles required to propagate the crack to the critical size. The crack growth rate typically increases with respect to crack length resulting in a crack growth curve resembling the curve shown in Figure 1.1. This analysis is commonly performed in LexTech Inc. AFGROW software [14]. AFGROW uses material da/dN versus ΔK data along with geometry-specific stress intensity factor solutions to predict the resulting fatigue life. The fatigue life of a component is defined as the number of loading cycles or flight hours required to propagate a fatigue crack from some initial flaw size (IFS) to component failure. The NDI minimum detectable flaw size is typically used as the IFS for analysis, but smaller values may be used in specially allowed instances.

1.2.2.4 Analysis

The calculated fatigue life of a structure is used to determine the proper frequency with which it should be inspected. Typically, the time between inspections is equal to half of the predicted time to failure [15]. By inspecting at regular intervals based on the level of component damage, aircraft safety is maintained.

Conservatism is an important concept for damage tolerant analysis. Analysis must always take a worst-case approach to predicting fatigue life. This is assured by using conservative assumptions in each area of damage tolerance analysis. Critical flaw size is calculated using a flaw in the most critical location under the most extreme loading conditions. NDI minimum detectable flaw sizes are based on conservative statistical analysis of inspection capabilities. Likewise, fatigue crack growth predictions use crack growth rate data higher than expected, resulting in conservative fatigue life. Any time an analysis or maintenance procedure is found to be unconservative, it must be changed to maintain safety of pilots and aircraft.

1.2.2.5 Maintenance

If during aircraft maintenance bolt hole eddy current inspection detects a flaw in a fastener hole, it is standard practice to oversize the hole until no flaw is detected. The flaw may be an actual crack, pit, or gouge, but it may also be caused my normal material variation. The hole is oversized in either instance. This can be detrimental to the residual strength and fatigue life of the structure. Oversizing also reduces the edge margin (e/D) of the hole. The edge margin is defined as the distance from the center of the hole to the edge of the part (e) divided by the diameter of the hole (D). Limitations are often set for

the smallest e/D, which is allowed for a certain part, below which replacement or repair is required. In other instances, a part is designed with a short edge margin to facilitate fitment with adjacent parts or other constraints. It should be noted that after oversizing a hole and detecting no flaws with NDI, a flaw may still be present based on the probability of detecting a flaw with that technique.

1.2.3 Increasing Fatigue Life

There are two logical ways to increase component life in a damage tolerant aircraft structure: increase the maximum allowable crack size or decrease crack growth rate. Increasing the allowable crack size would require decreasing applied loading. This would necessitate changing the usage of the aircraft which is undesirable. Also, the life increase would be minimal due to the tendency for crack growth rate to increase as crack size increases. For instance, doubling the critical crack size would increase the life by much less than double. Decreasing fatigue crack growth rate is a more practical method for increasing overall fatigue life.

The rate of fatigue crack growth can be decreased by introducing compressive residual stress into the material where a crack may form. Residual stress occurs due to material constraint and is not caused by external forces. Compressive residual stresses act by superposition to decrease net tensile stress, which slows fatigue crack growth. Residual stresses may be caused incidentally by heat treatment and manufacturing processes, but intentionally induced residual stresses are the focus of this research. Compressive residual stress may be applied in a variety of ways. For external surfaces, shot peening is a commonly used method. The surface of the part is bombarded with

small, hard particles (often steel) to cause local plastic deformation and compressive residual stress [16]. This process is not feasible for use on the interior of fastener holes due to space constraints.

1.2.3.1 Fastener Hole Cold Expansion

Cold expansion is the process of forcing a fastener hole to a larger diameter, causing yielding and inducing a zone of compressive circumferential residual stress near the edge of the hole. Fastener hole cold expansion was developed by the Boeing Company in the 1960s. A company now named Fatigue Technologies Incorporated (FTI) later developed Split Sleeve Cold Expansion™ technology [17]. Split Sleeve Cold Expansion™, illustrated in Figure 1.2, involves drawing a mandrel fitted with a thin, metal sleeve through the fastener hole. The mandrel used in this process is slightly smaller than the diameter of the hole, but the thickness of the sleeve combined with the mandrel is larger than the hole. The addition of the split sleeve allows cold expansion to be performed without access to the opposite side of the hole, making it much easier to implement on a large scale. Two side effects of this process are a ridge of material created in the bore of the hole by the gap in the split sleeve and surface deformation at the edge of the hole from the pulling operation known as surface upset. These features are shown in Figure 1.3. The split sleeve should be oriented such that the gap is aligned with the loading direction to prevent nucleation of cracks in this area. After cold expansion, the hole is reamed to its final size, removing this ridge. As illustrated in Figure 1.4, Split Sleeve Cold Expansion™ results in compressive residual stress approximately equal to the material's yield stress, which extends approximately one radius distance from the

edge of the hole. After this distance the residual stresses are tensile to maintain equilibrium. The tensile stress region is not detrimental to fatigue life because the life decrease caused by the tensile stress is very small compared to the life increase caused by the compressive stress. This is due to the fact that most of the fatigue life of a crack is spent as a small crack growing slowly. Reducing this already low growth rate with compressive stress extends life dramatically, but increasing growth rate when the crack is near failure has less impact on total life. The residual stress distribution produced by cold expansion is not uniform through the thickness of the part, but rather is lower at the face where the mandrel enters the part and higher at its exit. For this reason, care must be taken to note the direction of cold expansion. This stress gradient causes the characteristic "P" shaped crack front shown in Figure 1.5.

FTI Process Specification 8101D recommends that fastener holes have e/D greater than 1.75 for proper cold expansion [17]. It also notes that shorter edge margins may show deformation of the parent material visible at the edge of the component (usually at the edge nearest the hole). Deformation of the free edge indicates that the elastic stresses in the bulk of the part were not sufficient to completely constrain the plastic strains caused by cold expansion. This is a sign that cold expansion may be less effective for short e/D fastener holes as compared to holes with larger e/D.

1.3 Effects of Cold Expansion on Damage Tolerant Design

Many aircraft are pushed to be in service beyond their original design lifetime. As more components of these aircraft begin to show signs of aging, methods for slowing fatigue crack growth become increasingly important. Cold expansion is an attractive

method for extending the life of these aging aircraft due to its low cost and high effectiveness.

Increasing fatigue life is important, but incorporating the effect of cold expansion into analysis is the only way to reap the benefits. In order to gain the most benefit possible to the entire maintenance process, the effects of cold expansion must be well understood. Additionally, this understanding must be properly incorporated into the damage tolerant analysis process. If cold expansion is not properly accounted for in analysis, the resulting inspection intervals may be unconservative. Current practice for USAF damage tolerant analysis is to use an IFS of 0.005 inches instead of 0.05 inches to account for cold expansion [15]. This successfully increases the calculated life but inaccurately accounts for the cold expansion process.

The method of reducing the IFS for analysis to 0.005 inches to account for cold expansion is used for all fastener holes regardless of e/D. This assumes that the effectiveness of cold expansion is not reduced for smaller e/D. Improved understanding of the cold expansion process is required to produce accurate and conservative fatigue life predictions.

1.3.1 Previous Research

The effects of cold expansion on fatigue life have been researched quite extensively since its introduction in the 1960s. Early investigations into the propagation of cracks from cold-expanded holes yielded some important results. Pell et al. observed that crack growth rate of cracks emanating from cold-expanded holes was nearly constant for much of the fatigue life until rapidly increasing to failure [18]. This was contrasted

with the approximately linear increase in growth rate for cracks growing from noncold-expanded holes. It was also observed that the crack progressed faster near the mandrel entrance face of the sample than the exit face, producing a uniquely shaped crack front. This was attributed to the crack growing into lower compressive stress regions sooner at the mandrel entrance face than the exit face. Fatigue life increases of up to eight times were observed by Ball and Lowry for constant amplitude loading of cold-expanded holes in 2124-T851 aluminum alloy [19]. Carlson and Pilarczyk each observed larger increases in fatigue life in their testing of 2024-T351 and 7075-T651 aluminum alloys, respectively [20], [21]. Under variable amplitude aircraft wing loading spectra, Ball and Lowry reported life increases of up to five times. In this research they also discovered that fastener holes with through-thickness cracks had similar benefits from cold expansion as holes with corner cracks. Buxbaum and Huth also showed that cold expansion provides decreased life improvement under spectrum loading as compared to constant amplitude loading for 2024-T3 aluminum alloy [22]. In terms of damage tolerant analysis, it is important to note that basing fatigue life predictions on constant amplitude testing does not yield conservative results for spectrum loading conditions.

1.3.1.1 Fastener Holes with Preexisting Flaws

Researchers also recognized the importance of understanding the effects of cold expanding a hole with a preexisting flaw. Because damage tolerance analysis assumes the presence of flaws during service, their presence must also be assumed at the time of cold expansion. Research by Petrak and Stewart showed that the fatigue life of fastener holes with preexisting cracks approximately 0.1 inches long can be improved by cold expansion and interference fit fasteners [23]. It has been shown that cold expansion has

negligible effect on crack nucleation and the growth of both small cracks and very large cracks, but it can significantly slow the growth of cracks longer than about 0.039 inches and shorter than the radius of the hole [18], [24], [25], [26], [22]. This is an important finding for damage tolerant analysis because it indicates the growth of a crack at an IFS of 0.050 inches is slowed by cold expansion. Research performed by Buch and Berkovitz revealed that fastener holes with preexisting cracks benefitted more from cold expansion than holes without cracks [27]. It was also found by Zhang and Wang that fatigue life was improved most when a fastener hole was cold expanded after 25% of its noncold-expanded fatigue life [26]. Buxbaum and Huth found that cold expanding a fastener hole with a preexisting crack approximately 0.020 inches long can result in fatigue life longer than a noncold-expanded hole without a flaw [22].

Warner performed research on cold expansion of fastener holes in 2024-T351 aluminum alloy with preexisting cracks under constant amplitude and spectrum loading [28]. The research found that increasing the maximum stress used for spectrum loading caused a reduction in the life increase obtained by cold expansion. Maximum stresses of 25, 30, and 33 ksi produced fatigue lives approximately 8.1, 4.4, and 2.5 times the lives predicted by 0.005 inch IFS predictions, respectively. However, spectrum testing with a maximum stress of 43.25 ksi produced fatigue life lower than 0.005 inch IFS predictions. This shows that predicting crack growth life of cold-expanded holes using a 0.005 inch IFS is not conservative for all loading conditions.

1.3.1.2 Fastener Holes with Short Edge Margins

Many fastener holes in aircraft applications have short edge margins arising from being oversized during maintenance or by design. Brot and Nathan performed research on short edge margins and found that cold expansion was ineffective at increasing fatigue life of samples with e/D less than 1.0 [29]. The same research showed that specimens with e/D between 1.0 and 1.5 experienced approximately three times increase in fatigue life due to cold expansion. Ayatollahi researched the effect of short edge margins on residual stress fields of cold-expanded fastener holes using finite element modeling (FEM) [30]. The results showed that the radius of the compressive residual stress field did not vary with e/D greater than 2.0, but the radius of the compressive stress field decreased dramatically for holes with e/D less than 2.0. It was also found that elevated tensile stresses were developed at the free edge for e/D less than 2.0, which could contribute to accelerated failure. Ayatollahi also observed edge deformation in the FEM due to the cold expansion process similar to the bulging observed by Andrew in experimentation [31], [32]. The FEM showed that the magnitude of bulging was below 3% of the hole radius in all cases.

Andrew performed experiments on cold-expanded fastener holes with e/D of 1.2 containing preexisting cracks in 2024-T351 aluminum alloy. It was found that spectrum loading at 33 ksi maximum stress produced fatigue life below the life predicted by AFGROW using an IFS of 0.005 inches. Using identical material, loading spectra, and maximum stress of 33 ksi, Warner found that a hole with e/D of 4.0 produced fatigue life greater than AFGROW prediction. This indicates that an e/D exists between 1.2 and 4.0, which matches predictions based on a 0.005 inch IFS.

Research by Warner and Andrew each included fatigue crack growth rate measurement using ASTM E 647 standard specimens from the same material lot as their test specimens. From this data, material lookup files were used to accurately model the material response in analysis tools like AFGROW.

Hill Engineering, LLC performed testing to characterize the residual stress field caused by cold expansion of short edge margin holes in 2024-T351 aluminum alloy [33]. The stress field was characterized using the contour method. The contour method is a destructive method in which the sample is sectioned on a plane of interest using electrical discharge machining (see Figure 1.6). The shape change of the specimen after sectioning is measured and applied to a finite element model, which calculates the stress required to maintain equilibrium. A plot of residual stress data gathered using the contour method for e/D of 2.0 is shown in Figure 1.7.

1.3.2 Current Research

In the course of extending aircraft fatigue life, fastener holes are routinely inspected and cold expanded. In the instance that a flaw is not detected by NDI, a flaw of the minimum detectable size may still be present. It is important to understand the effect of cold expansion on holes with preexisting flaws. Specifically, this research investigates the effects of cold expansion on fastener holes with preexisting 0.050 inch cracks, the minimum detectable flaw size for bolt hole eddy current inspection.

In the case that a flaw is detected at a fastener hole by NDI, the hole is oversized until no flaw is detected before being cold expanded. Oversizing holes can give rise to short e/D situations. In other cases, parts may be designed with a short e/D for

functionality purposes. A short e/D is typically defined as 2.0 and below. The current damage tolerance analysis practices of the USAF use a 0.005 inch IFS to account for cold expansion regardless of part e/D. Research by Andrew showed that this assumption does not produce conservative predictions for fatigue life under all loading conditions. This research seeks to quantify the reduction in prediction conservatism caused by decreases in e/D.

1.3.2.1 Relevance to USAF Damage Tolerance Practices

The current research differs from previous research on similar topics due to its relevance to current USAF damage tolerant analysis practices. It has been demonstrated that type of loading (constant amplitude or spectrum), maximum applied stress, e/D, and material properties all contribute to the resulting fatigue life of cold-expanded fastener holes. This implies that testing that does not replicate service conditions should not be used to predict the service life aircraft components.

This research explores the benefit gained by cold expansion of short e/D holes under a fighter aircraft wing bending loading spectrum. This spectrum was designed to accurately replicate the stresses experienced by a fighter aircraft during flight and is currently used for USAF fatigue life prediction.

The maximum stress used in this research of 33 ksi is based on typical service conditions for fighter aircraft. Other researchers also used this stress level, making comparisons between research possible.

It is known that fatigue life predictions using current USAF techniques for holes with e/D of 1.2 can be unconservative, but the functional form of the decrease in

conservatism from e/D of 4.0 is not known. This research explores the benefit of cold expansion on holes with 1.3, 1.4, 1.5, and 2.0 e/D. These values represent situations encountered during routine aircraft maintenance. Testing these e/D values is important for improving analysis techniques to more closely match test results.

Finally, the 2024-T351 aluminum alloy used in this research represents a very common application for cold-expanded fastener holes. To facilitate comparison, the material used in this research is from the same lot as the material used in the research by Andrew and Warner. This reduces material-induced variability while maintaining relevance to common aircraft conditions. This also allows the previously developed material lookup files to be leveraged in the current research.

The results from this research will be compared to the current techniques used for damage tolerance analysis. Recommendations will be provided for the suitability of current analysis practices.

1.3.2.2 Research Objectives

The present research seeks to meet the following objectives:

1. Document the fatigue life of noncold-expanded, short e/D holes in 2024-T351 aluminum alloy.
2. Quantify the fatigue life gained by cold expanding fastener holes with preexisting cracks and varying e/D.
3. Determine if AFGROW predictions using a 0.005 inch initial flaw size produce conservative fatigue life predictions for all e/D compared to generated data.
4. Use numerical simulation to inform comparisons between cold-expanded and

noncold-expanded fastener holes at varying e/D.

5. Document fatigue crack growth behavior for each e/D.

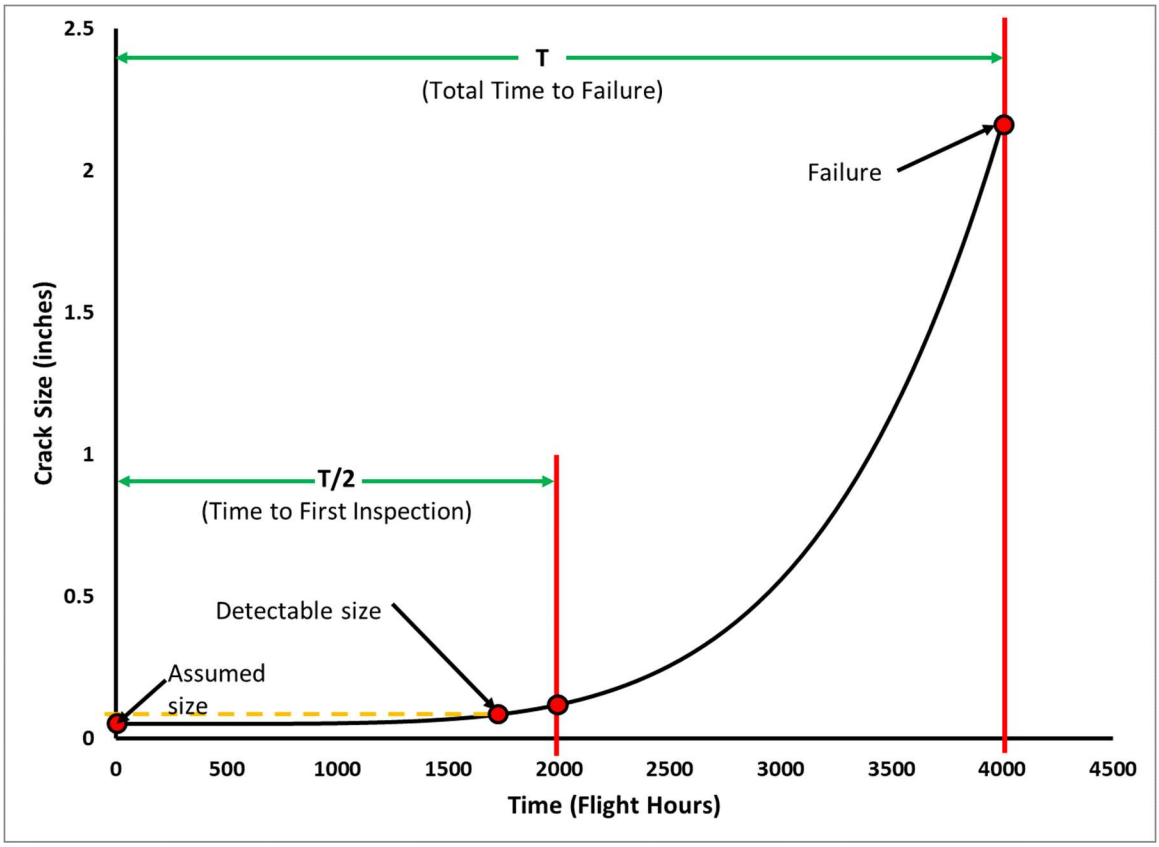

Figure 1.1: Illustration of damage tolerant design practices over the life of a component. Note that the assumed size may be equal to the detectable size.

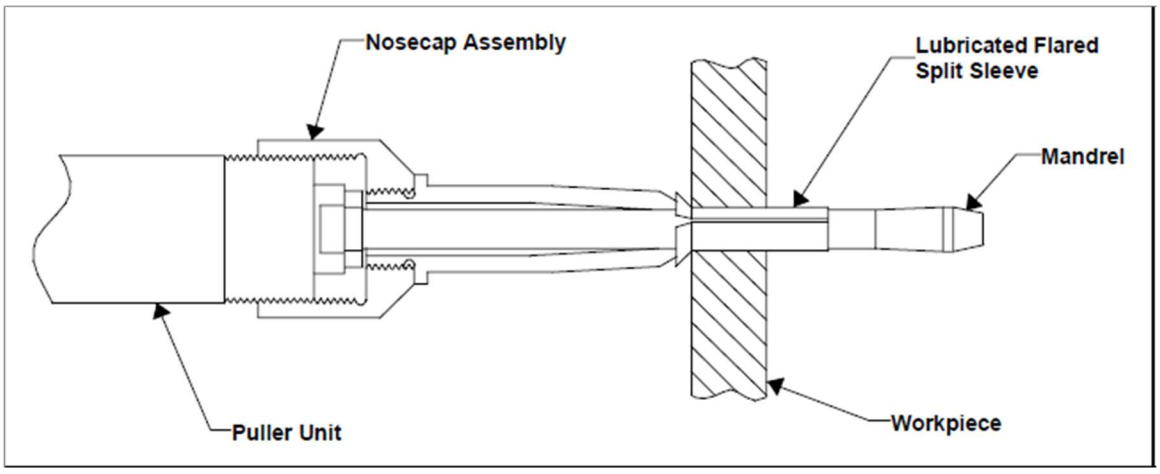

Figure 1.2: Illustration of Split Sleeve Cold Expansion™ process [17].

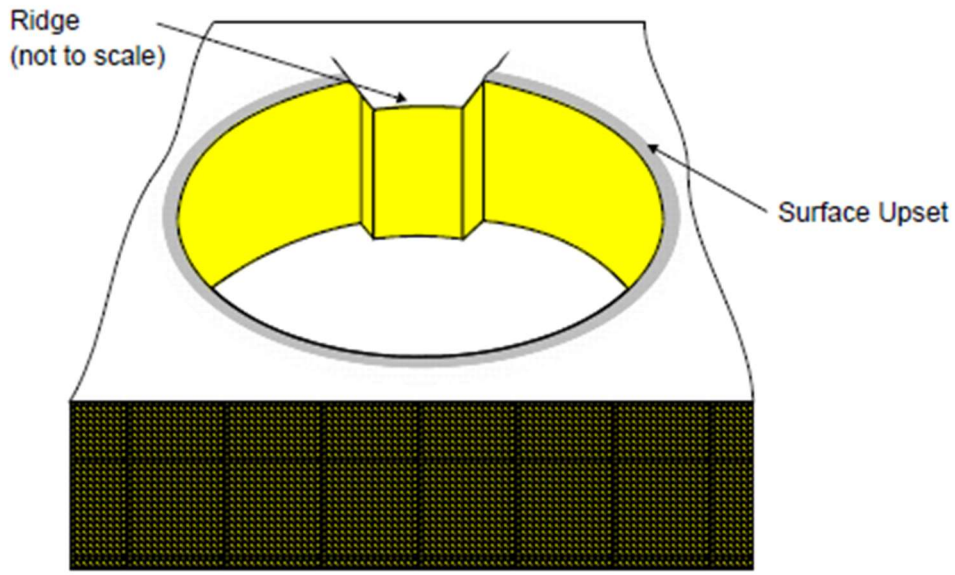

Figure 1.3: Ridge induced by split sleeve. Sleeve should be oriented such that the ridge is aligned with the direction of loading [17].

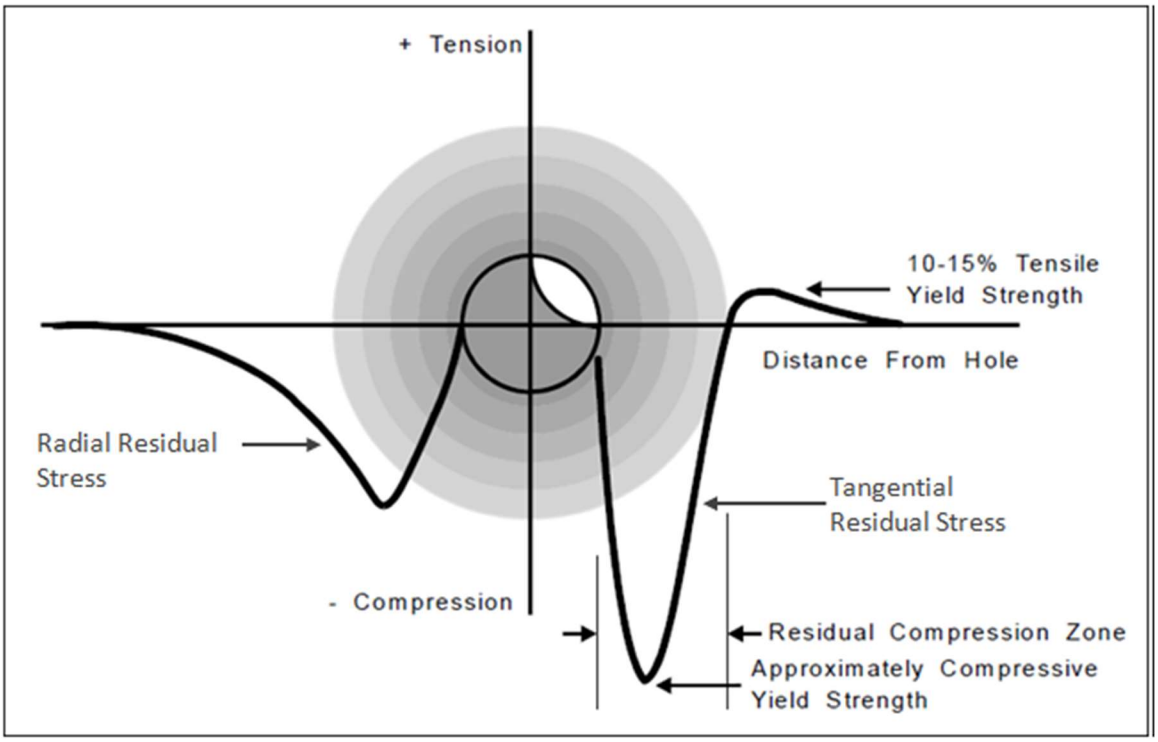

Figure 1.4: Residual stress fields induced by cold expansion. Peak compressive stress is greater in magnitude than peak tensile stress [17].

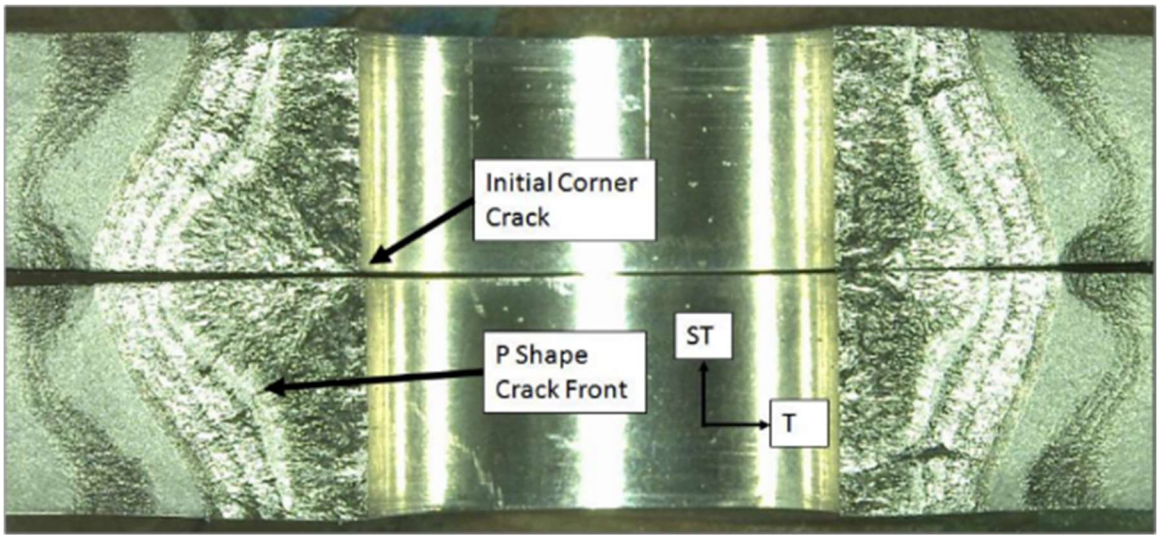

Figure 1.5: Characteristic "P" shaped crack front caused by through-thickness variation of residual stress fields. Specimen shown is from research performed by Warner [28]. The two mating crack surfaces are shown on top and bottom. Cracks emanated from the hole in the center outward.

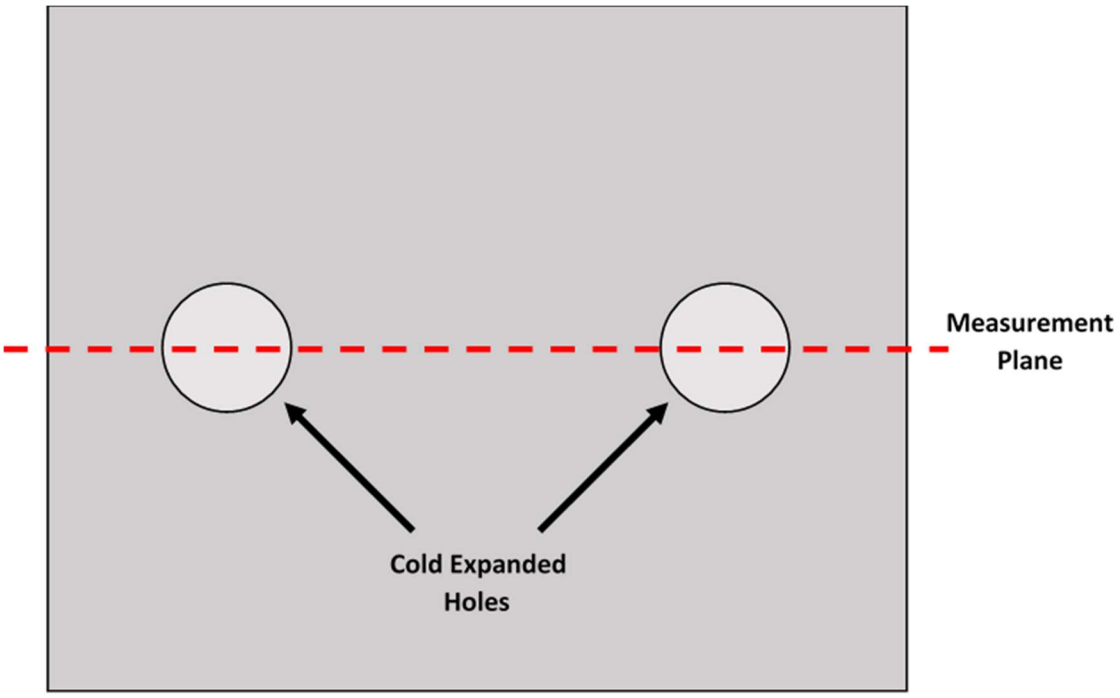

Figure 1.6: Specimen configuration for performing residual stress measurements with the contour method. The specimen is cut along the measurement plane using electrical discharge machining.

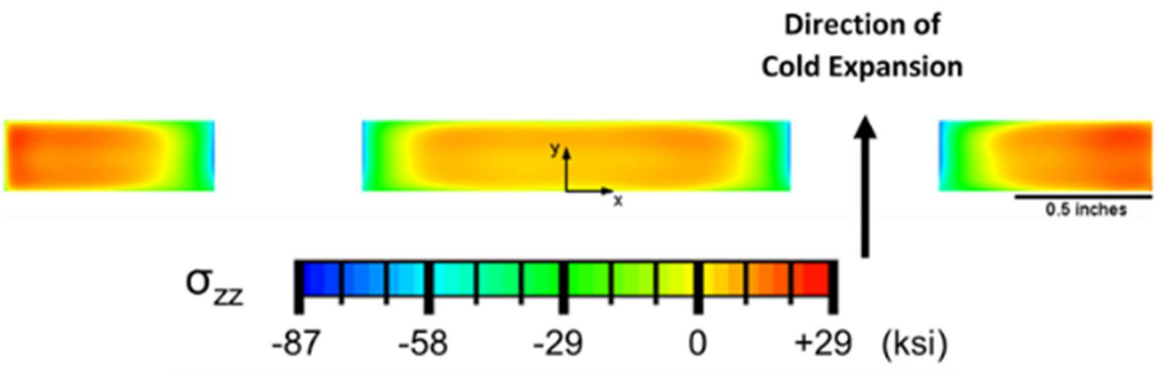

Figure 1.7: Plot of residual stress data gathered using the contour method. Note that the stress field varies based on direction of cold expansion.

2 TEST SETUP AND METHODS

2.1 Test Specimens

2.1.1 Test Matrix

The test matrix for this research is shown in Table 2.1. This experiment design was chosen to isolate the effect of edge margin on fatigue life of precracked, cold-expanded holes in 2024-T351 aluminum alloy. Variable amplitude (or spectrum) loading was used to test each specimen because it better replicates actual aircraft loading conditions than constant amplitude loading. This makes the results of this research readily applicable to aircraft design and maintenance. The loading spectrum used was based on the wing root bending moment of a fighter aircraft. Structure under this loading is a typical application of 2024-T351 aluminum. The maximum stress used in the loading spectrum was 33,000 pound-force per square inch (33 ksi) because it is representative of stress levels at the wing root of a fighter aircraft [34].

2.1.2 Specimen Material

All specimens were machined from the same piece of 2024-T351 aluminum alloy plate. This plate is from the same material lot as the testing performed by Andrew and Warner [31] [28]. Testing of this alloy is important because it is widely used in the aerospace industry for tension applications. It has low strength but exceptional toughness, making it suitable for damage tolerant design. The composition of alloying elements in

2024 aluminum is approximately 4.5, 1.5, and 0.6 weight percent copper, magnesium, manganese, respectively [REF]. The material certification sheet is included in Appendix A.

2.1.3 Specimen Geometry

A total of 20 specimens were used in this research. Five specimens were allocated to testing each edge margin. The overall specimen design was modeled after the middle tension specimen described in the ASTM E 647 standard with some notable differences. Instead of a small, centered hole with two through-thickness cracks, the specimens were fabricated with a 0.474 to 0.477 inch diameter offset hole and a single corner crack. This was designed to emulate common aircraft fastener hole geometry and damage. The holes were centered at edge distances (e) of 0.65, 0.70, 0.75, and 1.00 inches to achieve edge margins (e/D) of 1.30, 1.40, 1.50, and 2.00, respectively, for 0.50 inch diameter (D) holes (final diameter after final reaming). Figure 2.1 shows a test specimen, and specimen drawings are shown in Appendix B. The edge from which e is measured will be referred to as the free edge of specimen, and the material between the hole and the free edge will be referred to as the short ligament. The 20 specimens were divided into a noncold-expanded (NCX) control group with two replicates per e/D and a cold-expanded (CX) test group with three replicates per e/D.

2.1.4 Specimen Fabrication

All test specimens were fabricated by Southwest Research Institute (SwRI) for the purpose of this research. Each specimen was milled from the same plate of material

before drilling and reaming the through hole. An approximate 0.010 by 0.010 inch electrical discharge machined (EDM) notch was created at the corner of each hole nearest the short ligament. A representative EDM notch is shown in Figure 2.2. The bore of the hole and both faces of the specimen were polished to a mirror-like finish to aid in crack measurement. Aluminum tabs of 0.063 inch thickness were bonded to the grip area of the cold-expanded specimens to prevent crack nucleation from marks induced by the gripping operation.

2.1.5 Specimen Identification

SwRI added specimen identification markings to both ends of each specimen as shown in Figure 2.3. The first two or three letters in the identification designate if the specimen is to be cold expanded. “CX” indicates the specimen will be tested after cold expansion, and “NCX” indicates it will be tested in the noncold-expanded state. The following three numbers and two letters indicate the edge margin (e/D) of the specimen. “130ED” indicates that the specimen has an e/D of 1.30. The final number following a hyphen designates individual replicates within each treatment group. For example, the third specimen, which is allocated for cold expansion with e/D of 1.40, is identified as “CX140ED-3.”

Areas of interest on each specimen are referred to by specific names for ease of communication. The face of the specimen containing the EDM notch is denoted as the front of the specimen, and the opposite face is denoted as the back. The area between the hole and the free edge of the specimen is denoted as Side A, and the opposite as Side B.

2.2 Equipment Used

All test equipment used in this research is owned and maintained by the USAF Hill Air Force Base (HAFB) Science and Engineering Laboratory. Various pieces of equipment were used for testing, measuring, machining, and imaging the test specimens. The most recent certificates of calibration can be found in Appendix C. Note that calibration was performed during the course of testing, but the machine was certified as-found with no changes from the previous calibration.

2.2.1 Servo-hydraulic Tester

All specimens were precracked and tested on the same servo-hydraulic fatigue machine with approximately the same settings. The configuration of the machine is described in the following sections. The machine is shown in Figure 2.4.

2.2.1.1 Load Frame

The load frame used for this research is an MTS Landmark with 55 kip capacity. This machine is equipped with two valves capable of 15 gallons per minute (gpm) hydraulic fluid flow (30 gpm total). The upper grip is fixed while the other is mounted to the piston which actuates to apply force.

2.2.1.2 Hydraulic Grips

The grips used in this research are MTS 647.25A hydraulic wedge grips. These grips are matched to the load frame and have a load capacity of 55 kip. They are capable of 10,000 psi grip pressure, but 5,000 psi was used for this research. This pressure was

chosen because it provided sufficient gripping ability and stiffness. At lower pressures the grips shifted slightly at high loads.

Standard 4-inch-wide, diamond pattern MTS wedge grip faces, model 046-198-804 were used to grip the specimen. These grip faces can specimen thicknesses between 0.04 and 0.47 inches, allowing specimens with and without bonded tabs (CX and NXC specimens, respectively) to be tested.

2.2.1.3 Controller

The controller sends command signals to the load frame while simultaneously processing feedback signals of load and displacement. An MTS Flex-Test 40 controller was used in this research. The controller uses proportional, integral, derivative, and feedforward (PIDF) gain settings to process feedback signals and produce the proper command signals.

2.2.1.4 Software

Test software is the interface between the operator and the controller. It performs many tasks including managing test flow, data acquisition (DAQ), safety features, and sending loading information to the controller. Multipurpose Elite (MPE) by MTS is the test software used for this research. The test flow was designed specifically for this research and allowed the operator to control and monitor each aspect of the test. It also visualized data from user input such as crack length over time.

2.2.2 Measurement Equipment

Specimen dimensions were measured initially and after each processing step to document any changes.

2.2.2.1 Digital Outside Micrometers

The thickness of each specimen was measured with a 0 – 1.2 inch digital micrometer with 0.00005 inch accuracy. The width was measured with a 4 – 5 inch micrometer with 0.00015 inch accuracy.

2.2.2.2 Digital Microscope

A Keyence VHX 6000 digital microscope was used to measure multiple features in this research including hole diameter at each stage of processing, edge distance, amount of specimen edge deformation, and EDM size. This microscope is shown in Figure 2.5.

2.2.2.3 Travelling Microscopes

Gaertner Scientific microscopes, Model M303LE, were used with Model NV11RS Fagor digital readouts to measure crack growth during testing. This system has a display resolution of 0.00002 inches, which is superior to the minimum values suggested in ASTM E 647 for fatigue crack growth measurement [13]. These microscopes have filar eyepieces, which allow for precise positioning with respect to the crack. Two travelling microscopes were mounted on the load frame with custom hardware. One was used to measure the crack on the front of the specimen while the

other was used to measure the crack in the bore of the hole and the back of the sample. Figure 2.6 shows the travelling microscope mounting configuration used.

2.2.3 Imaging Equipment

2.2.3.1 Stationary Digital Microscope

The Keyence VHX 6000 digital microscope was also used for qualitative imaging of specimen features such as ridges left by the cold expansion process and scratches from reaming. It was instrumental in documenting the appearance of the specimens at each stage of testing. It is capable of 20 – 2000 times magnification, automatic image stitching, and three-dimensional optical measurement. This digital microscope was also used for postmortem fractographic analysis.

2.2.3.2 Scanning Electron Microscope

High magnification imaging of fracture surfaces was performed with a Jeol scanning electron microscope (SEM). With maximum magnification up to 300,000 times and large depth of field, it provides high quality images that cannot be captured in other ways. The SEM used is shown in Figure 2.7.

2.2.3.3 USB Digital Microscope

A Dino-Lite USB digital microscope was used to document the crack growth process during testing. Up to two of these small microscopes were mounted on the load frame to capture magnified images of the surface crack growth at specific intervals. The USB interface allowed the microscopes to be controlled by the test software. Figure 2.8

shows an image captured with this method.

2.3 Test Procedure

The steps taken to prepare the specimens for testing and to perform the tests are as follows:

1. Initial measurement
2. Constant amplitude fatigue precracking
3. Cold expansion (CX specimens only)
4. Hole measurement
5. Reaming and polishing
6. Hole measurement
7. Variable amplitude fatigue testing
8. Fractographic analysis

Each step will be explained in the following sections.

2.3.1 Specimen Measurement

The first step in the testing process was to measure the specimens as-received. The thickness and width were measured using outside micrometers. The hole diameter, edge distance, and EDM notch dimensions were then measured using the Keyence digital microscope.

2.3.2 Fatigue Precracking

To accurately represent a crack in an aircraft component, a fatigue crack was propagated from the EDM notch at the corner of each hole. To create a fatigue crack,

each specimen was subjected to constant amplitude fatigue loading at the root mean square (RMS) peak stress value of the test spectrum, 14.4 kip, and stress ratio of R = 0.1 as defined by (2.1).

$$R = \frac{\sigma_{min}}{\sigma_{max}} \tag{2.1}$$

According to the guidelines in ASTM E647, it was determined that fatigue precracking at the RMS stress would not appreciably affect the subsequent testing [13]. The cracks were propagated until they reached a length of approximately 0.050 inches, the minimum detectable flaw size for bolt hole eddy current inspection [12].

2.3.3 Cold Expansion

Each CX specimen was cold expanded according to FTI process specification 8101D using FTI 16-0-N tooling in the HAFB Wing Shop [17]. This resulted in an expanded hole with a ridge from the lubricated split sleeve, shown in Figure 2.9. The split sleeve was oriented such that the produced ridge aligned with the direction of loading. This prevents cracks from nucleating at this discontinuity. The pulling direction of cold expansion was from the front of the specimen to the back for all specimens. This caused the compressive residual stresses to be lower at the crack than on the opposite face. This represents a conservative approach because cracks are expected to grow faster in lower residual compressive stress fields. The diameter of each hole was measured to calculate the amount of applied and residual expansion using (2.2) and (2.3), respectively [17].

$$I_a = \frac{D_m + 2t_s - D_i}{D_i} \tag{2.2}$$

$$I_r = \frac{D_f - D_i}{D_i} \tag{2.3}$$

where D_m is the major diameter of the mandrel, t_s is the thickness of the sleeve, D_i is the initial diameter of the hole, and D_f is the diameter of the hole after cold expansion. The resulting calculations are summarized in Table 2.2. Applied and residual expansion are generally used measurements for the degree of cold expansion.

As observed by Andrew, the free edge of the specimens became permanently deformed by the cold expansion process. This slight deformation is shown in Figure 2.9. The amount of deformation for each specimen was measured using the Keyence digital microscope and tabulated in Table 2.3.

2.3.4 Reaming and Polishing

To remove the ridge left by cold expansion and produce the desired 0.5 inch diameter, the hole was reamed to its final size. Reaming also removes the EDM notch, leaving only a true fatigue crack. This process was performed on all specimens, CX and NCX, to produce uniform hole size. Reaming was performed on the standard manual mill shown in Figure 2.10 using a reamer provided by the HAFB Wing Shop. Shims were used to protect the deformed edge of CX specimens from the mill vice during reaming. An image of this setup is shown in Figure 2.11.

After reaming, axial scratches from removing the reamer remained in the holes. These scratches are shown in Figure 2.12. A pneumatic die grinder with custom bit was used to lightly sand and polish the bore of each hole to a mirror-like finish. This process was performed to reduce the likelihood of cracks nucleating at these locations and to make the crack more readily visible for measurement. All sanding and polishing was performed circumferentially in the bore to prevent leaving scratches in the direction of

expected crack growth. The resulting appearance of the hole is shown in Figure 2.13. After polishing, each specimen was measured to document the dimensions for testing.

2.3.5 Fatigue Testing

Each sample was clamped in the upper grip of the load frame first. Machinist parallels were used to ensure the specimen was aligned vertically when gripped as shown in Figure 2.14. The load cell was then balanced to account for the weight of the specimen. The lower grip was raised into position, and the bottom of the sample was gripped. The load was then returned to zero to remove any loading caused by the gripping process. Test parameters were entered into the test software and the crack was initially measured. Then, the test was run until specimen failure, pausing after each approximately 0.02 inches of crack growth for measurement. Specimen failure is defined as crack propagation completely through the nearest edge of the specimen, the specimen ligament, as shown in Figure 2.15. Although some specimens (specifically specimens with e/D of 2.0) fractured completely at the point of ligament failure, this was not a requirement for failure.

2.3.5.1 Loading Spectrum

A fighter aircraft wing root bending loading spectrum was used to test each specimen. This spectrum consists of 7,368 cycles which represents 240 aircraft flight hours. Loading spectra are typically defined by their maximum stress. The file containing each peak and trough of the loading sequence is normalized such that a value of 1.0 corresponds to the maximum stress. This allows the spectrum file to be utilized in testing

and analysis at varying stress levels. The maximum stress used in this research was 33 ksi. Figure 2.16 shows a section of the normalized loading spectrum. This spectrum was repeated continuously until specimen failure, only interrupted by crack measurement and marker band sequences. The loading rate used for this testing was 165 kip per second.

2.3.5.2 Marker Banding

Periodically, marker band loading sequences were applied. Marker banding is the process of changing fatigue loading conditions to leave a visible artifact on the fracture surface. These artifacts are useful for documenting the shape of the crack front at particular times. T space marker bands consistently between NCX and CX specimens, marker band sequences were applied after every four main spectrum passes for NCX specimens and after every 16 main spectrum passes for CX specimens. This implies the assumption that CX specimens have an approximately four times greater fatigue life than NCX specimens. The marker band sequence used in this research is illustrated in Figure 2.17. The first three cycles reach maximum spectrum stress, 33 ksi, at $R = 0.1$, and the following 300 cycles reach 80% of maximum stress at $R = 0.5$. This marker band sequence is based on research performed by Fawaz who determined that its effect on total fatigue life is negligible [35]. Comparisons were also performed using AFGROW software and the resulting differences were negligible. A fracture surface with evident marker bands is shown in Figure 2.18. Marker banding was performed on noncold-expanded specimens after every four spectrum loading blocks. For cold-expanded specimens, marker bands were applied after every 15 spectrum loading blocks.

2.3.5.3 Surface Crack Measurement Procedure

The crack was measured at the start of each test and at growth increments of approximately 0.020 inches throughout testing. Before each measurement, the specimen was loaded to approximately the RMS peak stress of the spectrum (15 ksi) to open the crack slightly and improve measurement accuracy. The digital readout was set to zero while the travelling microscope filars were aligned with the edge of the hole before each measurement. This assured the accuracy of each measurement by accounting for any movement of the microscope or shape change of the hole. The microscope was then translated horizontally until the filars aligned with the edge of the crack, and the distance measured by the readout was recorded.

2.3.5.4 Bore Crack Measurement Procedure

Cracks within the bore of the hole were measured differently because it is impossible to view the crack from a direction normal to the surface of the hole. To accommodate this limitation, a travelling microscope was set at an angle to the specimen, directed at the bore of the hole. The method used to correct the crack measurement for the angled measurement is illustrated in Figure 2.19, with the actual microscope orientation shown in Figure 2.20. The digital readout was zeroed at the edge of the hole on the front face of the specimen (A), the microscope was translated horizontally to the tip of the crack (B), and the distance measured by the digital readout was recorded. An additional step was taken to correct for the angled measurement: the microscope was further translated past the tip of the crack to view the edge of the hole at the back face of the specimen (C). The distance measured by the digital readout was recorded. This total

distance (AC) is the thickness of the specimen when measured from the angle of the microscope. The ratio of the measured length of the crack (AB) to the measured thickness of the specimen (AC) is equal to the ratio of the actual length of the crack to the actual thickness of the specimen. Based on this relationship, the actual crack length was calculated using (2.4).

$$a = AC\,\frac{AB}{t} \tag{2.4}$$

where a is the actual bore crack length, and t is the actual thickness of the specimen.

Once the bore crack propagated completely through the thickness of the specimen, the travelling microscope was rotated to view the back surface of the specimen squarely. The crack was then measured using the same method as the front of the specimen.

2.4 Data Analysis Methods

This section will describe the methods used to analyze the data gathered in this research.

2.4.1 AFGROW Analysis

The primary tool used for data analysis was AFGROW because it is the main tool used by the USAF for damage tolerance analysis. Individual AFGROW models were created for each specimen using the measured dimensions.

2.4.2 Analysis Parameters

AFGROW analysis requires the input of multiple parameters to describe material, model geometry, loading spectrum, and crack growth retardation. Each input parameter will be described in the following sections.

2.4.2.1 Material Lookup File

AFGROW uses material lookup files to determine the response of the material based on loading inputs. Most notably, the da/dN versus ΔK curve calculates fatigue crack growth increments based on cyclic loading. ASTM E 647 fatigue crack growth rate measurement experiments were performed by Andrew and Warner to characterize the material used in this research [31] [28]. Figure 2.21 shows the da/dN versus ΔK data that they developed.

2.4.2.2 Simulation Model

The Single Corner Crack at Hole AFGROW model was used to simulate the test specimen crack growth. This model, shown in Figure 2.22, uses each specimen cross-sectional dimension including width, thickness, hole diameter, edge distance, and crack size and shape. The crack size and shape are defined by the surface crack length, *c*, and the bore crack length, *a*, as shown in Figure 2.23. Optionally, the ratio of bore crack length to surface crack length, *a/c*, may be held constant. In this research, *a/c* was held constant, and the average between the actual bore crack length and the surface crack length was used for both *a* and *c*. This method was used because the resulting simulated crack growth most closely matched test data. This method was also used by Andrew and

Warner [31] [28]. In some instances, the crack dimensions used for AFGROW analysis were not the actual specimen crack dimensions, but rather 0.05 or 0.005 inch initial flaws were used for damage tolerance analysis.

2.4.2.3 Loading Spectrum

The loading spectrum described previously, including marker band sequences, was used for all AFGROW simulations with 33 ksi maximum stress. Note that the spacing between marker band blocks varied between NCX and CX specimens. This was included in analysis.

2.4.2.4 Crack Growth Retardation

When a tensile overload is applied to a fatigue crack, a large plastically deformed zone is created near the crack tip. This zone decreases fatigue crack growth rates and increases overall fatigue life. This effect is known as crack growth retardation. This is especially important under spectrum loading because occasional large loads may marginalize the effects of subsequent smaller loads. Also, crack growth retardation may be induced by incidental overloads from test machine loading error. Loading accuracy must be closely monitored to ensure accurate test results. The generalized Willenborg model is the most commonly used method for accounting for crack growth retardation in AFGROW. It estimates the size of the plastically deformed zone at the tip of the crack and reduces the stress intensity of subsequent loads accordingly, which serves to reduce crack growth rate and increase overall fatigue life. The generalized Willenborg model requires a single input parameter, shutoff overload ratio (SOLR) to define crack growth

retardation. SOLR is affected by both material properties and loading conditions. Lower values of SOLR provide more crack growth retardation and longer fatigue life.

2.4.3 Noncold-Expanded Specimens

NCX specimens were used to create a baseline for crack growth comparison. This was achieved by adjusting AFGROW simulations to match test results. The primary adjustment parameter was SOLR. Fatigue crack growth analysis was performed on each NCX specimen, and SOLR was adjusted until the predicted fatigue life was equal to the measured fatigue life. The mean of the resulting SOLR values was used for AFGROW predictions. It was assumed that SOLR is only material and loading spectrum dependent, and does not vary significantly by e/D. This allows using the mean of all SOLR values, regardless of e/D, to produce the most accurate predictions possible.

2.4.4 Cold-Expanded Specimens

Multiple methods were used to evaluate the effect of cold expansion on precracked, short e/D, cold-expanded holes. The methods used in this research are described in the following sections.

2.4.4.1 Baseline Comparison

Multiple types of comparisons may be made between NCX and CX specimen fatigue life results. One such comparison is between the total fatigue life measured for CX and NCX specimens. Life Improvement Factor (LIF), as defined in (2.5), was used to quantify the effect of cold expansion on fatigue life.

$$LIF = \frac{CX\ Life}{NCX\ Life} \tag{2.5}$$

2.4.4.2 Initial Flaw Size Reduction

In accordance with USAF damage tolerance design practices, AFGROW analyses were performed with the average SOLR values and initial crack size of 0.005 inches. This is the minimum IFS that may be used to account for cold expansion [15]. This approach was used to evaluate the conservatism of USAF fatigue crack growth predictions.

2.4.5 Numerical Simulation

In addition to traditional AFGROW analysis, numerical simulation was used to model crack growth behavior. Numerical simulation was performed using a combination of StressCheck®, AGROW, and Broad Application for Modeling Failure (BAMF) [36] [14] [37]. StressCheck® is a finite element analysis (FEA) software which has robust functionality for fracture mechanics. It allows the user to model cracks in complex structures and calculate parameters related to fracture, such as stress intensity. Residual stresses can also be modeled within the program. The three-dimensional simulations produced by StressCheck® are typically more robust and have more flexibility than the solutions implemented in AFGROW. Despite the strengths of StressCheck®, AFGROW is more optimized for fatigue crack growth. Also, AFGROW is widely accepted as an aerospace industry standard for fatigue crack growth predictions. BAMF was created to utilize the strengths of each software to solve complex problems. Standard analysis methods are limited in the crack front shapes that they can simulate. AFGROW typically uses two points to define a crack front and interpolates the crack shape, but BAMF allows

AFGROW solutions to be applied to complex crack geometries.

The flow of crack growth prediction using BAMF, StressCheck®, and AFGROW (referred to as BAMF predictions from this point) is illustrated in Figure 2.24. A finite element model is used to calculate the stress state at certain points along the crack front. BAMF supplies this information to AFGROW, which calculates the resulting crack growth increment for each location. These data are passed to StressCheck® by BAMF to update the finite element model. This process is repeated recursively until the analysis is complete. During this process, the crack front freely changes shape based on the growth of the crack at each calculated point. The final data output from BAMF contains crack growth information and the stress state at each point on the crack front for each growth increment. One limitation of the current BAMF implementation is the assumption that the crack remains on its initial plane for all increments of crack growth. This can produce varying levels of accuracy depending on geometry and loading conditions.

Finite element models were created using nominal specimen geometry for each e/D. Figure 2.25 shows the model and boundary conditions used. The lower face of the model is fully fixed, and the loading is applied to the top face. A convergence study was performed for the stress output of the model. A *P*-level of three was found to provide approximately 4% error. Because stress intensity is more convergent than stress in StressCheck®, and stress intensity was the parameter used in this research, this level of stress convergence was determined to be acceptable. Each model contained the nominal 0.050 inch crack at the edge of the hole. When simulating CX specimens, residual stress fields from experiments by Hill Engineering, LLC were applied in the plane of crack growth [33]. Crack growth, stress state, and β correction factors for use in LEFM were

among the data produced for all crack front points at each increment of growth. These data can be used to replicate results from BAMF predictions using only AFGROW if the crack front geometry remains constant. This is useful for changing minor test parameters without repeating entire 8-hour simulations.

2.4.6 Fractographic Analysis

One specimen from each combination of cold expansion and edge margin (eight in total) was sectioned for fractographic analysis. Sectioning was performed with a diamond saw, and the fracture surfaces were stored individually to avoid damage. The fracture surfaces were examined under both an optical microscopes and a scanning electron microscope.

Table 2.1: Research test matrix.

Material	Thickness	Width	Length	Hole Diameter	Loading	Max Stress	Edge Margin	Specimen ID	CX/NCX	Count
2024-T351	0.25 in.	4 in.	16 in.	0.5 in.	Variable Amplitude	33 ksi	1.3	NCX130ED	NCX	2
								CX130ED	CX	3
							1.4	NCX140ED	NCX	2
								CX140ED	CX	3
							1.5	NCX150ED	NCX	2
								CX150ED	CX	3
							2.0	NCX200ED	NCX	2
								CX200ED	CX	3
CX = Cold Expanded NCX = Non-Cold Expanded								Total Specimens		20

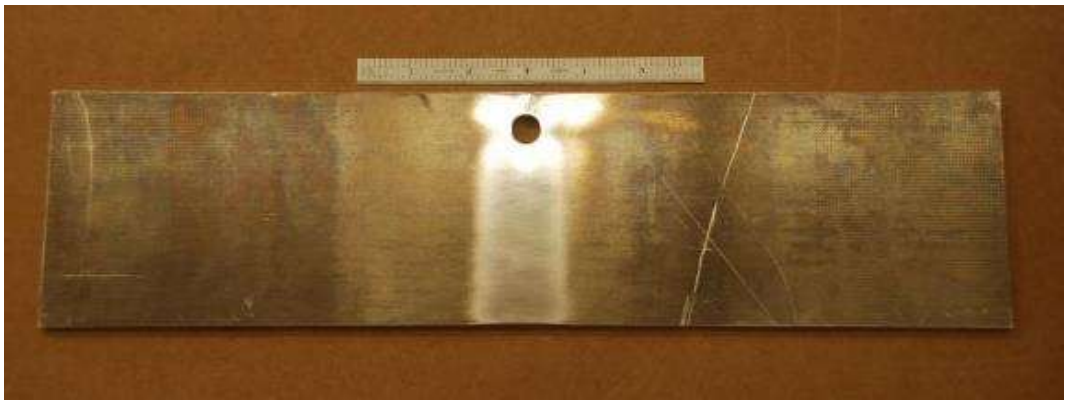

Figure 2.1: Short edge margin specimen.

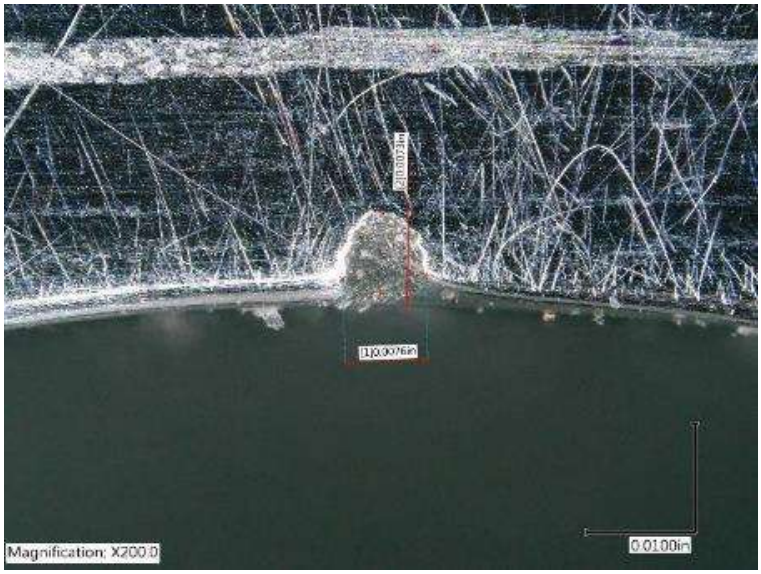

Figure 2.2: Electrical discharge machined (EDM) notch at edge of hole.

Figure 2.3: Specimen identification markings.

Figure 2.4: Servo-hydraulic load frame used for fatigue testing.

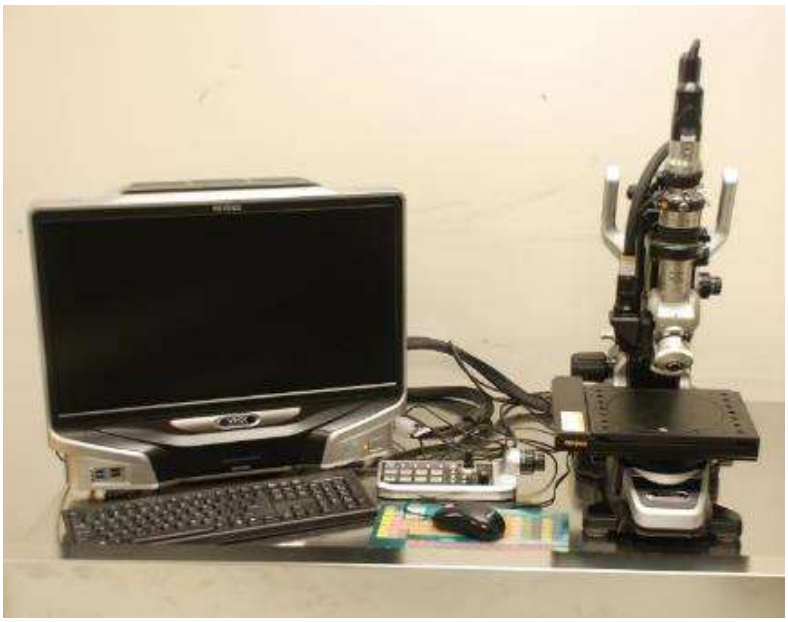

Figure 2.5: Keyence VHX 6000 digital microscope.

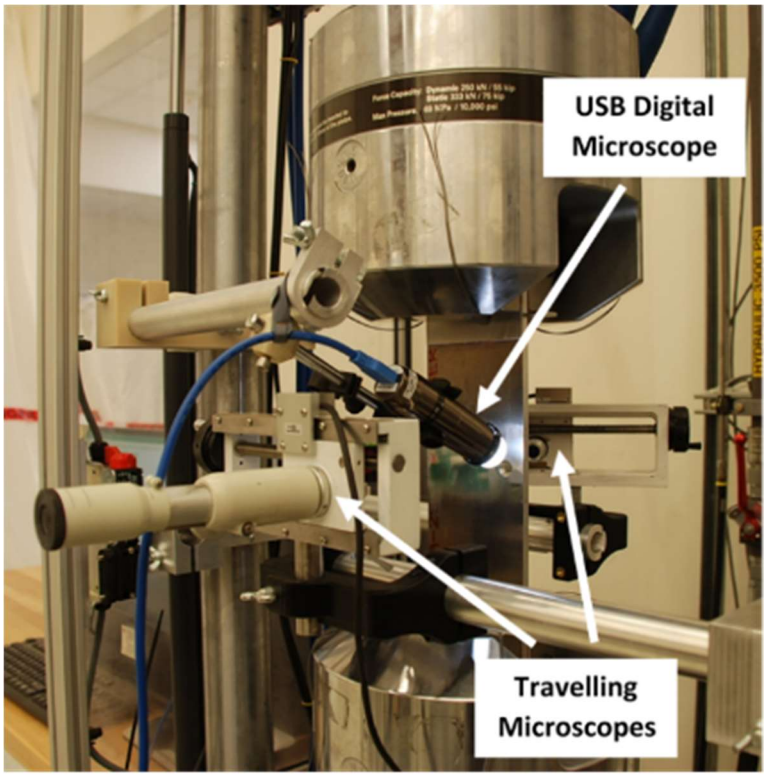

Figure 2.6: Mounting configuration for travelling microscopes and USB digital microscope.

Figure 2.7: Scanning electron microscope.

Figure 2.8: Crack growth image captured with USB digital microscope.

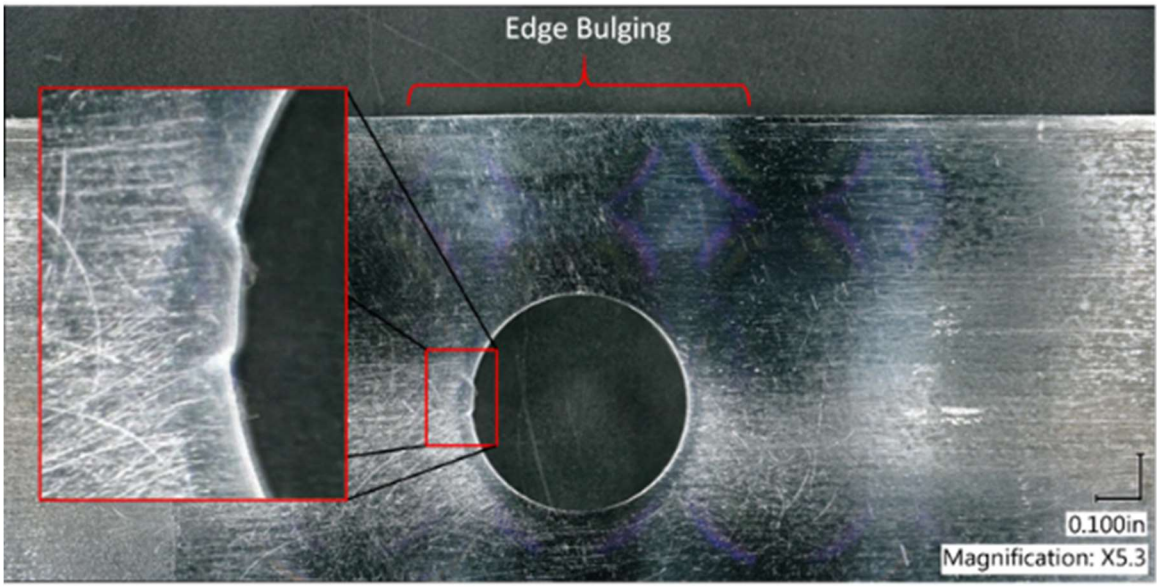

Figure 2.9: Digital microscope image of ridge and slight edge bulging caused by cold expansion.

Table 2.2: Applied and residual expansion values.

Specimen ID	Initial Hole Diameter (in.)	Mandrel Diameter (in.)	Sleeve (in.)	Applied Expansion	Final Hole Diameter (in.)	Residual Expansion
CX130ED-1	0.4741	0.4695	0.0125	4.30%	0.4858	2.47%
CX130ED-2	0.4742	0.4695	0.0125	4.28%	0.4854	2.36%
CX130ED-3	0.4718	0.4695	0.0125	4.81%	0.4859	2.99%
CX140ED-1	0.4732	0.4695	0.0125	4.50%	0.4855	2.60%
CX140ED-2	0.4738	0.4695	0.0125	4.37%	0.4855	2.47%
CX140ED-3	0.4748	0.4695	0.0125	4.15%	0.4864	2.44%
CX150ED-1	0.4735	0.4695	0.0125	4.44%	0.4862	2.68%
CX150ED-2	0.4729	0.4695	0.0125	4.57%	0.4861	2.79%
CX150ED-3	0.4734	0.4695	0.0125	4.46%	0.4860	2.66%
CX200ED-1	0.4740	0.4695	0.0125	4.32%	0.4857	2.47%
CX200ED-2	0.4733	0.4695	0.0125	4.48%	0.4859	2.66%
CX200ED-3	0.4743	0.4695	0.0125	4.26%	0.4859	2.45%

Table 2.3: Amount of edge deformation caused by cold expansion.

Specimen ID	Initial Hole Radius (in.)	e/D	Edge Deformation (in)	Percent of Hole Radius
CX130ED-1	0.2371	1.30	0.0063	2.66%
CX130ED-2	0.2371	1.30	0.0094	3.96%
CX130ED-3	0.2359	1.30	0.0061	2.59%
CX140ED-1	0.2366	1.40	0.0043	1.82%
CX140ED-2	0.2369	1.40	0.0055	2.32%
CX140ED-3	0.2374	1.40	0.0056	2.36%
CX150ED-1	0.2368	1.50	0.0069	2.91%
CX150ED-2	0.2365	1.50	0.0042	1.78%
CX150ED-3	0.2367	1.50	0.0059	2.49%
CX200ED-1	0.2370	2.00	0.0009	0.38%
CX200ED-2	0.2367	2.00	0.0009	0.38%
CX200ED-3	0.2372	2.00	0.0006	0.25%

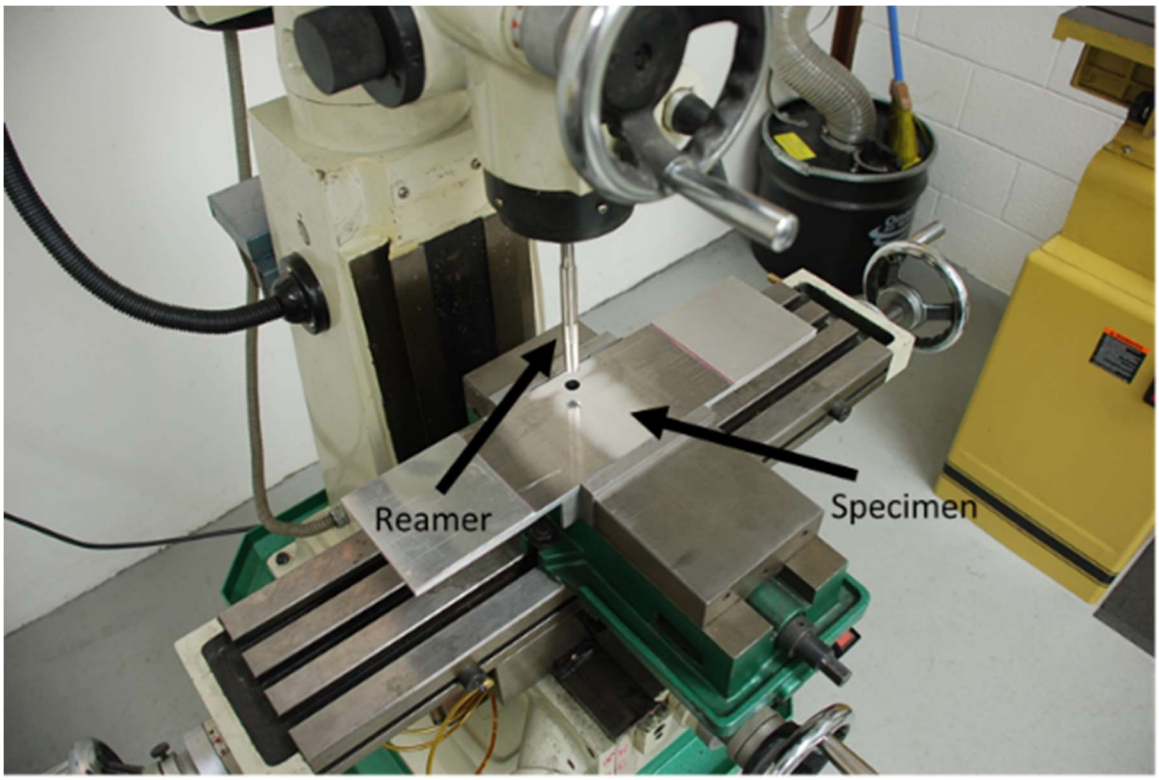

Figure 2.10: Setup used for reaming CX specimens.

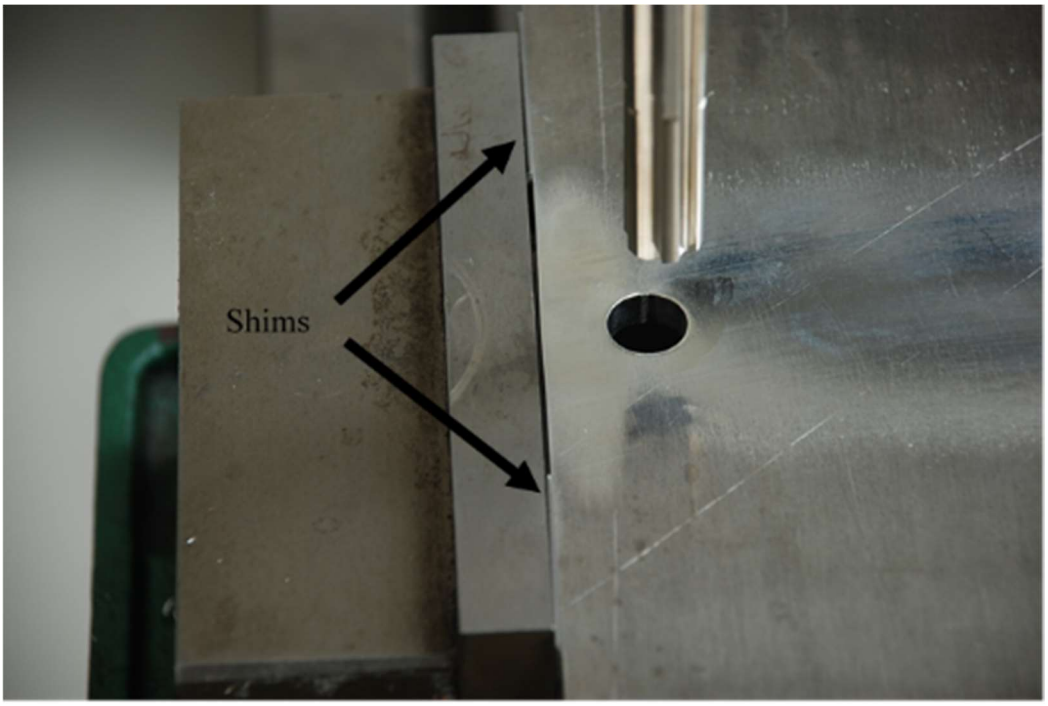

Figure 2.11: Shims used to protect bulged edge of specimen from mill vice.

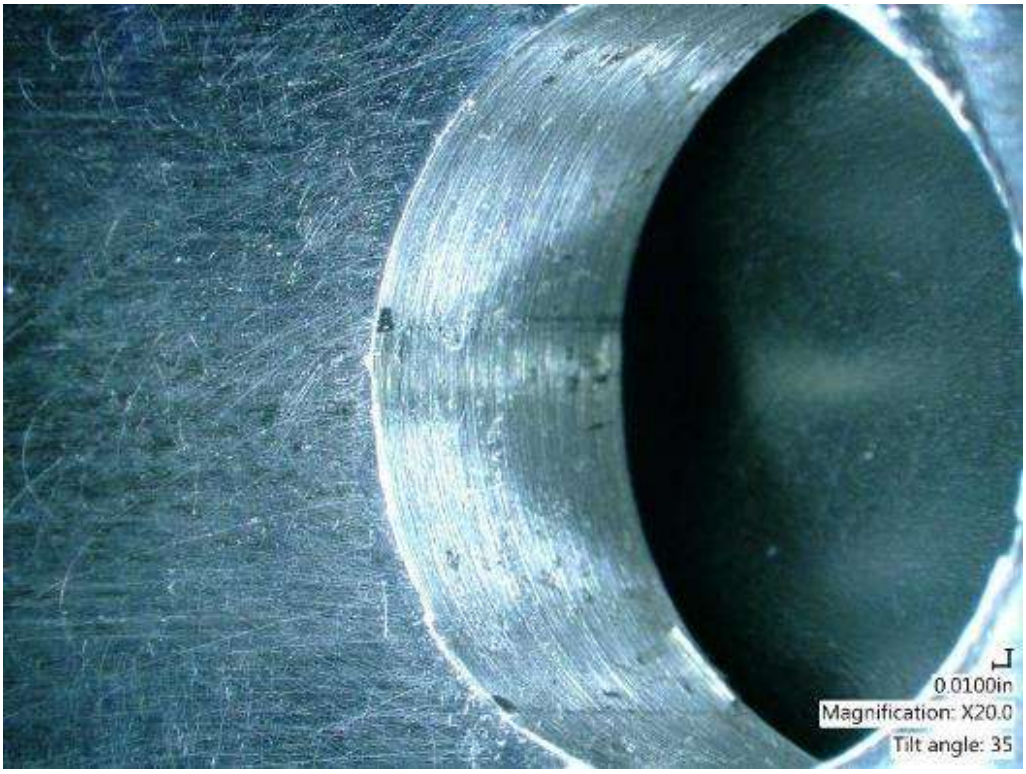

Figure 2.12: Scratches left in bore by reaming process.

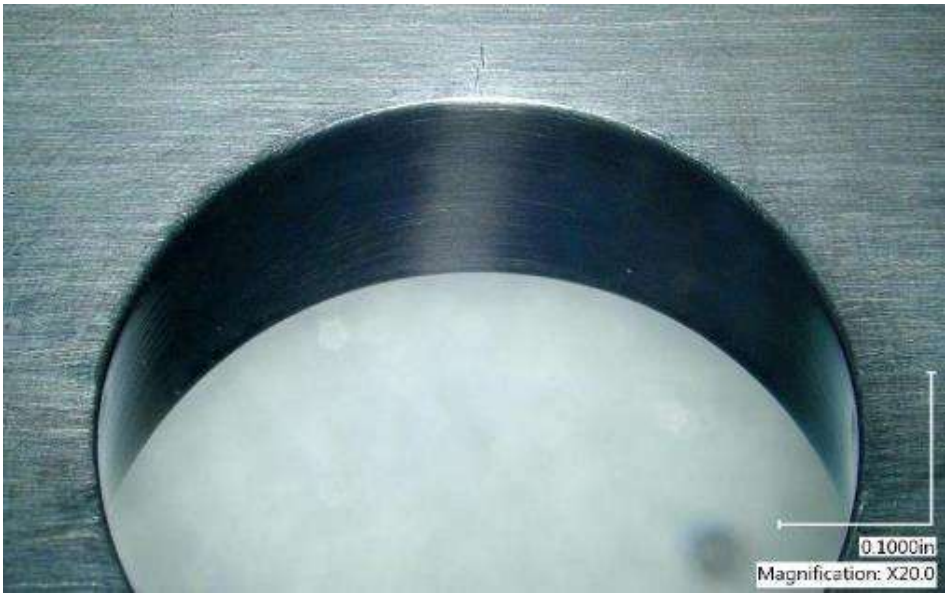

Figure 2.13: Bore appearance after sanding and polishing.

Figure 2.14: Machinist parallel used to align specimen vertically in test machine grips.

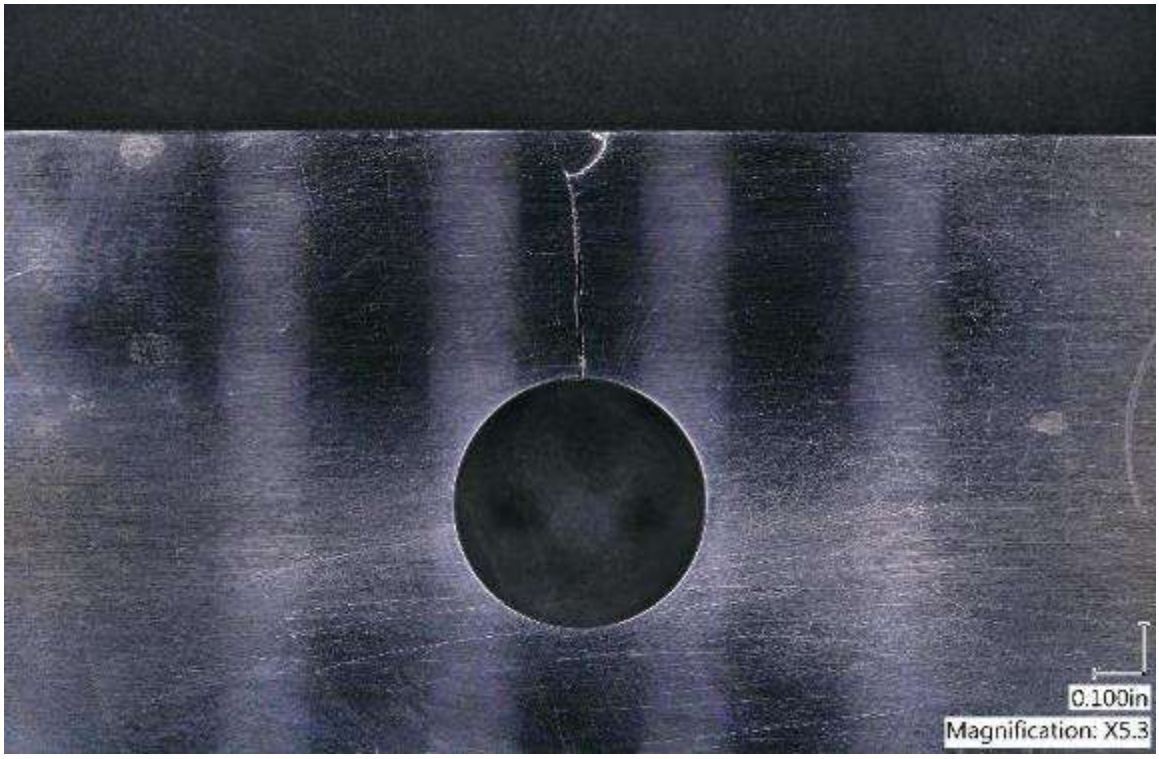

Figure 2.15: Specimen that has undergone ligament failure.

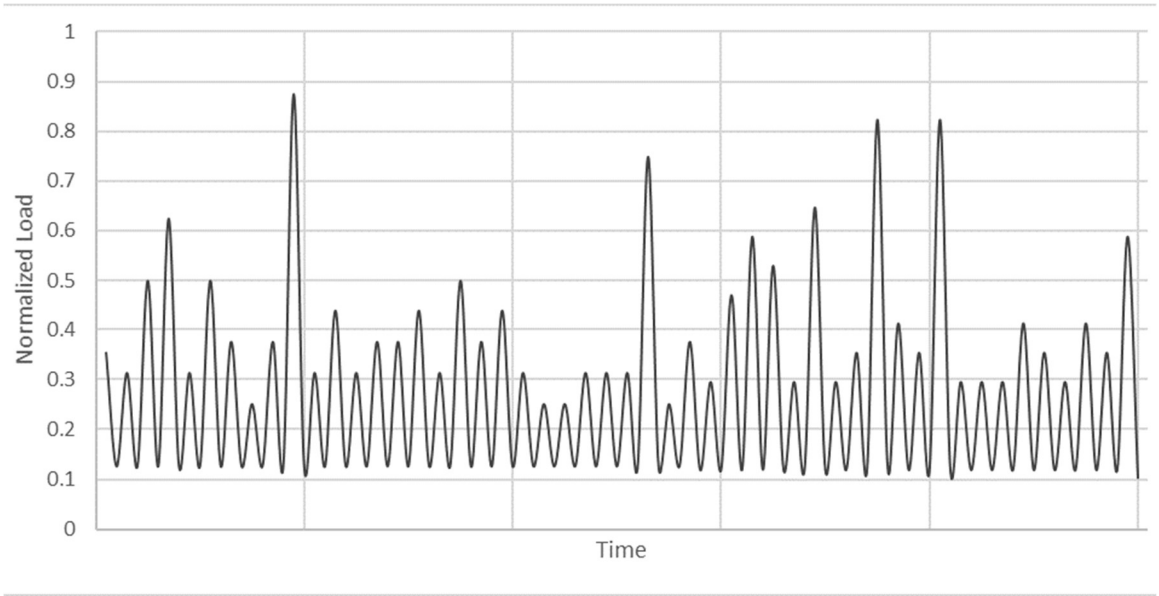

Figure 2.16: Section of normalized fighter aircraft wing root bending spectrum.

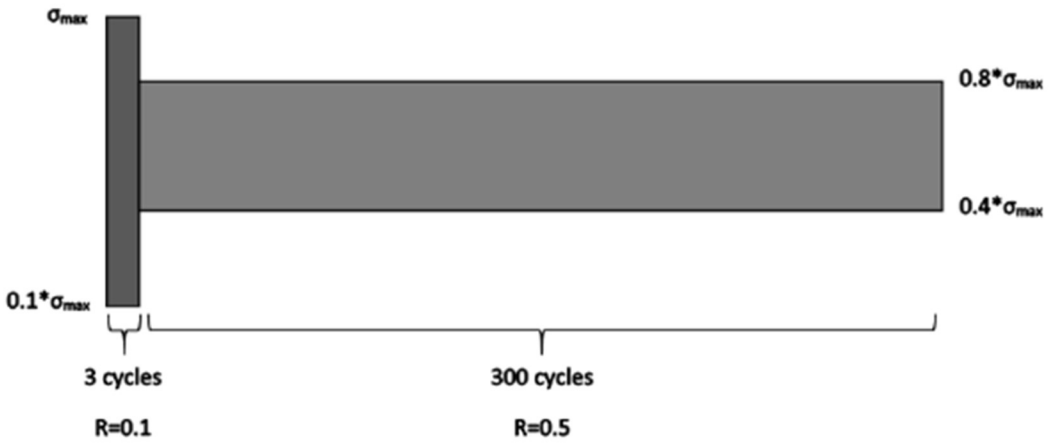

Figure 2.17: Illustration of marker band loading. σ_{max} is 33 ksi.

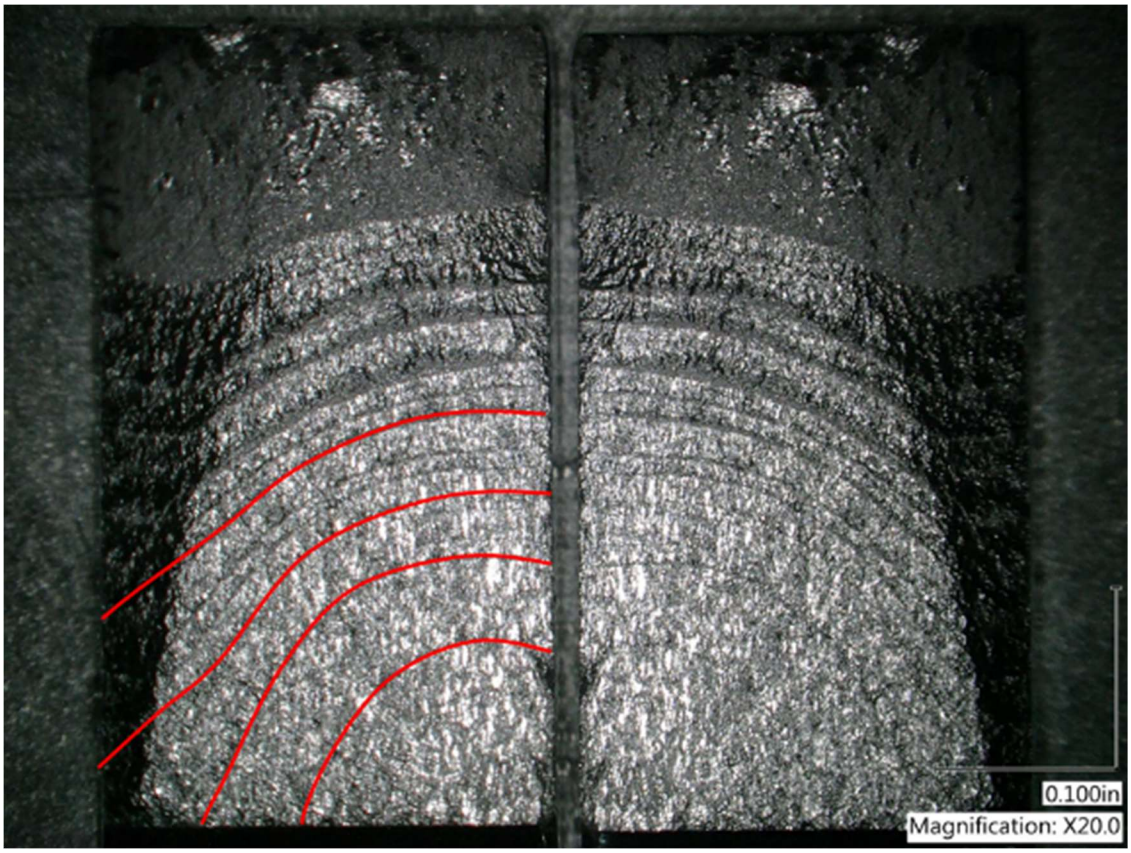

Figure 2.18: Specimen fracture surfaces with marker bands highlighted. Original image taken at 20X Matching fracture surfaces are shown side by side. The crack originated from the bottom center of the image and propagated upward and outward.

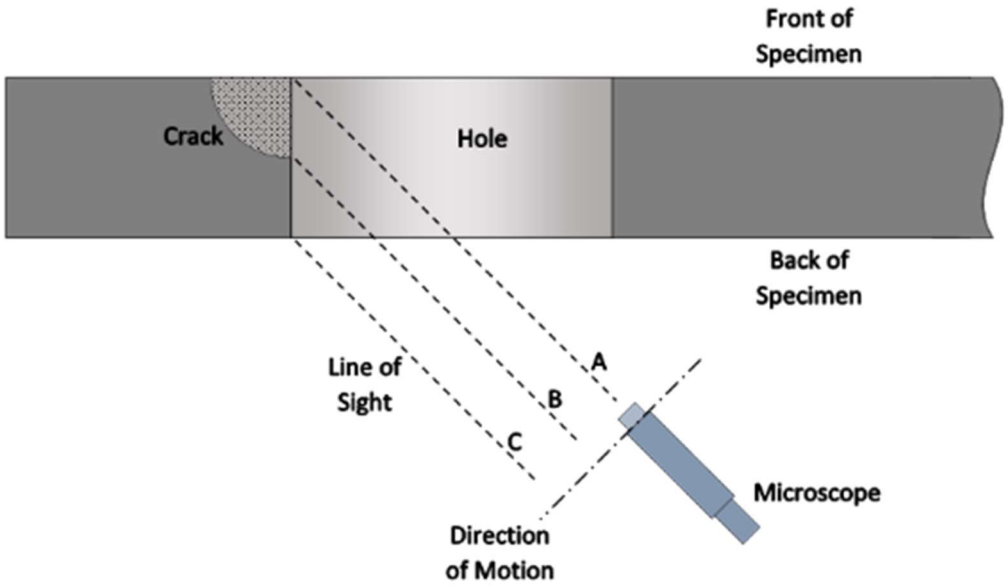

Figure 2.19: Illustration of bore crack measurement procedure.

Figure 2.20: Travelling microscope orientation for measuring bore crack length.

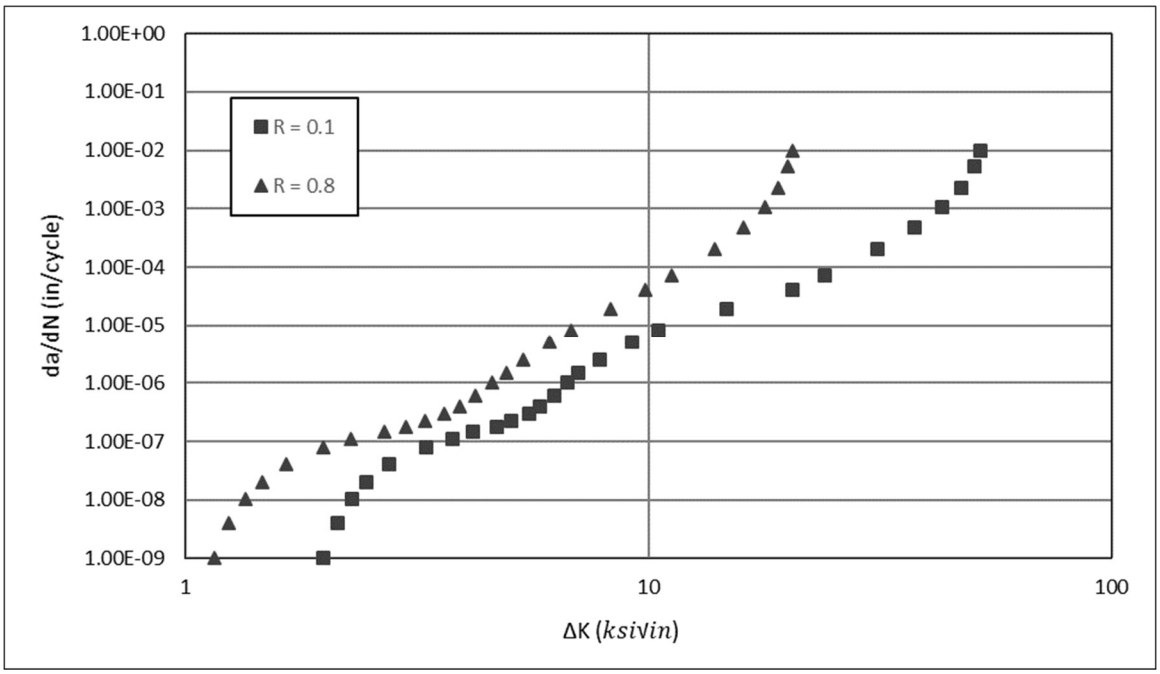

Figure 2.21: da/dN versus dK curve developed through ASTM E 647 testing by Andrew and Warner for 2024-T351 aluminum alloy. The specimens used in this research are from the same material lot as the specimens that generated the data shown.

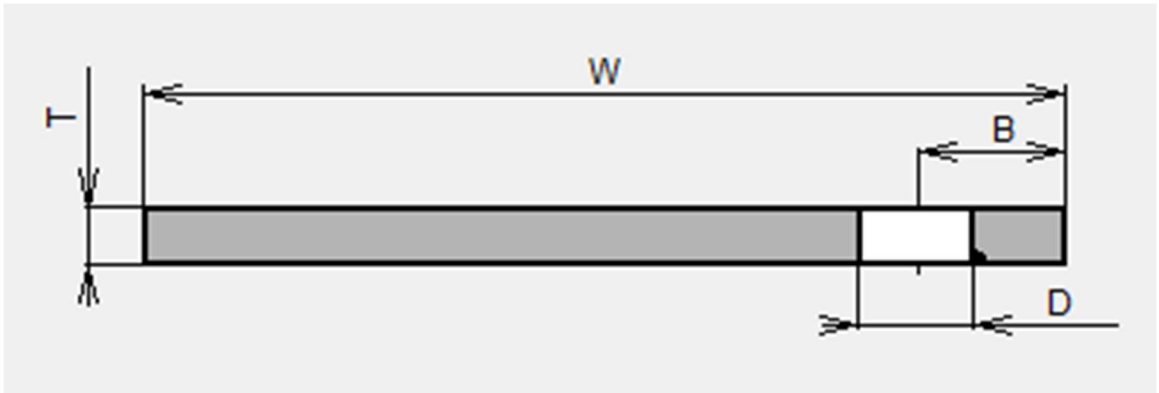

Figure 2.22: AFGROW Single Corner Crack at Hole model used for all simulations.

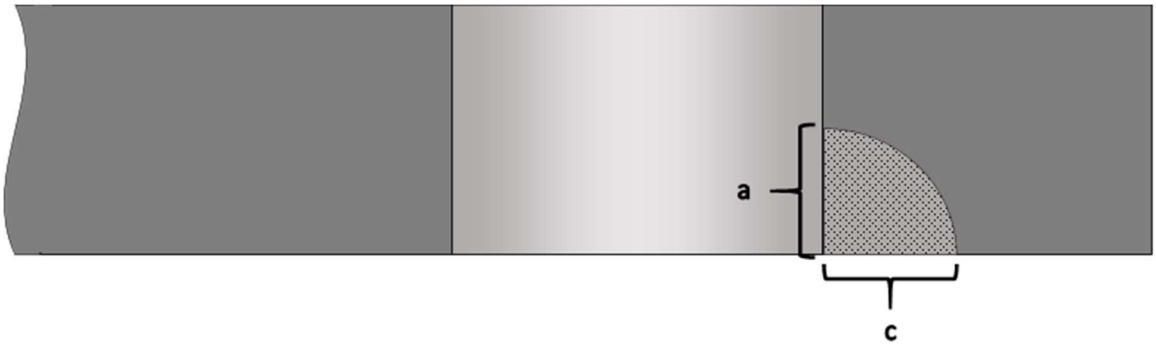

Figure 2.23: Definition of crack size parameters.

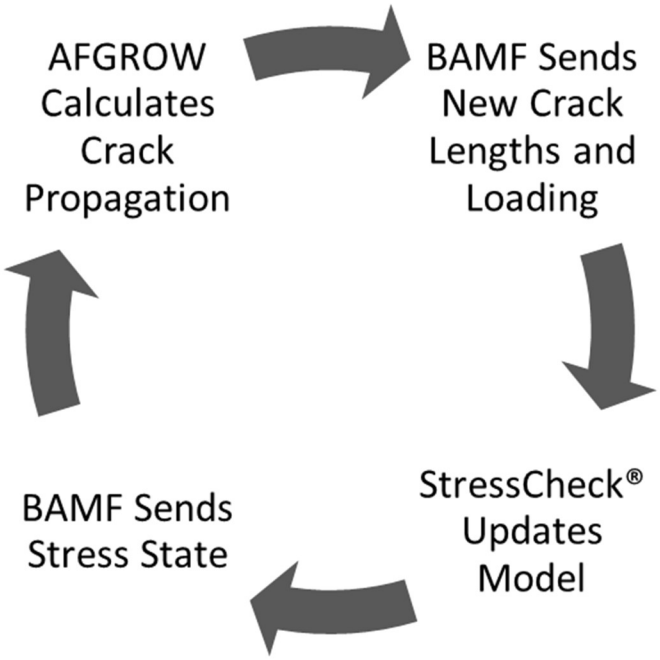

Figure 2.24: Data flow during BAMF analysis.

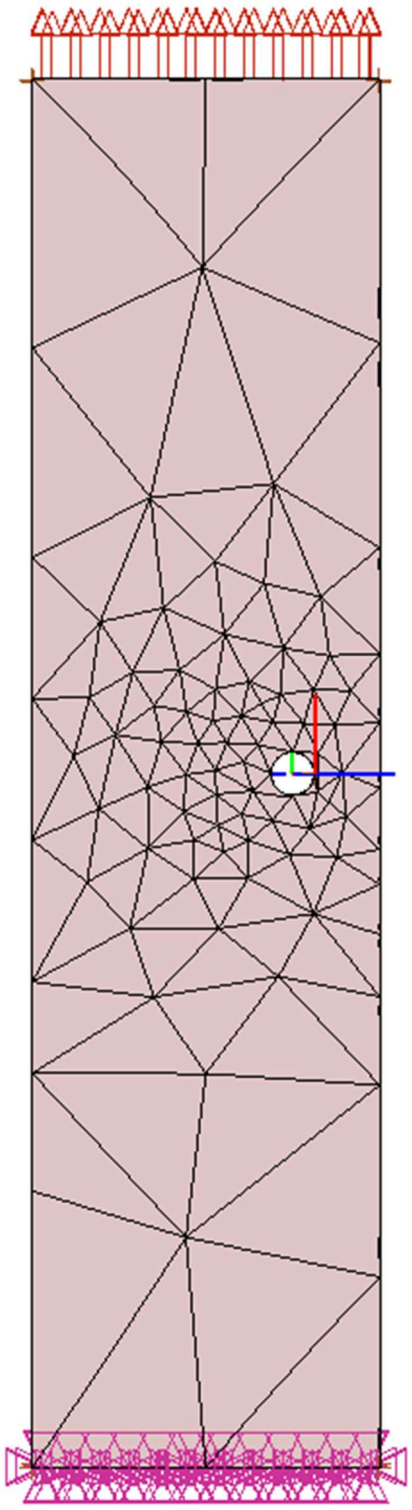

Figure 2.25: Finite element model showing mesh, constraints on the bottom surface, and loading on the top surface.

3 RESULTS

3.1 Experiment Summary

Fatigue testing was completed on 20 short e/D 2024-T351 aluminum alloy specimens. Four different edge margins were tested in this research: 1.3, 1.4, 1.5, and 2.0. Five specimens were dedicated to testing each edge margin. Two of the five specimens were not cold expanded and were used to create a baseline of fatigue life. The remaining three specimens of each e/D were cold expanded according to FTI Process Specification 8101D [17]. Each specimen was fatigue precracked from an EDM notch at the corner of the hole prior to cold expansion (if applicable). All specimens were tested under a fighter aircraft wing root bending spectrum with 33 ksi maximum stress. A summary of all completed testing is shown in Table 3.1. Because each loading block of the test spectrum represents 240 hours of aircraft flight, the cycle count provided by the fatigue test machine was converted to flight hours using (3.1).

$$Flight\ Hours = \frac{Current\ Cycles \times 240\,\frac{hou}{block}}{7{,}368\,\frac{cycles}{block}} \tag{3.1}$$

where a cycle is defined as two load reversals, one maximum and one minimum.

3.1.1 Applied Force Validation

The test software captured data from each cycle of every test. These data included force command, applied force, displacement, cycle count, and current time. The intended load for a given cycle is referred to as the force command. Based on feedback signal

accuracy, loading rate, and other factors, the actual force applied may differ from the force command. Force data from testing were analyzed to verify that the applied force was acceptably close to the force command. The largest observed loading error, as defined by (3.2), was approximately 0.25 kip, or 0.76% of maximum load.

$$Loading\ Error = \ Applied\ Force - Force\ Command \tag{3.2}$$

This was determined to have a negligible effect on specimen life. A histogram showing the distribution of loading error is shown in Figure 3.1. It shows a bimodal distribution that, upon further inspection, is due to the error incurred at the maximum and minimum of each loading cycle. The error tended to be negative at load maxima, meaning the actual force was lower than the force command, and positive at load minima. Because negative error occurred at load maxima, it can be assumed that overloads did not produce undesirable crack growth retardation effects.

3.2 Crack Growth Datasheets

A crack growth datasheet was created for each specimen during testing. Figure 3.2 shows a typical datasheet. The crack length measured on each face of the specimen was recorded along with the current cycle count of the test. The cycle count was later converted to flight hours. Note that each crack originated on the front face of the specimen and grew through-thickness (down the bore of the hole) and toward the edge of the specimen. Once the crack propagated through-thickness, data were no longer gathered for the bore of the hole. Instead, data from back surface crack measurements were collected. An example of the resulting data are shown graphically in Figure 3.3. In the following sections, the crack growth will be represented by only the crack growth on the

front face of the specimen for legibility. All crack growth data sheets are included in Appendix D.

3.3 Test Results

The fatigue crack growth of all noncold-expanded specimens is shown in Figure 3.4, and the fatigue crack growth of cold-expanded specimens is shown in Figure 3.5. The fatigue life measured for each e/D is shown in Table 3.2, and the LIF for each e/D based on the test results is also shown. The LIF decreases rapidly with decreasing e/D, as shown in Figure 3.6.

3.3.1 Edge Margin of 1.3

The fatigue crack growth of all 1.3 e/D specimens is shown in Figure 3.7. The average fatigue life of noncold-expanded specimens was 3,592 flight hours, and the average fatigue life of cold-expanded specimens was 12,365 flight hours. This resulted in a LIF of 3.44.

3.3.2 Edge Margin of 1.4

The fatigue crack growth of all 1.4 e/D specimens is shown in Figure 3.8. The average fatigue life of noncold-expanded specimens was 4,252 flight hours, and the average fatigue life of cold-expanded specimens was 18,304 flight hours. This resulted in a LIF of 4.30.

3.3.3 Edge Margin of 1.5

The fatigue crack growth of all 1.5 e/D specimens is shown in Figure 3.9. The average fatigue life of noncold-expanded specimens was 4,989 flight hours, and the average fatigue life of cold-expanded specimens was 21,894 flight hours. This resulted in a LIF of 4.39.

3.3.4 Edge Margin of 2.0

The fatigue crack growth of all 2.0 e/D specimens is shown in Figure 3.10. The average fatigue life of noncold-expanded specimens was 7,680 flight hours, and the average fatigue life of cold-expanded specimens was 63,139 flight hours. This resulted in a LIF of 8.22.

3.4 Simulation Results

3.4.1 AFGROW Predictions

AFGROW predictions of each NCX specimen were compared to test data to determine proper SOLR values. The mean of all SOLR values was used to produce 0.05 and 0.005 inch IFS predictions for each e/D, representing the minimum detectable flaw size for bolt hole eddy current inspection and the IFS benefit for cold expansion, respectively. Table 3.3 shows SOLR values determined for each specimen and e/D, the average SOLR, percent disagreement between a 0.05 inch IFS prediction and test results, and the LIF between a 0.05 and 0.005 inch IFS predicted life. The average disagreement between the 0.05 inch IFS predictions and test data was -5.7%. The variation in SOLR values between specimens of the same e/D is simply caused by variation in the test

fatigue life from which they were derived. The average LIF between 0.05 and 0.005 inch IFS predictions was 3.69. Figure 3.11 shows 0.05 inch IFS predictions with NCX test data, and Figure 3.12 shows 0.005 IFS prediction results with CX test data. The correlation ratio, defined in (3.3), was used to evaluate the conservatism of 0.005 IFS predictions compared to test results.

$$Correlation\ Ratio = \frac{Test\ Life}{Predicted\ Life} \tag{3.3}$$

A correlation ratio equal to one indicates that the predicted fatigue life matches test results perfectly. Unconservative predictions result in a value less than one, while conservative predictions are greater than one. The correlation ratios calculated for each e/D are shown in Table 3.4.

3.4.2 BAMF Predictions

Several BAMF predictions were performed using both CX and NCX data. All predictions of CX crack growth behavior utilized the residual stress data gathered by Hill Engineering, LLC [33]. Each prediction used 11 points to define the crack front, allowing the shape to vary naturally as the crack grows. This produces more accurate predictions due to the more accurate crack shape. Figure 3.13 shows a sample fracture surface with an overlay of the crack front progression predicted by BAMF for the same NCX specimen. The prediction is nearly identical to test results. A similar overlay comparison of the produced CX crack shape is shown in Figure 3.14. The BAMF prediction varies from the crack front shape observed.

One set of predictions was based solely on residual stress and did not account for crack growth retardation. The resulting crack growth curves are shown alongside

experimental CX data in Figure 3.15. The correlation ratio between test data and predictions with no retardation were calculated and are shown in Table 3.5. The correlation ratio was greater than one for all e/D with an average of 1.833. Subsequently, SOLR values were adjusted such that the BAMF predictions matched the average experimental life of each e/D. The resulting SOLR values were averaged and used as the SOLR for further predictions. For NCX specimens the resulting predictions, summarized in Table 3.6, showed high agreement with test results, with average percent difference of 0.6. CX predictions are summarized in Table 3.7. The predictions for NCX specimens and CX specimens are shown with test data in Figure 3.16 and Figure 3.17, respectively. These SOLR-tuned BAMF predictions represent the most accurate prediction of crack growth behavior addressed in this research. The LIF between NCX and CX BAMF predictions was calculated as 3.51, 4.53, 4.51, and 7.49 for e/D of 1.3, 1.4, 1.5, and 2.0, respectively.

3.5 Fractographic Results

Fractography was performed on selected specimens to observe crack front and fracture surface morphology. Figure 3.18 shows a sample from this research, which exhibits the slightly "P" shaped crack front described by Carlson in his research of cold-expanded holes in 2024-T351 aluminum alloy [20]. Figure 3.19 shows an SEM image of fatigue striations caused by spectrum loading visible at 500X magnification. Figure 3.20 shows an 8,000X magnification SEM image of fatigue striations formed during constant amplitude precracking of the same specimen at a maximum stress of 14.4 ksi and stress ratio of 0.1. By comparison, the striations in the spectrum loading region are more

prominent and spaced further apart than the striations in the constant amplitude precracking region, indicating increased crack growth rate. Figure 3.21 shows an SEM image of a fracture surface at the point of transition from fatigue crack growth to fast fracture.

3.6 Crack Closure Data

Crack closure is a mechanism which is believed to contribute to the fatigue life extension caused by cold expansion. The force required to cause a crack to open fully is a point of interest for understanding this mechanism. Images were captured using a Dino-Lite digital microscope at varying stress levels at different points in the fatigue life, which may provide information about this mechanism.

Table 3.8 shows the stress required to open the crack in the test specimen at varying e/D and crack length. Note that crack length measurements were not available for the time the images were captured, so the crack lengths given were found by interpolation and are approximate. Additionally, the images were captured at stress increments of 3.3 ksi (10% of max stress), and the stress level given corresponds to the first image which appeared to show crack opening. Appendix E shows a set of these images for each e/D.

Table 3.1: Summary of tests performed.

Specimen ID	Edge Margin (e/D)	Applied Cold Expansion	Loading Type	Maximum Load (ksi)	Test Date	Initial Surface Crack Length (in)	Initial Bore Crack Length (in)	Cycles to Ligament Failure	Flight Hours to Ligament Failure
NCX130ED-1	1.285	N/A	Spectrum	33	26-Dec-18	0.04170	0.05594	97090	3130
NCX130ED-2	1.297	N/A	Spectrum	33	14-Jan-19	0.04296	0.04566	123473	3981
CX130ED-1	1.289	4.30%	Spectrum	33	9-Feb-19	0.04616	0.04971	357593	11616
CX130ED-2	1.292	4.28%	Spectrum	33	8-Mar-19	0.04582	0.05015	382526	12426
CX130ED-3	1.294	4.81%	Spectrum	33	27-Mar-19	0.04838	0.05179	398703	12952
NCX140ED-1	1.396	N/A	Spectrum	33	19-Dec-18	0.03592	0.04394	129486	4175
NCX140ED-2	1.397	N/A	Spectrum	33	11-Jan-19	0.03934	0.05021	131627	4244
CX140ED-1	1.396	4.50%	Spectrum	33	6-Feb-19	0.04298	0.04718	634041	20597
CX140ED-2	1.389	4.37%	Spectrum	33	4-Mar-19	0.04452	0.03957	536913	17441
CX140ED-3	1.394	4.15%	Spectrum	33	25-Mar-19	0.04438	0.04847	514808	16723
NCX150ED-1	1.490	N/A	Spectrum	33	17-Dec-18	0.04084	0.05278	146421	4721
NCX150ED-2	1.489	N/A	Spectrum	33	8-Jan-19	0.03684	0.05508	159915	5156
CX150ED-1	1.494	4.44%	Spectrum	33	31-Jan-19	0.04630	0.05646	690053	22416
CX150ED-2	1.503	4.57%	Spectrum	33	25-Feb-19	0.04328	0.05667	677509	22009
CX150ED-3	1.494	4.46%	Spectrum	33	23-Mar-19	0.04780	0.06788	648834	21077
NCX200ED-1	1.994	N/A	Spectrum	33	6-Dec-18	0.04440	0.04106	235873	7605
NCX200ED-2	1.990	N/A	Spectrum	33	27-Dec-18	0.03930	0.05704	235708	7600
CX200ED-1	1.997	4.32%	Spectrum	33	18-Jan-19	0.04790	0.05428	1655081	53765
CX200ED-2	1.994	4.48%	Spectrum	33	25-Jan-19	0.04318	0.04746	2029311	65921
CX200ED-3	1.993	4.26%	Spectrum	33	18-Mar-19	0.04294	0.05523	2130697	69215

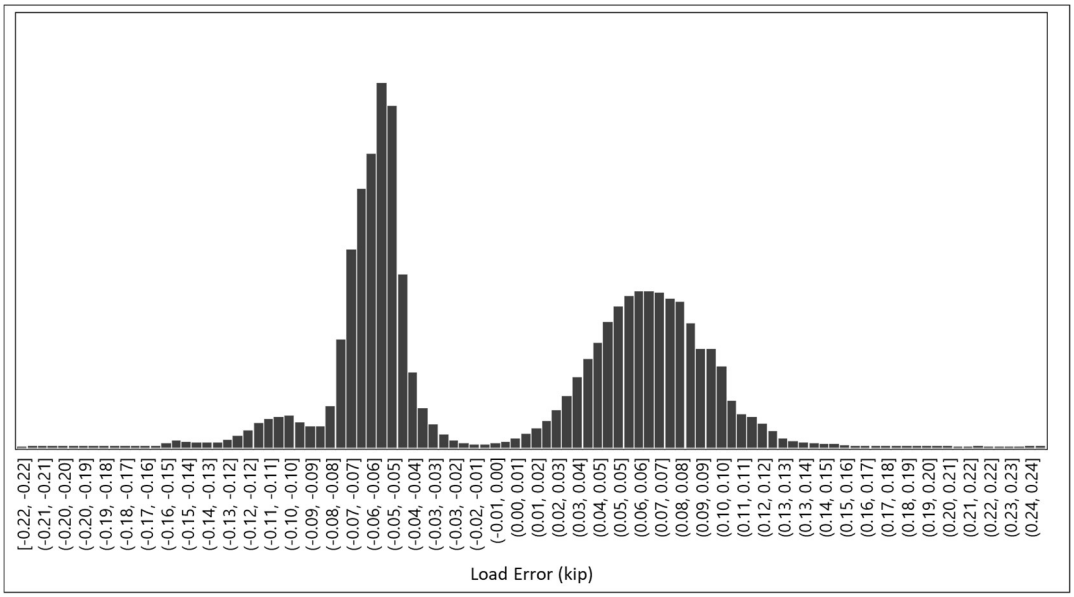

Figure 3.1: Loading error distribution showing bimodal shape. Positive errors occurred more often at load minima and negative errors tended to occur at load maxima. This indicates that unintentional overloading did not occur.

NCX130ED-1 Crack Growth Datasheet

Test Date: 12/26/2018 10:10:47 AM **Width (in): 4.0025**

Max Stress (ksi): 33 **Thickness (in): 0.2529**

Loading Rate (kip/sec): 165 **Area (in^2): 1.012**

Hole Diameter (in): 0.5047 **Ligament Length (in): 0.3963**

Flight Hours	Crack Length (inches)			Comments
	Front Surface	Back Surface	Bore	
0.00	0.04170		0.05594	
237.57	0.05876		0.07130	
475.13	0.06672		0.08383	
950.26	0.08210		0.11264	
1435.10	0.10276		0.13511	
1910.23	0.12724		0.17129	
2157.47	0.15302		0.19594	
2395.03	0.17576	0.00000	0.23117	
2513.82	0.18912	0.02812	0.25290	Through Thickness
2632.60	0.20858	0.07588		
2870.17	0.24472	0.15762		
2998.65	0.28386	0.23168		
3117.44	0.35930	0.31262		
3130.46	0.39630	0.39630		Ligament Failure

Figure 3.2: Typical noncold-expanded crack growth datasheet: NCX130ED-1, wing root bending spectrum, and 33ksi max stress.

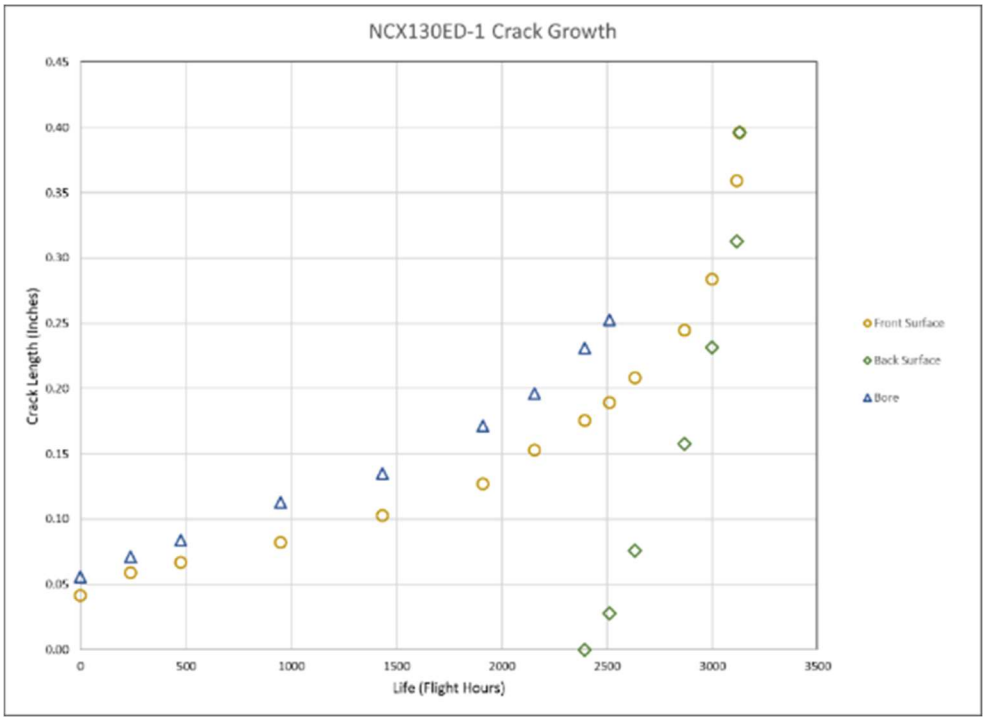

Figure 3.3: Typical noncold-expanded crack growth curve: NCX130ED-1, wing root bending spectrum, and 33ksi max stress.

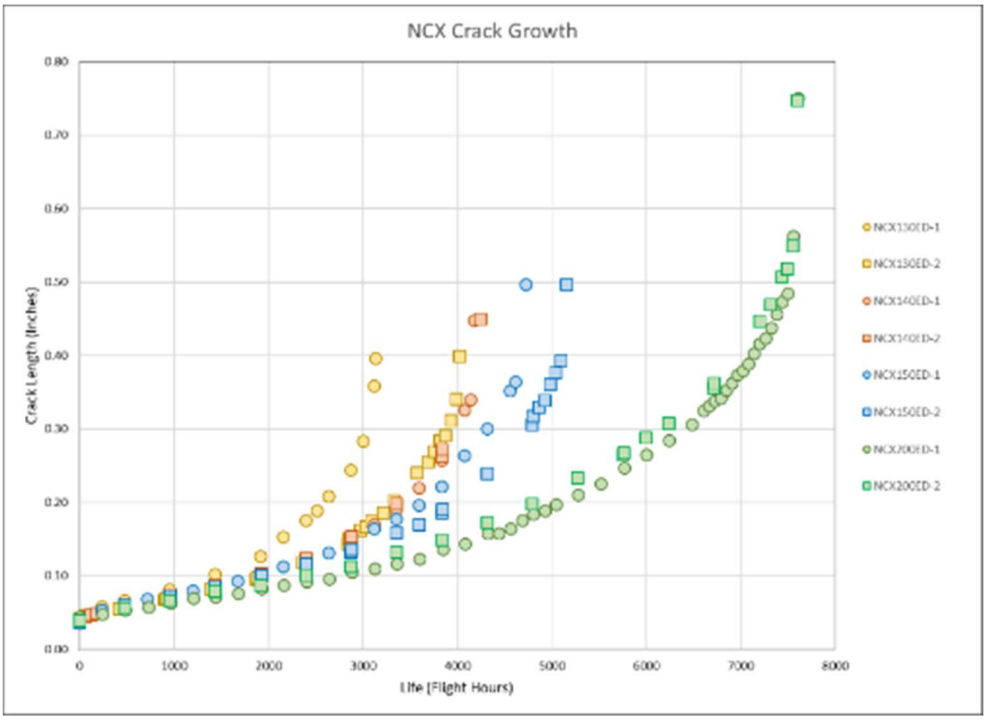

Figure 3.4: Crack growth curves of all NCX test specimens.

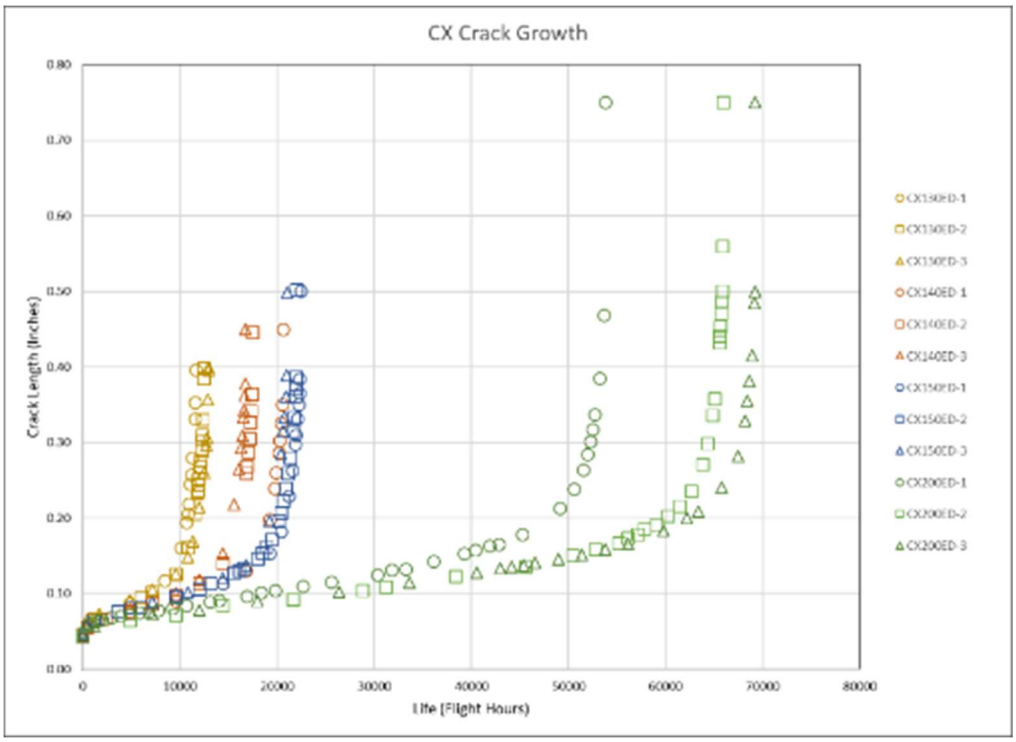

Figure 3.5: Crack growth curves of all CX test specimens.

Table 3.2: Test life improvement factor.

e/D	Average NCX Life (Flight Hours)	Average CX Life (Flight Hours)	LIF
1.3	3592.2	12365.1	3.44
1.4	4252.7	18303.6	4.30
1.5	4989.2	21893.6	4.39
2	7680.5	63138.9	8.22

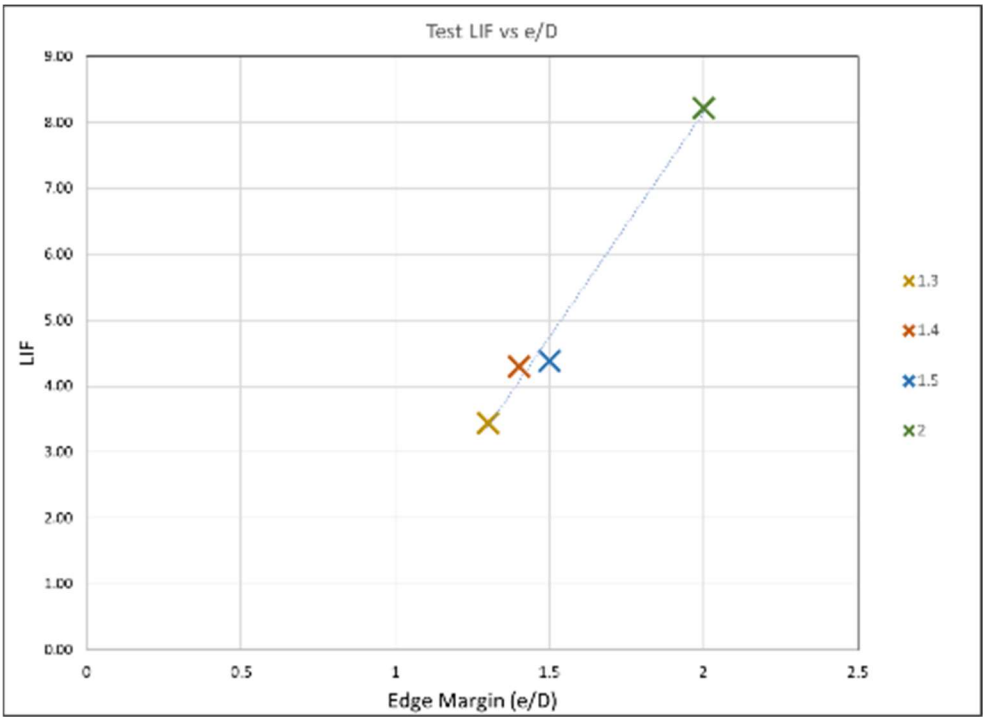

Figure 3.6: LIF versus e/D for test data. LIF decreases with decreasing e/D.

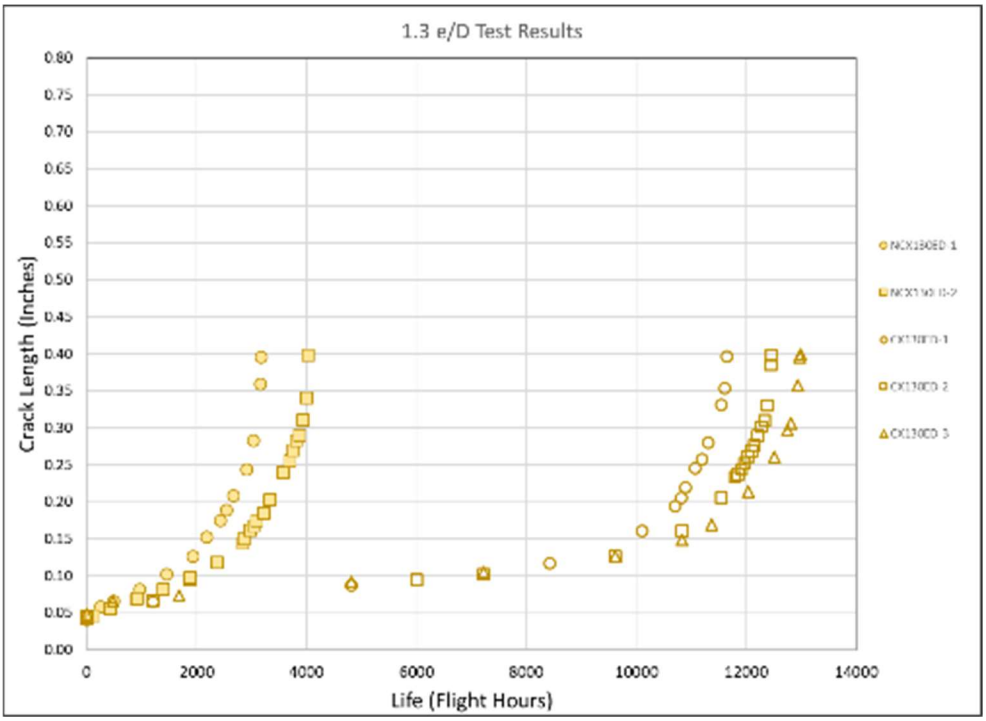

Figure 3.7: Fatigue crack growth data from all 1.3 e/D tests. The resulting LIF was 3.44.

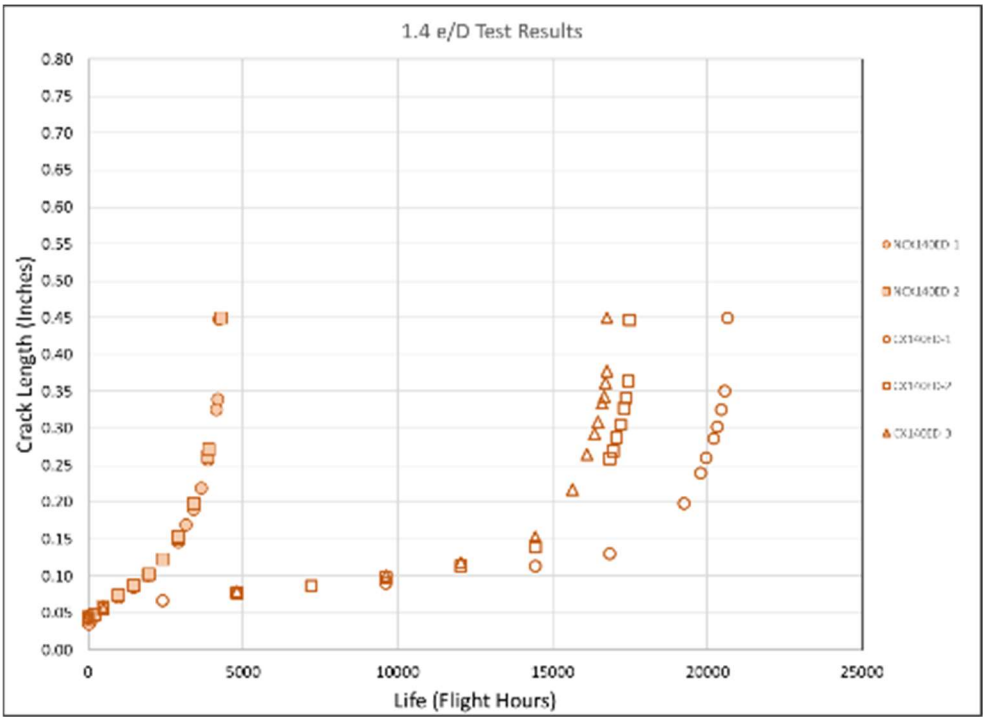

Figure 3.8: Fatigue crack growth data from all 1.4 e/D tests. The resulting LIF was 4.30.

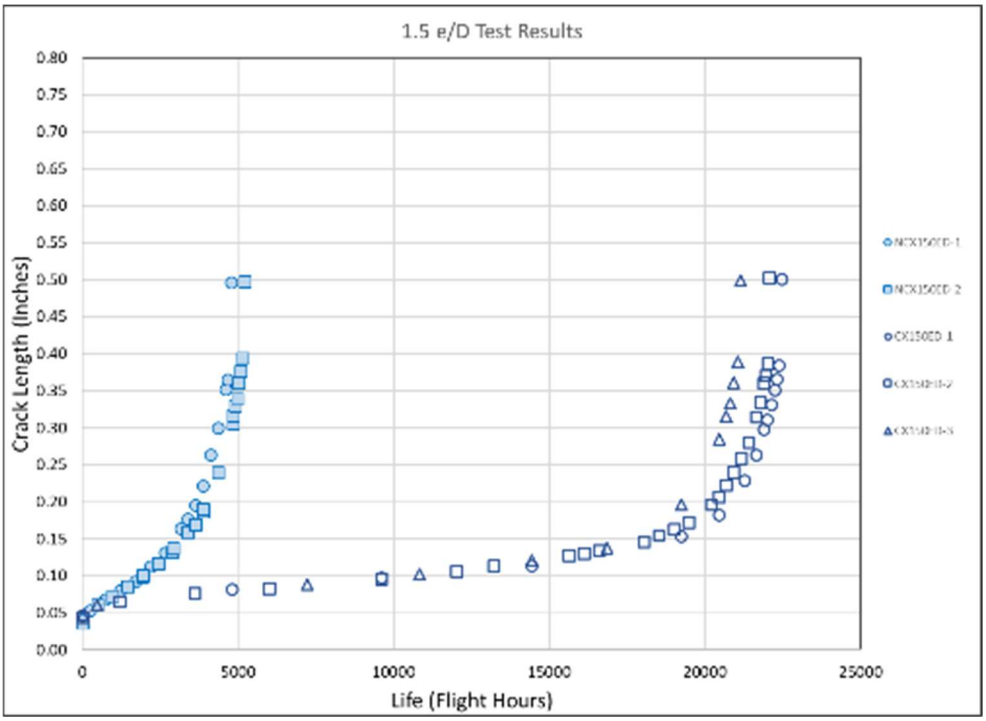

Figure 3.9: Fatigue crack growth data from all 1.5 e/D tests. The resulting LIF was 4.39.

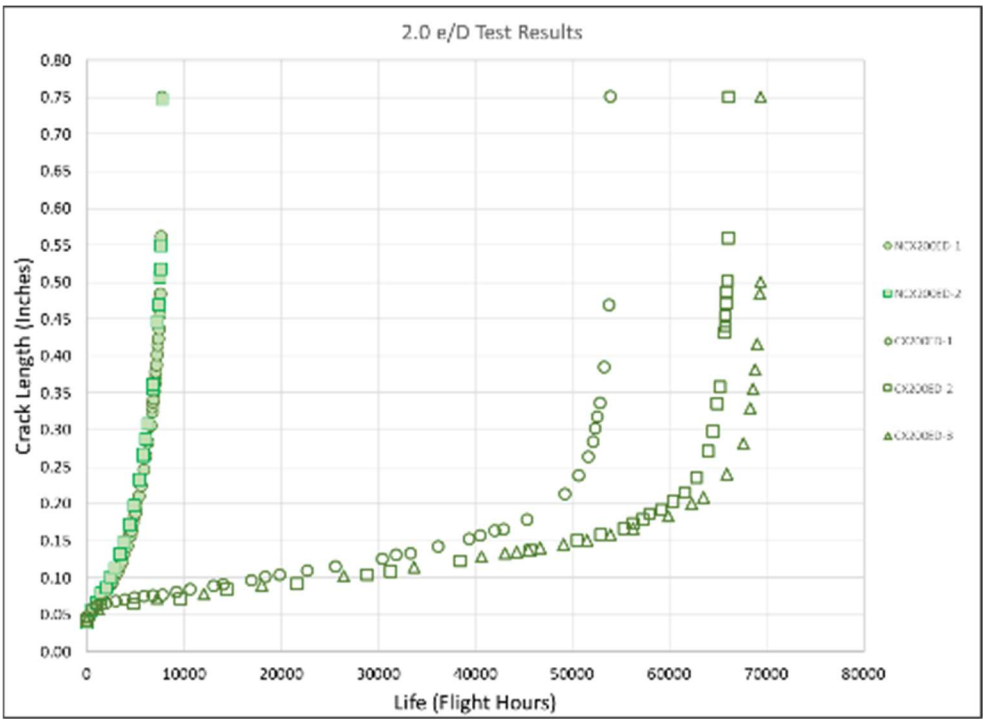

Figure 3.10: Fatigue crack growth data from all 2.0 e/D tests. The resulting LIF was 8.22.

Table 3.3: AFGROW prediction parameters and results.

Specimen ID	SOLR	Average SOLR	0.05 inch IFS Life (Flight Hours)	Difference From Test	Average Difference	0.005 inch IFS Life (Flight Hours)	0.05/0.005 IFS Prediction LIF	Average LIF
NCX130ED-1	1.979	1.865	3864.10	7.6%	-5.7%	15047.85	3.89	3.69
NCX130ED-2	1.8695							
NCX140ED-1	1.937		4160.16	-2.2%		16002.41	3.85	
NCX140ED-2	1.886							
NCX150ED-1	1.86		4563.49	-8.5%		16966.16	3.72	
NCX150ED-2	1.819							
NCX200ED-1	1.799		6167.65	-19.7%		20415.15	3.31	
NCX200ED-2	1.772							

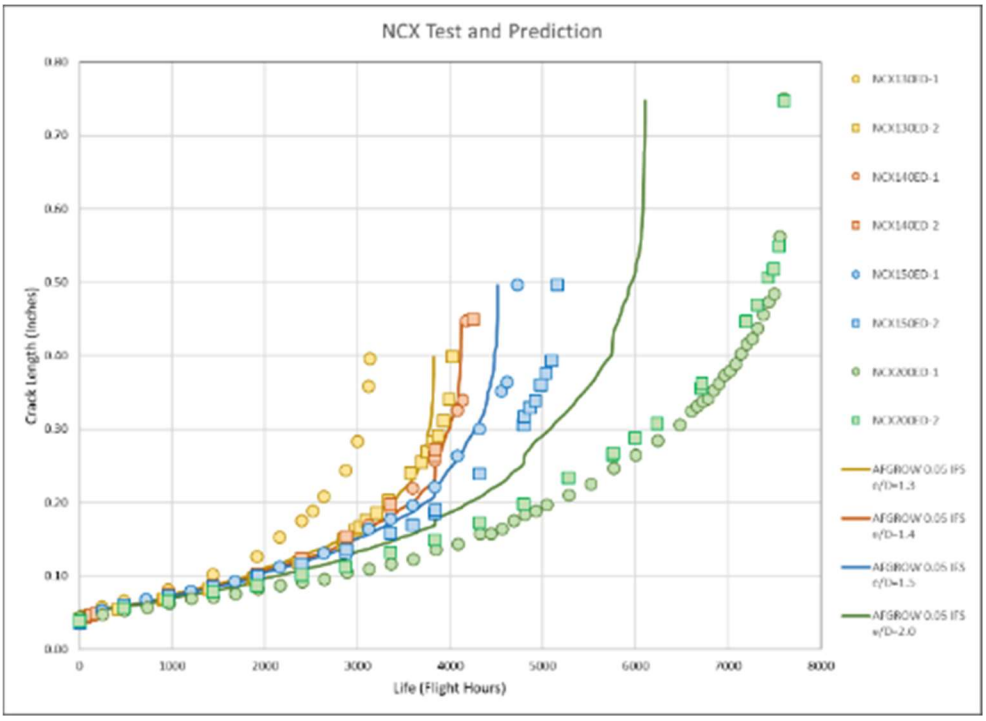

Figure 3.11: Plot comparing NCX test data with the derived 0.05 inch IFS AFGROW predictions.

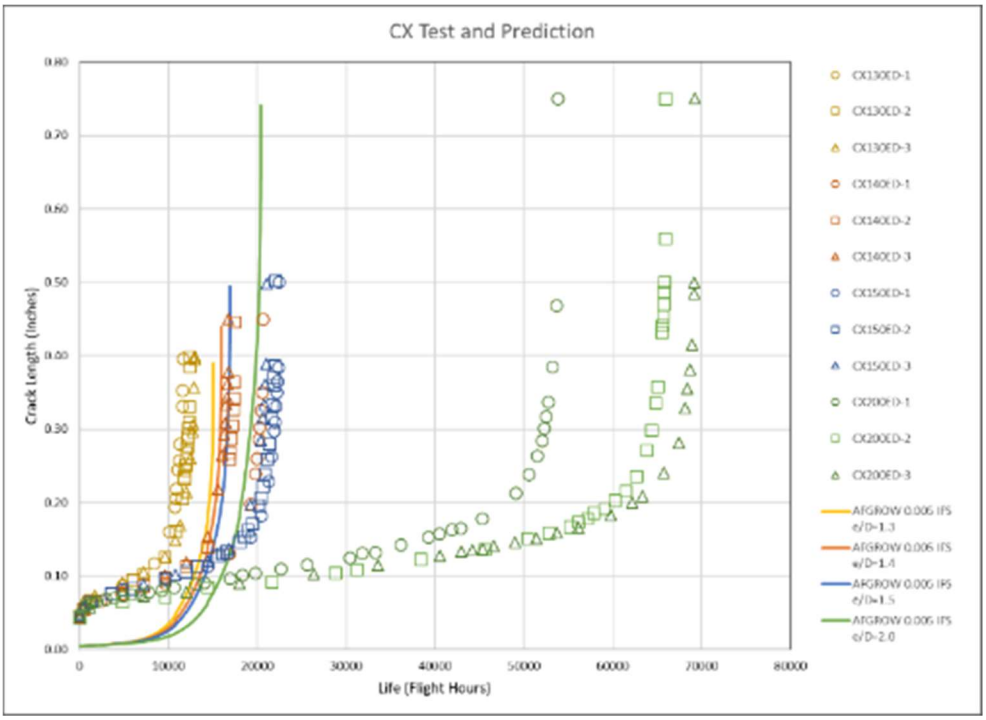

Figure 3.12: Plot comparing CX test data with 0.005 inch IFS AFGROW predictions.

Table 3.4: Correlation ratio between test and 0.005 IFS AFGROW predictions for each e/D.

e/D	Average CX Life (Flight Hours)	0.005 inch IFS Life (Flight Hours)	Correlation Ratio
1.3	12054.06	15047.85	0.80
1.4	19070.91	16002.41	1.19
1.5	22273.00	16966.16	1.31
2.0	60006.38	20415.15	2.94

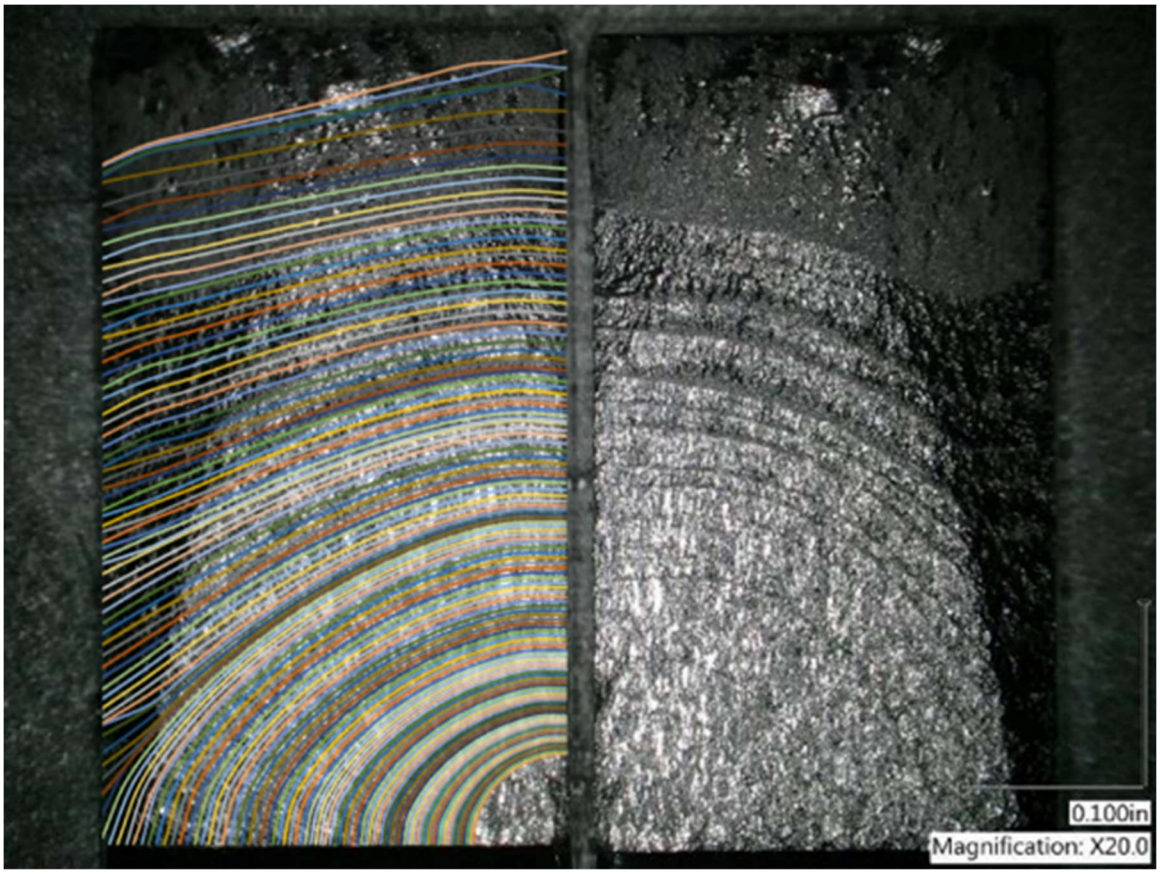

Figure 3.13: NCX140ED-1 fracture surface with overlay of crack progression predicted by BAMF. Mating fracture surfaces are shown. Crack propagation occurred from bottom center, upward and outward for each half of the fracture.

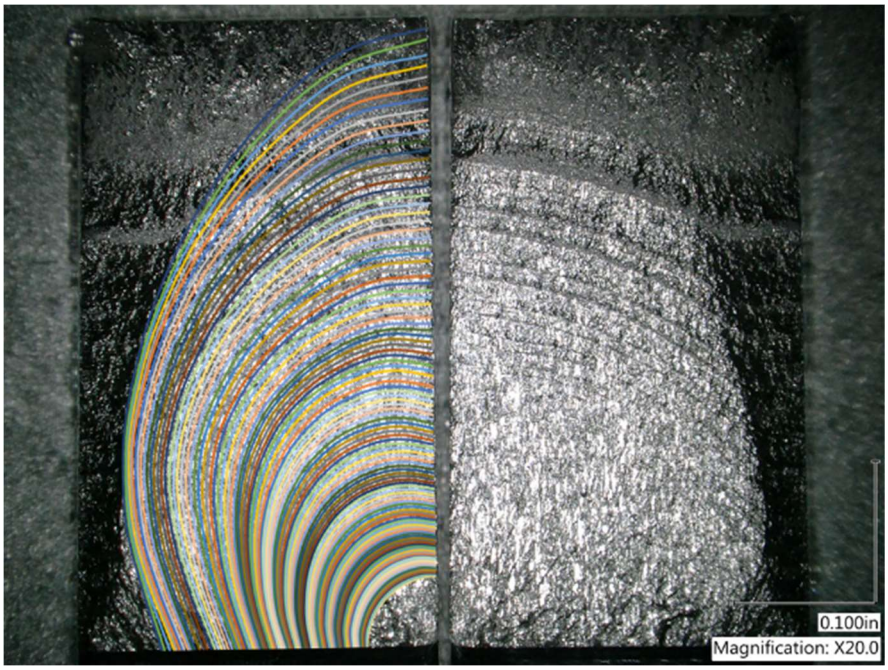

Figure 3.14: CX140ED-2 fracture surface with overlay of crack progression predicted by BAMF. Mating fracture surfaces are shown. Crack propagation occurred from bottom center, upward and outward for each half of the fracture.

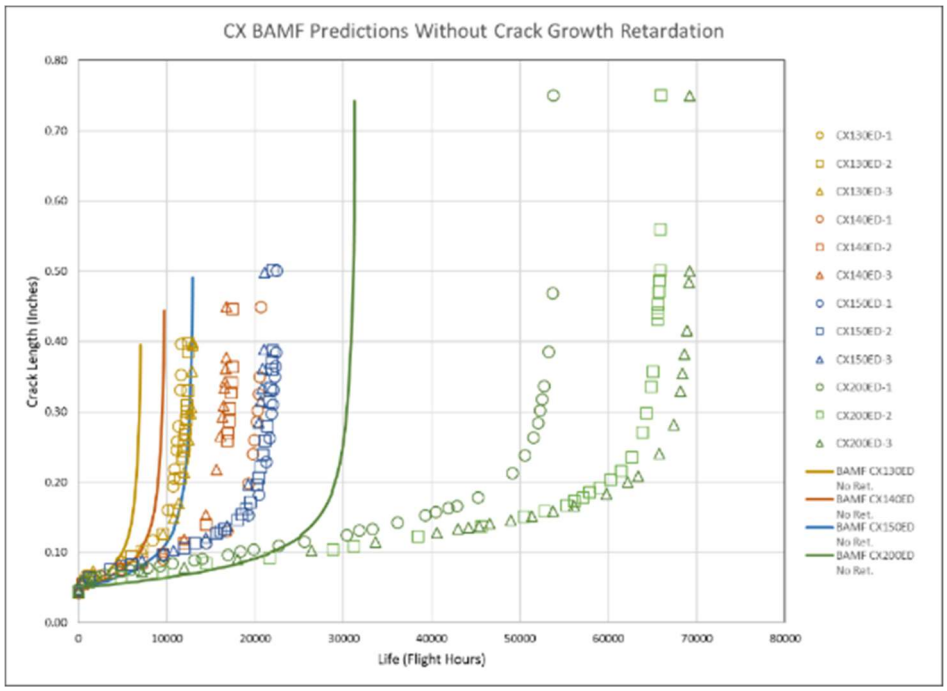

Figure 3.15: BAMF predictions of CX crack growth without retardation plotted with CX test data.

Table 3.5: Correlation ratio between test data and BAMF prediction not accounting for crack growth retardation.

e/D	Average Test Life (Flight Hours)	Predicted Life Without Retardation (Flight Hours)	Correlation Ratio
1.3	12365.06	7048.37	1.754
1.4	18303.60	9768.31	1.874
1.5	21893.55	12942.90	1.692
2	63138.86	31345.54	2.014

Table 3.6: Summary of BAMF predictions for NCX specimens.

e/D	Average Test Life (Flight Hours)	SOLR	Average SOLR	Predicted Life (Flight Hours)	Difference From Test	Average Difference
1.3	3592.23	1.748	1.734	3690.85	-2.7%	0.6%
1.4	4252.65	1.714		3976.48	6.5%	
1.5	4989.19	1.756		5211.07	-4.4%	
2	7680.47	1.720		7450.55	3.0%	

Table 3.7: Summary of BAMF predictions for CX specimens.

e/D	Average Test Life (Flight Hours)	SOLR	Average SOLR	Predicted Life (Flight Hours)	Difference From Test	Average Difference
1.3	12365.06	4.475	4.219	12955.34	4.6%	-0.9%
1.4	18303.60	4.095		17996.74	-1.7%	
1.5	21893.55	4.648		23492.80	6.8%	
2	63138.86	3.658		55838.53	-13.1%	

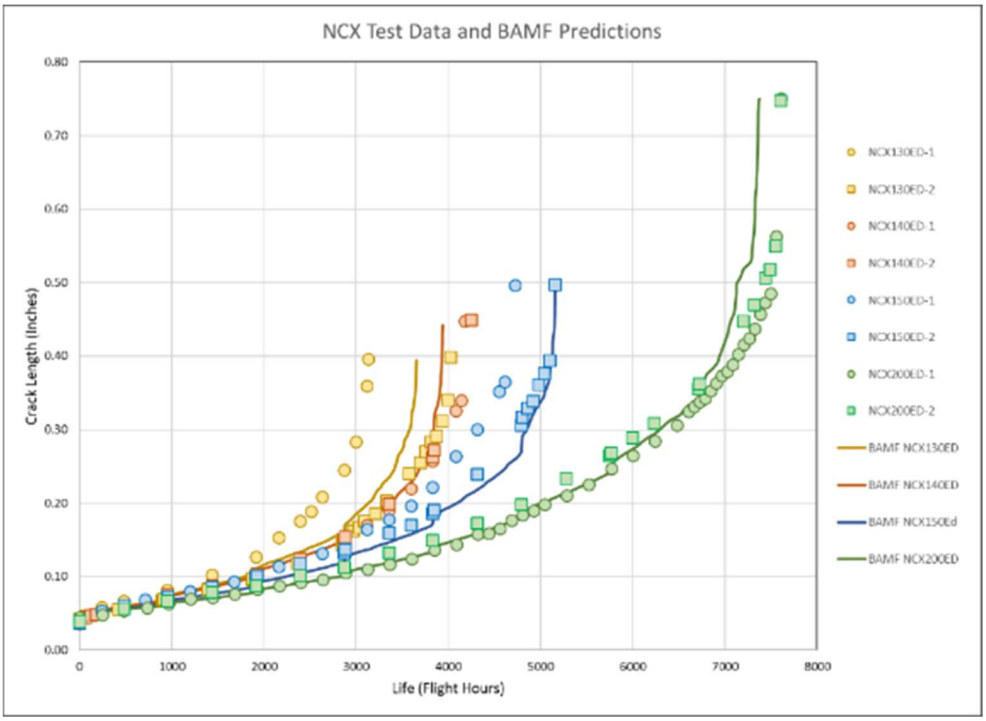

Figure 3.16: BAMF predictions for NCX specimens plotted with test data.

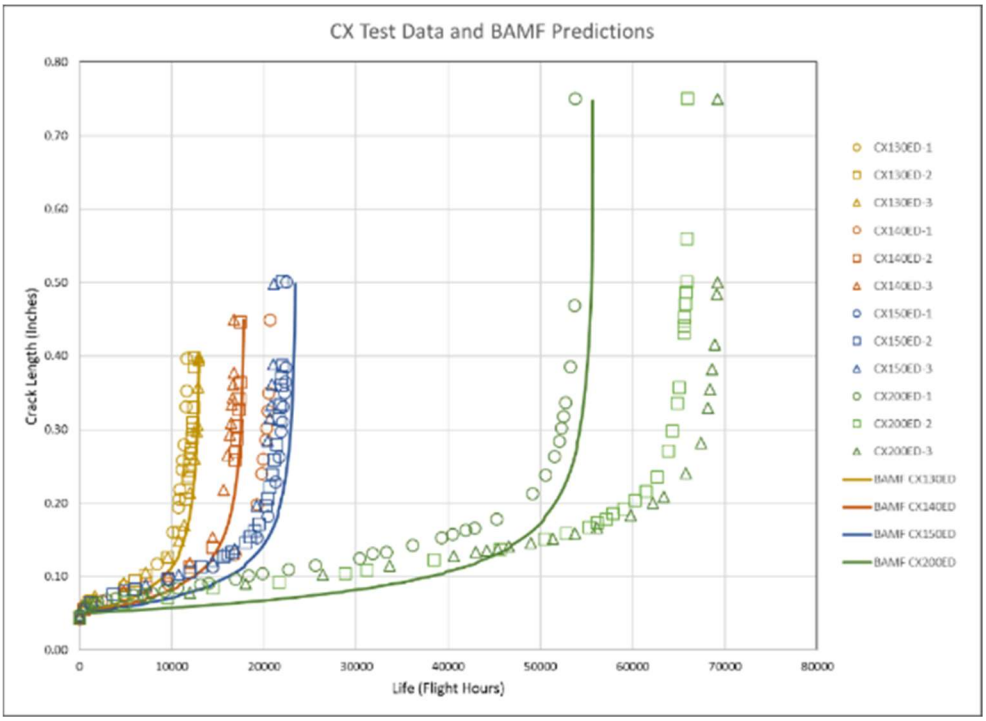

Figure 3.17: BAMF predictions for CX specimens plotted with test data.

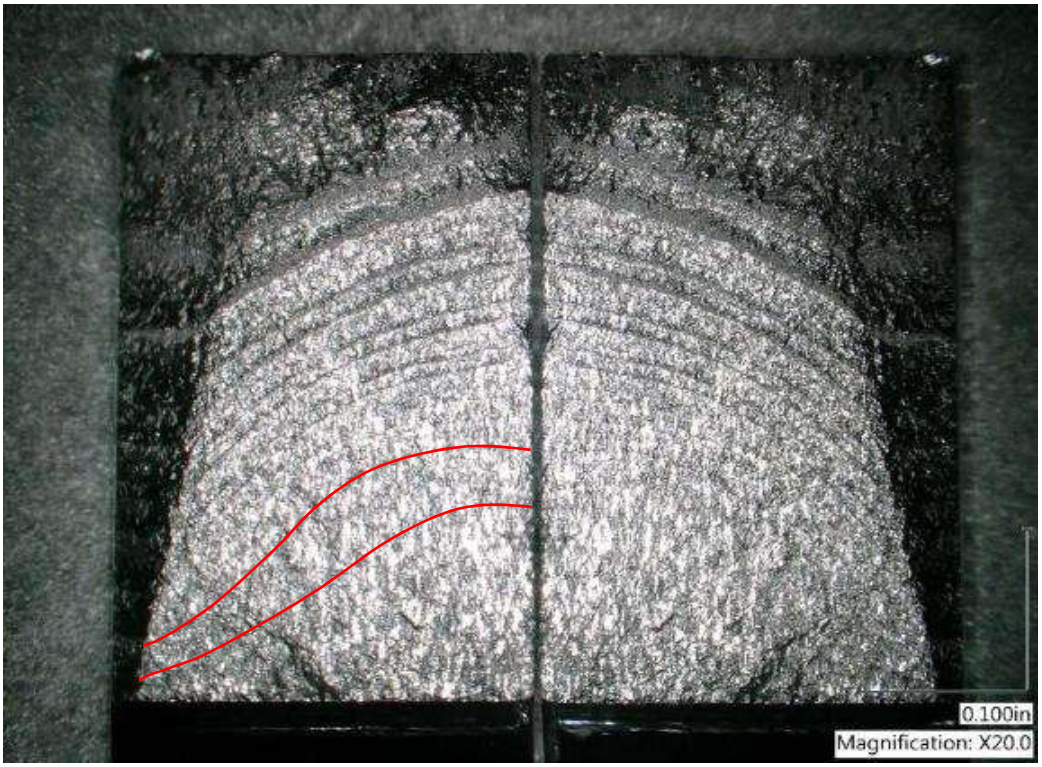

Figure 3.18: Optical image of slightly "P" shaped crack front traced on CX130ED-2. Both mating surfaces of the fracture are shown with the crack origin in the bottom center of the image.

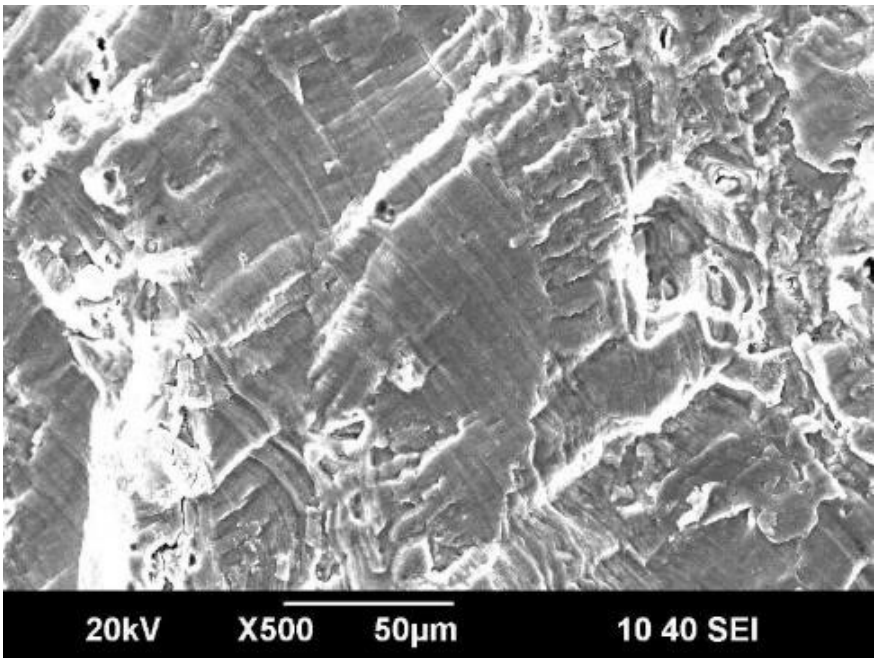

Figure 3.19: SEM image of visible fatigue striations at 500X magnification in region of spectrum testing. Direction of propagation was from the bottom-left to the top-right of this image.

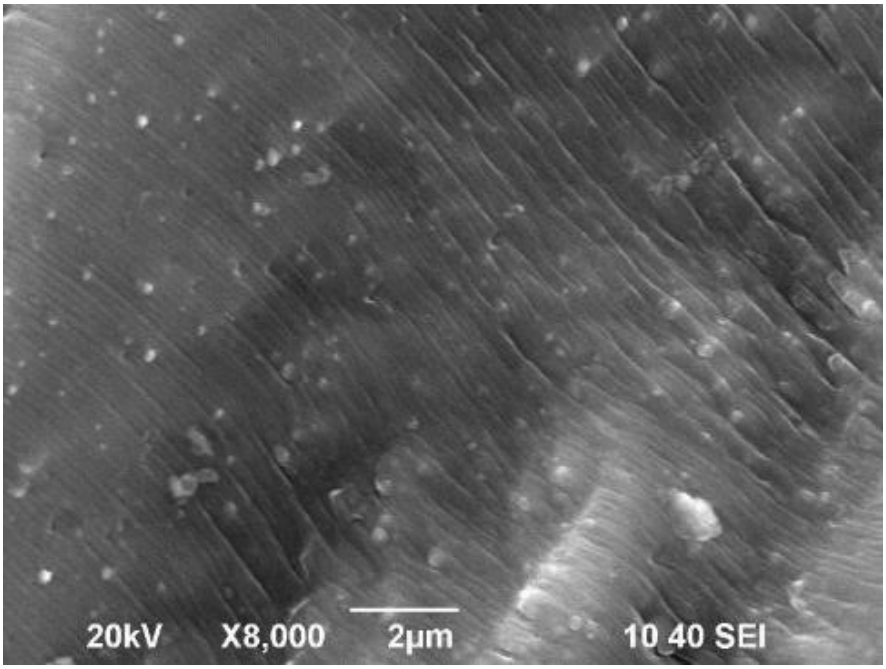

Figure 3.20: SEM image of visible fatigue striations at 8,000X magnification in constant amplitude precrack region. Direction of propagation was from the bottom-left to the top-right of this image.

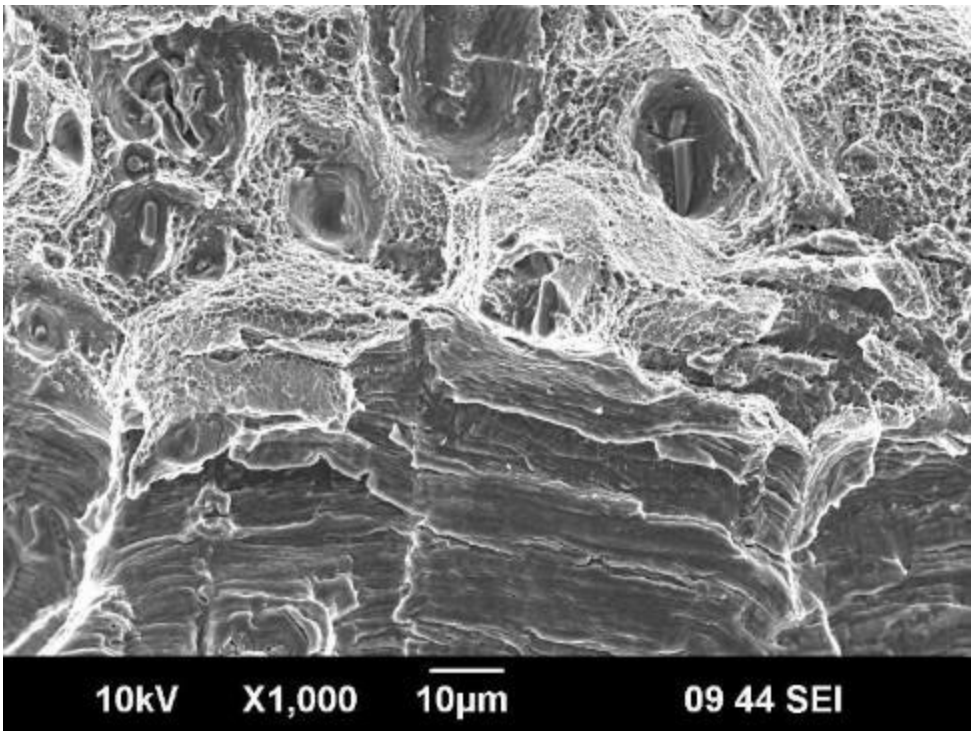

Figure 3.21: SEM image at 1,000X magnification of fracture transition from fatigue (bottom) to tensile overstress (top).

Table 3.8: Stress required to cause crack opening for cold-expanded specimens at varying crack lengths.

Edge Margin	Stress at Crack Opening (ksi)	Approximate Crack Length (in)
1.3	19.8	0.081
	16.5	0.103
	9.9	0.161
1.4	19.8	0.071
	16.5	0.087
	16.5	0.106
	13.2	0.140
1.5	19.8	0.073
	16.5	0.089
	16.5	0.102
	13.2	0.120
	13.2	0.167
2	19.8	0.072
	19.8	0.083
	19.8	0.096
	19.8	0.107
	19.8	0.119
	19.8	0.134
	19.8	0.148
	16.5	0.175
	16.5	0.235

4 DISCUSSION

4.1 Test Results

This research found that precracked, cold-expanded 2024-T351 aluminum alloy specimens with hole edge margins of 1.3, 1.4, 1.5, and 2.0 showed LIFs of 3.44, 4.30, 4.39, and 8.22, respectively, as compared to precracked, noncold-expanded specimens. Andrew observed an average LIF of 2.27 for specimens from the same material lot and e/D of 1.2 under spectrum loading [31]. Additionally, Warner found that center hole specimens (e/D of 4.0) of the same material under spectrum loading at 33 ksi max stress had an average LIF of 6.57 [28]. It was expected that a larger e/D contributes to greater benefit from cold expansion, but specimens tested in this research with e/d of 2.0 exhibited greater LIF than the specimens tested by Warner. This may be attributed to differences in crack nucleation in the bore of the hole. The specimens tested in this research tended to only propagate cracks from the hole toward the nearest edge of the specimen, although some did produce small cracks on the opposite side of the hole when nearing failure. The specimens used in Warner's research had centered holes with single corner cracks. Invariably, additional cracks nucleated on the opposite side of the hole from the original corner crack. An example is shown in Figure 4.1. Differences in crack nucleation times between cold-expanded and noncold-expanded specimens may contribute to the LIF reported. Overall, the test results from this research agreed with other similar research.

4.2 AFGROW Predictions

AFGROW was used for crack growth predictions because it is widely accepted in the aerospace industry for fatigue crack growth analysis. Also, it is the current method used by the USAF for performing damage tolerance analysis. The SOLR was adjusted to make predictions match test results for each NCX sample. The average across all samples was used for performing further predictions. The SOLR was averaged across all specimens regardless of e/D in order to encompass more of the variability observed in the small sample sizes tested. In general, this was effective, but it was observed that specimens with e/D of 2.0 often produced lower SOLR values than other specimens.

The mean SOLR was used to predict the fatigue life of a flaw at the minimum detectable flaw size of 0.05 inches. In accordance with current USAF damage tolerance analysis practices, an IFS of 0.005 inches was used to predict fatigue life of CX specimens using the mean SOLR calculated from NCX specimens [15]. LIF was calculated between the 0.05 and 0.005 inch AFGROW predictions, yielding .3.89, 3.85, 3.72, and 3.31 times life increase for 1.3, 1.4, 1.5, and 2.0 e/D, respectively. This is an average LIF of 3.69. The LIF is nearly constant over the range of e/D tested. This is inconsistent with the LIF observed for testing that increased with increasing e/D. This is an indication that the fatigue life predicted using a 0.005 IFS may not be conservative for all tested e/D.

The correlation ratio between the tested fatigue life and the 0.005 inch IFS predicted life is important to this research. It was found by Andrew that the correlation ratio for e/D of 1.2 was below one, and this research seeks to quantify the transition from conservative to unconservative prediction based on e/D. Recall that a correlation ratio

less than one indicates an unconservative prediction. This research found that the correlation ratio was less than one for e/D of 1.3 and increased with increasing edge margin. The correlation ratio for this research and the research performed by Andrew and Warner at the same maximum stress and loading spectrum are plotted against edge margin in Figure 4.2. A nearly linear relationship between correlation ratio and e/D can be seen for e/D between 1.2 and 2.0. Data from the centered hole testing performed by Warner do not appear to relate in the same way. This may be caused by the different crack growth behavior of center hole specimens previously discussed. A least-squares line fit through the short e/D data has an R^2 of 0.990 and predicts that an e/D of 1.36 would produce a correlation coefficient of one. This indicates that a 0.005 inch IFS model would produce conservative predictions of crack growth from precracked, cold-expanded holes with e/D greater than 1.36, but the predicted life of holes with e/D below 1.36 would be unconservative.

It should be noted that predictions using the average SOLR produced the largest error between prediction and test for e/D of 2.0. The SOLR from only 2.0 e/D (not the average) was used to produce a 0.005 IFS prediction to evaluate the possible variation. The least-squares line through the resulting data had an improved R^2 of 0.998, but the predicted e/D value at which the correlation ratio was equal to one remained unchanged at 1.36.

4.3 BAMF Predictions

The Broad Application for Modeling Failure was used to predict specimen fatigue crack growth. Simulating residual stress fields inside the test specimen provides a physics-based approach to modeling the fatigue life of cold-expanded holes. Predictions

performed without accounting for crack growth retardation showed correlation ratios above one for all tested e/D. This is shown graphically in Figure 4.3. The least-squares line through the data has a much lower slope than that of the 0.005 inch IFS predictions in Figure 4.2. Mathematically, the line would predict a correlation ratio of one at a negative value for e/D. This shows that BAMF predictions with no crack growth retardation produce conservative predictions of fatigue life for more values of e/D compared to 0.005 inch IFS predictions. This is true because BAMF predictions employ a physics-based approach, which naturally predicts crack growth more accurately than nonphysics-based approaches due to the consideration of residual stress.

SOLR values were found with which BAMF predictions reproduced test results. These values were averaged and used to predict fatigue life. The largest error produced between prediction and test for NCX specimens was 6.5% and 11.6% for CX specimens. This was determined to be an acceptable level of predictive accuracy, given the small sample sizes tested. These SOLR-adjusted predictions represent the best prediction of crack growth for the methods used in this research. The LIF of these BAMF predictions matched test LIF within 8.8% for all e/D. This shows the accuracy capability of physics based approaches in fatigue crack growth simulation.

4.3.1 Crack Shape

The crack shape progression predicted by BAMF for NCX specimens was nearly identical to test results. However, the actual crack shape of CX specimens varied from the predicted shape. BAMF predicted that the crack would halt crack growth in the bore and continue on the front surface where the crack was beyond the maximum compressive

residual stress, but instead the crack continued growth in the hole bore continuously. Initially, it was hypothesized that this was due to multiple cracks nucleating along the bore surface and combining, resulting in apparent crack growth. Upon fractographic inspection, no evidence of multiple crack origins was identified. Alternatively, this anomaly may be caused by the fact that, currently, BAMF predictions invariably produce planar crack paths. Variations in residual stress likely induce multiaxial stress states, which causes the crack to deviate slightly from a planar path during tests. This is not accounted for by BAMF predictions. Also, the contour method, used to produce the residual stress fields for the BAMF predictions in this research, is less accurate for predicting the stresses very near the hole bore. These stresses may be fictitiously high, stopping crack growth.

4.4 Fractography

SEM fractography qualitatively showed the difference in fatigue striation spacing between the constant amplitude precrack region and the spectrum loading test region. From this information, it may be deduced that the precracking stress was sufficiently low as to not produce crack growth retardation which would skew test results. As mentioned previously, no additional crack nucleation sites were identified on the fracture surfaces observed.

4.5 Error Analysis

4.5.1 Hole Measurement

One source of error that may affect multiple areas of this research is hole measurement error. All hole measurements were performed optically using a digital microscope. The resulting measurements were not validated using physical measurement techniques like bore gauges, and therefore, the level of inaccuracy is unknown. This imparts significant levels of uncertainty into the applied and residual hole expansion calculations. Because predictions were typically tuned with the SOLR and used nominal specimen dimensions, the impact to conclusions of this research are minimal.

4.5.2 Residual Stress Fields

Recently, it was shown by Carlson that residual stress fields around a hole change as cracks propagate through them [38]. The residual stress fields used for numerical simulation in this research were assumed to remain constant during the entire fatigue life. Additionally, the residual stress fields were derived from specimens that were uncracked at the time of cold expansion. This differs from the test conditions in this research. However, it was determined that the analysis completed using these residual stress fields remains relevant as a demonstration of the power of analytical models explicitly using residual stress fields to predict failure.

4.5.3 Crack Shape

As previously discussed, BAMF predictions assumed planar crack growth and utilized residual stresses from the contour method, which may have skewed results.

Overall, this is assumed to be an insignificant factor in predicting the fatigue life of short edge margin cold-expanded holes.

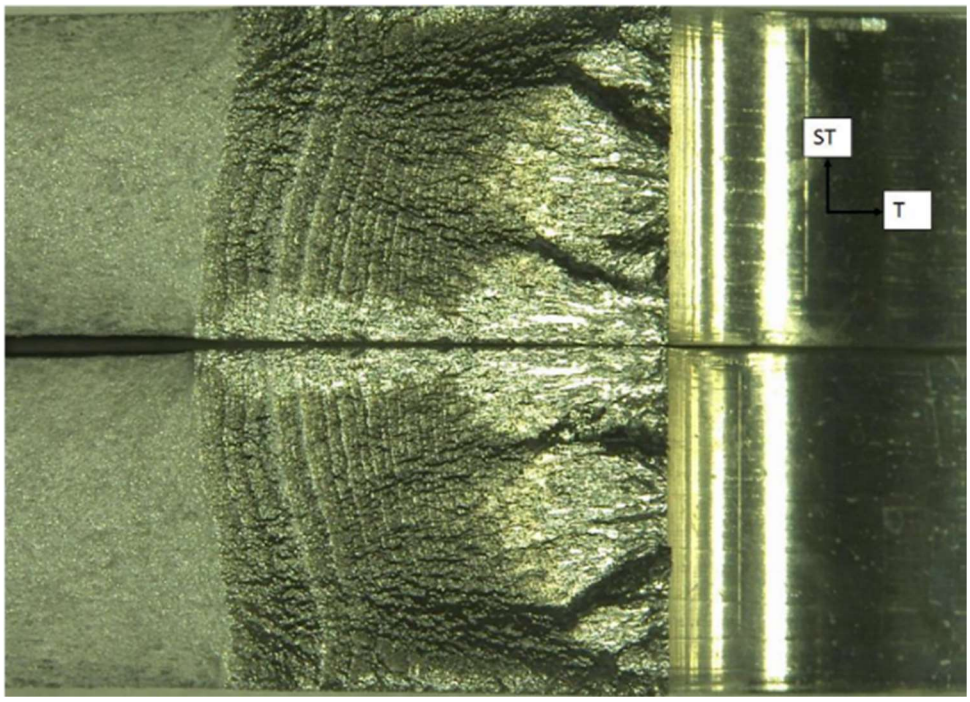

Figure 4.1: Multiple crack nucleation sites on the originally uncracked side of a centered hole in research by Warner [28]. The fracture faces shown are mating surfaces, which are placed side-by-side for viewing.

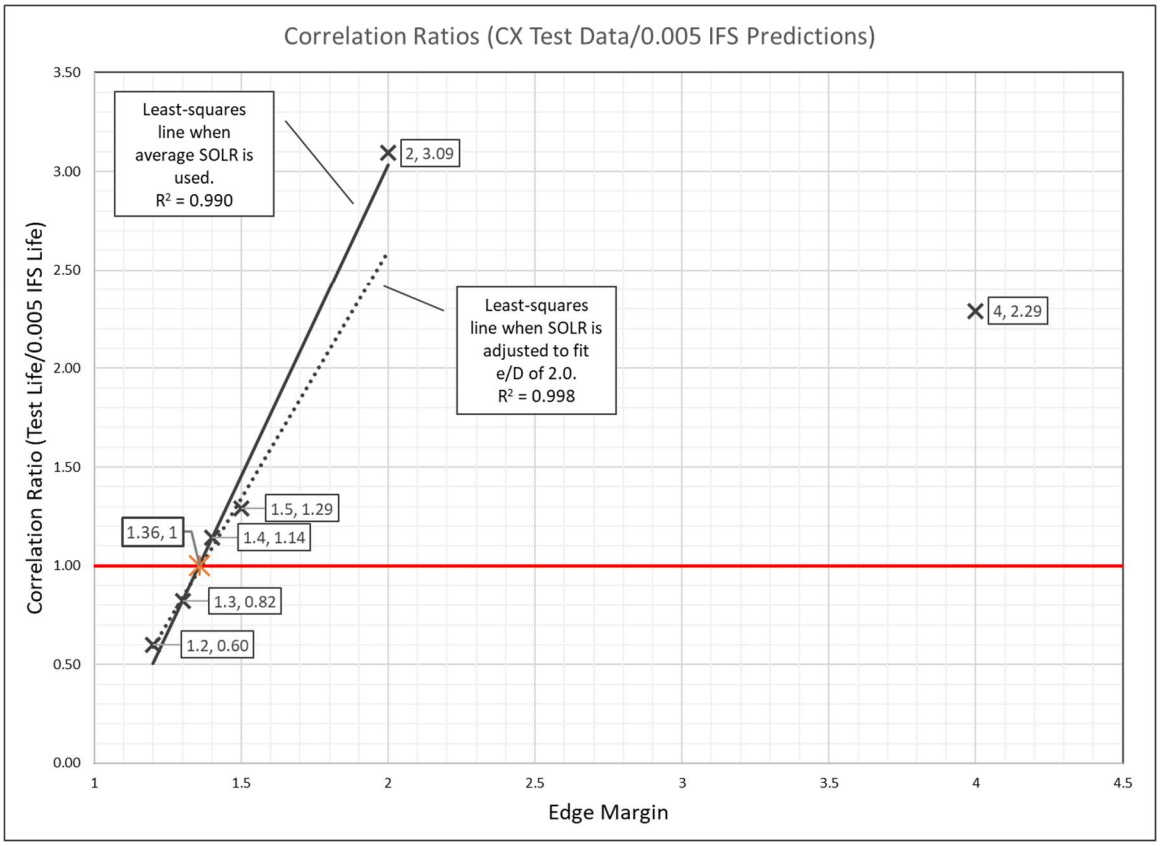

Figure 4.2: Correlation ratio versus e/D comparing test results to AFGROW predictions using 0.005 inch IFS. Data at e/D of 1.2 and 4 are from research by Andrew and Warner, respectively [31] [28].

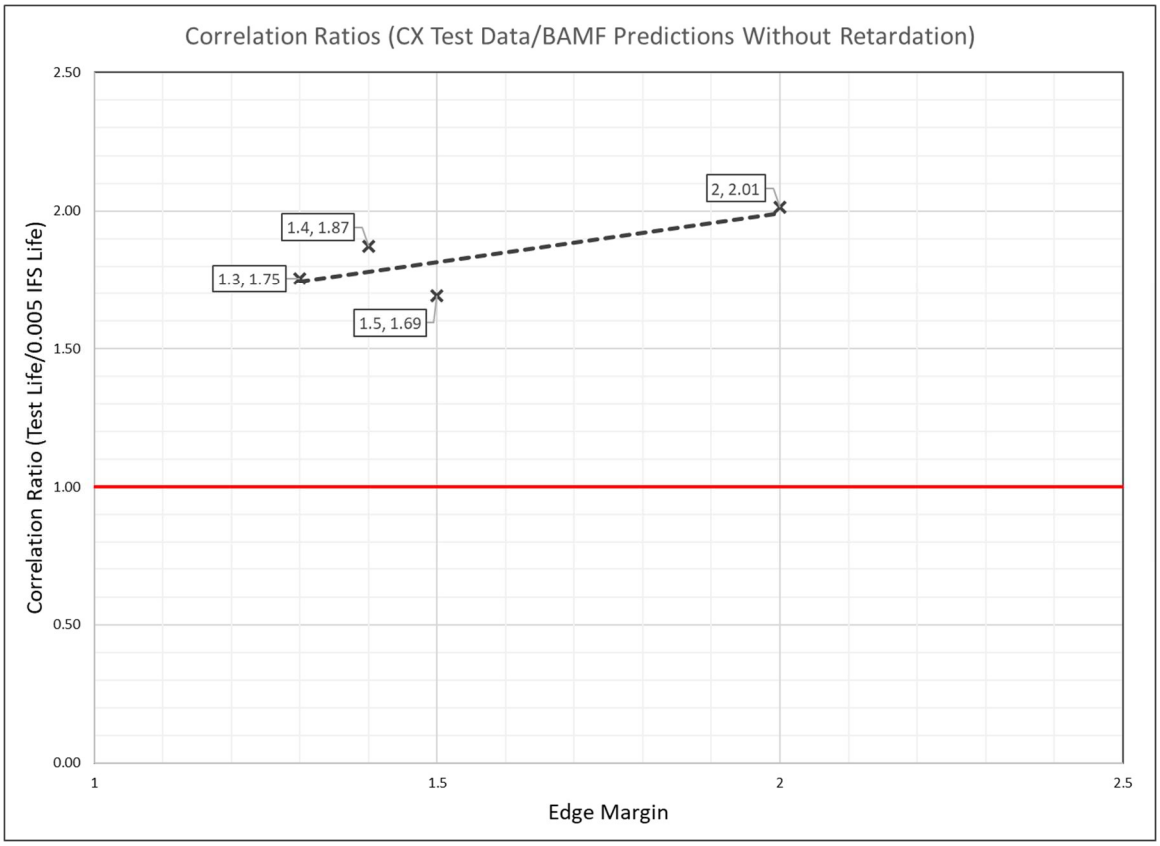

Figure 4.3: Correlation ratio versus e/D comparing test results to BAMF predictions without crack growth retardation

5 SUMMARY

5.1 Conclusions

5.1.1 Noncold-Expanded Hole Specimens

The average fatigue life of NCX specimens with the tested geometry and loading spectrum was 3,592 flight hours for e/D of 1.3, 4,253 flight hours for e/D of 1.4, 4,989 flight hours for e/D of 1.5, and 7,680 flight hours for e/D of 2.0.

5.1.2 Cold-Expanded Hole Specimens

The average fatigue life of CX specimens with the selected geometry and loading spectrum was 12,365 flight hours for e/D of 1.3, 18,304 flight hours for e/D of 1.4, 21,894 flight hours for e/D of 1.5, and 63,139 flight hours for e/D of 2.0. This corresponds to a factor of 3.44, 4.30, 4.39, and 8.22 life increase for 1.3, 1.4, 1.5, and 2.0 e/D specimens, respectively.

5.1.3 Reduced Initial Flaw Size for Predicting CX Specimen Fatigue Life

The current USAF practice of predicting cold-expanded hole fatigue life by reducing the initial flaw size to 0.005 inches produced unconservative results for specimens with 1.3 e/D. The results suggested that the lowest e/D for which the 0.005 inch IFS produces conservative results is 1.36.

5.2 Significance

The results of this research apply directly to aircraft sustainability because the test conditions replicate aircraft service conditions. Specimens were tested using a fighter aircraft wing root bending loading spectrum. Previous research showed that the benefit of cold expansion is reduced under spectrum loading as opposed to constant amplitude [19], [22], [31], [28]. Therefore, testing with spectrum loading is necessary to produce results, which allow for conservative damage tolerance analysis. It has also been shown that maximum spectrum stress can significantly affect the conservatism of predictions [28]. The maximum spectrum stress of 33 ksi was selected to closely match aircraft service conditions. The material used in this research is a commonly used alloy in aircraft structures allowing for broader application of these findings. Vast differences in material behavior make it nearly impossible to predict the behavior of one material from the testing of another. Finally, it has been shown that edge margin is an important factor in predicting fatigue life of cold-expanded holes, even producing unconservative crack growth predictions if accounted for improperly.

In the context of USAF damage tolerance analysis, the findings of this research are important. First, this research showed that short edge margin fastener holes with preexisting cracks benefit substantially from cold expansion under the test conditions of this research. Second, although fatigue life is increased by cold expansion, current USAF analysis methods do not properly account for this improvement. This can result in unconservative fatigue life predictions and unsafe aircraft operating conditions. Namely, fatigue life predictions of cold-expanded holes with edge margins of 1.30 were found to be unconservative. This research has shown, however, that analysis methods exist that

can conservatively predict the fatigue life of short edge margin, cold-expanded holes with preexisting cracks with accuracies within 10% of test, as shown in Table 5.1.

In the past, the inaccuracies of the 0.005 inch IFS method have been accepted because its downfall was thought to be its extreme conservatism. The findings of this research, along with the findings from previous research by Andrew and Warner, have shown that the 0.005 inch IFS method for accounting for cold expansion used by much of the aerospace industry is unconservative for various combinations of e/D and loading conditions [31], [32], [28]. This shows that this method, which was designed to be extremely conservative, fails to protect pilots and aircraft. This research provides data that may help improve damage tolerance procedures across the aerospace industry.

5.3 Recommendations

Based on the findings of this research, the following recommendations were developed:

1. Limit the use of 0.005 inch initial flaw size models for predicting the fatigue life of cold-expanded holes in 2024-T351 aluminum alloy with edge margins below approximately 1.36. Predictions below this edge margin have been shown to be unconservative.
2. Utilize current residual stress measurement techniques to quantify the residual stress field around cold-expanded fastener holes for geometries of interest.
3. Use residual stress data with numerical simulation to produce high-fidelity predictions for the fatigue life of cold-expanded fastener holes. These models produced conservative results for all feasible edge margins.

4. Cold expand short edge margin fastener holes for which extended fatigue life is desired. The resulting fatigue life is between 3.44 and 8.22 times the noncold-expanded life for the edge margins tested in this research.

5.4 Future Research

The following topics were identified as areas that require more research to fully understand:

1. Behavior of other materials under the conditions tested in this research.
2. Effects of various types of damage (e.g., scratches, gouges, reaming marks) on fatigue life of short edge margin holes.
3. Measurement of residual stresses induced by cold expansion of cracked holes.
4. Three-dimensional modeling of residual stress fields.
5. Effects of edge margin and applied stress on residual stress fields around cold-expanded holes.
6. Residual stress relaxation due to exposure to elevated temperature.

Table 5.1: LIF for SOLR-adjusted BAMF predictions compared to LIF observed in test.

e/D	NCX SOLR-Adjusted BAMF Prediction	CX SOLR-Adjusted BAMF Prediction	BAMF LIF	Test LIF	LIF Difference
1.3	3690.85	12955.34	3.51	3.44	2.0%
1.4	3976.48	17996.74	4.53	4.30	5.2%
1.5	5211.07	23492.80	4.51	4.39	2.7%
2	7450.55	55838.53	7.49	8.22	-8.8%

APPENDIX A

MATERIAL CERTIFICATION SHEET

KAISER ALUMINUM
FABRICATED PRODUCTS

Best in Class

CERTIFIED TEST REPORT
http://Certs.KaiserAluminum.com

Kaiser Aluminum
Trentwood Works
Spokane, WA 99205-5108
(800) 367-2586

CUSTOMER PO NUMBER:	WORK PACKAGE:	CUSTOMER PART NUMBER:	PRODUCT DESCRIPTION:
5400078947-0010		ALFLR00822-48.5	Sawed Plate

KAISER ORDER NUMBER:	LINE ITEM:	SHIP DATE:	ALLOY:	CLAD:	TEMPER:
1105438	1	11/12/2010	2024	BARE	T351
WEIGHT SHIPPED:	**QUANTITY:**	**B/L NUMBER:**	**GAUGE:**	**WIDTH:**	**LENGTH:**
4172 LB	23 PCS EST.	2029605	0.2500 IN	48.500 IN	144.500 IN

SHIP TO:	SOLD TO:
COPPER & BRASS SALES 5450 EAST HOME FRESNO, CA 93727 US	COPPER & BRASS SALES ATTN: ACCOUNTS PAYABLE P.O. Box 5116 SOUTHFIELD, MI 48086 US

Certified Specifications

AMS 4037/RevN AMS-QQ-A-250/4/RevA ASTM B 209/Rev07 CMMP 025/RevT

Test Results:

Test Code: 1504

LOT: 521928A2 CAST: 513 DROP: 05 INGOT: 3

(ASTM E8/B557)
(EN 2002-1)

Tensile: Temper	Dir/#Tests	Ultimate KSI (MPA)	Yield KSI (MPA)	Elongation %
T351	LT / 02 (Min:Max)	68.4 : 69.0 (472 : 476)	48.1 : 48.6 (332 : 335)	17.4 : 17.6

(ASTM E1251)

Chemistry:	SI	FE	CU	MN	MG	CR	ZN	TI	V	ZR		OTHER
Actual	0.08	0.20	4.4	0.56	1.3	0.01	0.16	0.02	0.01	0.00	TOT	0.03

Chemistry:		SI	FE	CU	MN	MG	CR	ZN	TI	V	ZR		OTHER
2024	MIN	0.00	0.00	3.8	0.30	1.2	0.00	0.00	0.00	0.00	0.00	MAX	0.05
	MAX	0.50	0.50	4.9	0.9	1.8	0.10	0.25	0.15	0.05	0.05	TOT	0.15

Aluminum Remainder

CERTIFICATION

Kaiser Aluminum Fabricated Products, LLC (Kaiser) hereby certifies that metal shipped under this order was melted in the United States of America or a qualifying country per DFARS 225.872-1(a), was manufactured in the United States of America, and meets the requirements of DFARS 252.225 for domestic content. This material has been inspected, tested and found in conformance with the requirements of the applicable specifications as indicated herein. All metal which is solution heat treated complies with AMS 2772. Any warranty is limited to that shown on Kaiser's standard general terms and conditions of sale. Test reports are on file, subject to examination. Test reports shall not be reproduced except in full, without the written approval of Kaiser Aluminum Fabricated Products, LLC laboratory. The recording of false, fictitious or fraudulent statements or entries on the certificate may be punished as a felony under federal law. ISO-9001:2000 certified.

BILL POYNOR, LABORATORIES SUPERVISOR

Plant Serial: 4210062

Kaiser Order Number: 1105438

Line Item: 1

Figure A.1: Material certification sheet

APPENDIX B

SPECIMEN DRAWINGS

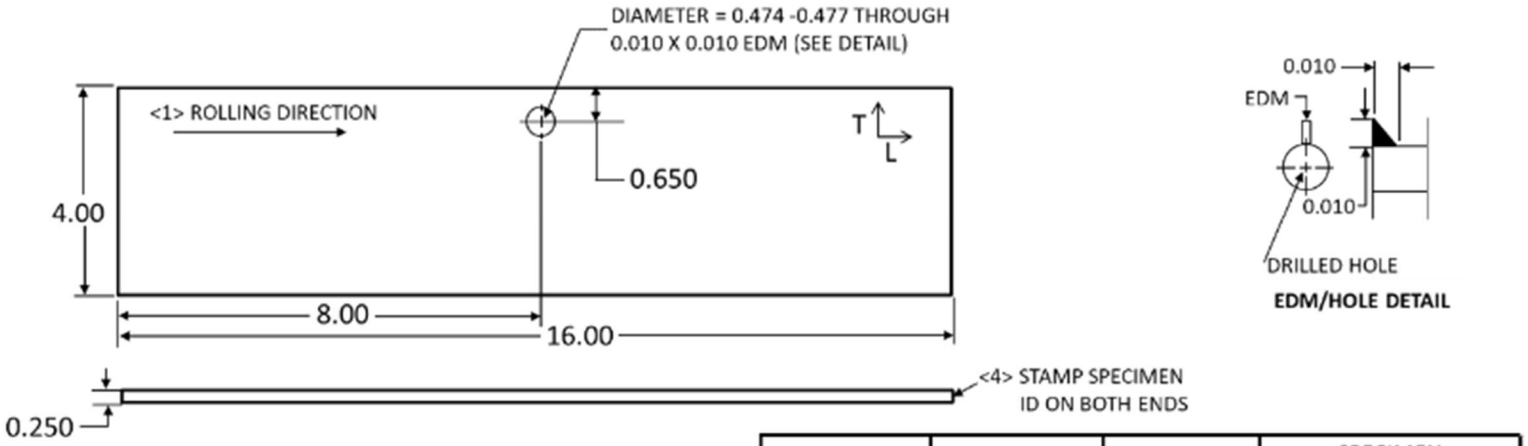

MATERIAL	QUANTITY	THICKNESS	SPECIMEN IDENTIFICATION
2024-T351	2	0.250	NCX130ED-X (1 TO 2)

<1> ROLLING DIRECTION IS CRITICAL FOR ALL SPECIMENS
<2> ALL SPECIMENS SHOULD COME FROM THE SAME PLATE
<3> DEBURR AND POLISH EDGES OF SPECIMEN. DO NOT CHAMFER OR RADIUS EDGE OF HOLE. POLISH AREA AROUND HOLE.
<4> STEEL STAMP SPECIMEN ID ON BOTH ENDS IN A VISIBLE LOCATION
<5> MATERIAL CERTIFICATIONS ARE REQUIRED

	NAME	DATE			
DRAWN	DALLEN ANDREW	2/22/2012	TITLE : NON COLD EXPANDED E/D =1.3 SPECIMEN		
MATERIAL	SEE TABLE				
QTY. REQD	SEE TABLE				
FINISH	64 RMS		SIZE	DWG. NO.	REV
UNLESS OTHERWISE SPECIFIED: DIMENSIONS ARE IN INCHES TOLERANCES: X.XX = ±0.01 X.XXX = ±0.001					
				WEIGHT:	SHEET 1 OF 1

Figure B.1: Specimen drawing for NCX 130ED-1,-2 specimens.

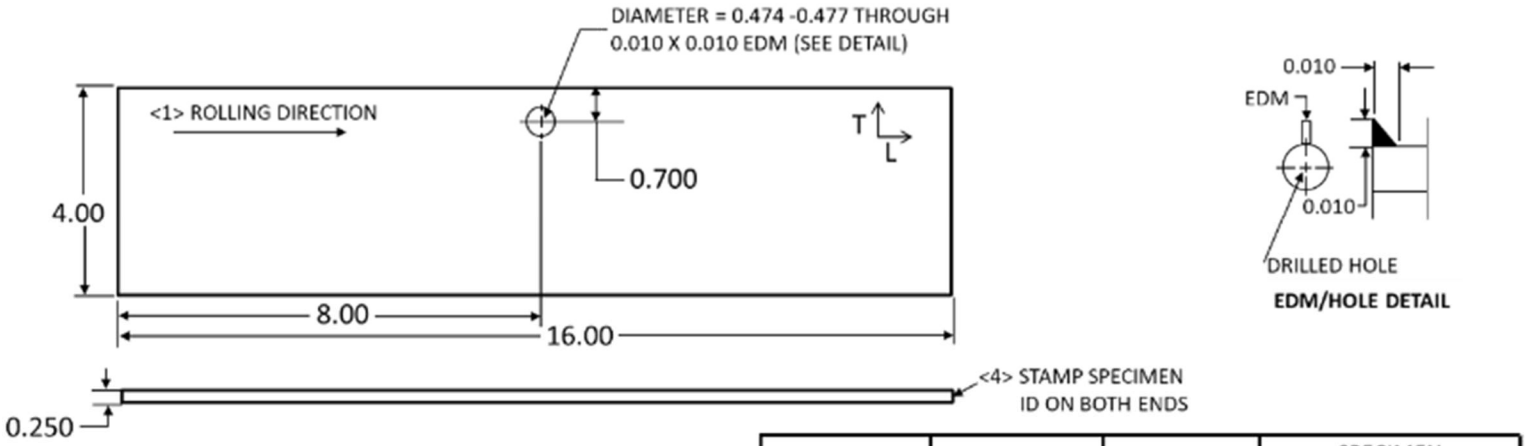

MATERIAL	QUANTITY	THICKNESS	SPECIMEN IDENTIFICATION
2024-T351	2	0.250	NCX140ED-X (1 TO 2)

<1> ROLLING DIRECTION IS CRITICAL FOR ALL SPECIMENS
<2> ALL SPECIMENS SHOULD COME FROM THE SAME PLATE
<3> DEBURR AND POLISH EDGES OF SPECIMEN. DO NOT CHAMFER OR RADIUS EDGE OF HOLE. POLISH AREA AROUND HOLE.
<4> STEEL STAMP SPECIMEN ID ON BOTH ENDS IN A VISIBLE LOCATION
<5> MATERIAL CERTIFICATIONS ARE REQUIRED

	NAME	DATE			
DRAWN	DALLEN ANDREW	2/22/2012	TITLE : NON COLD EXPANDED E/D =1.4 SPECIMEN		
MATERIAL	SEE TABLE				
QTY. REQD	SEE TABLE				
FINISH	64 RMS		SIZE	DWG. NO.	REV
UNLESS OTHERWISE SPECIFIED: DIMENSIONS ARE IN INCHES TOLERANCES: X.XX = ±0.01 X.XXX = ±0.001					
				WEIGHT:	SHEET 1 OF 1

Figure B.2: Specimen drawing for NCX 140ED-1,-2 specimens.

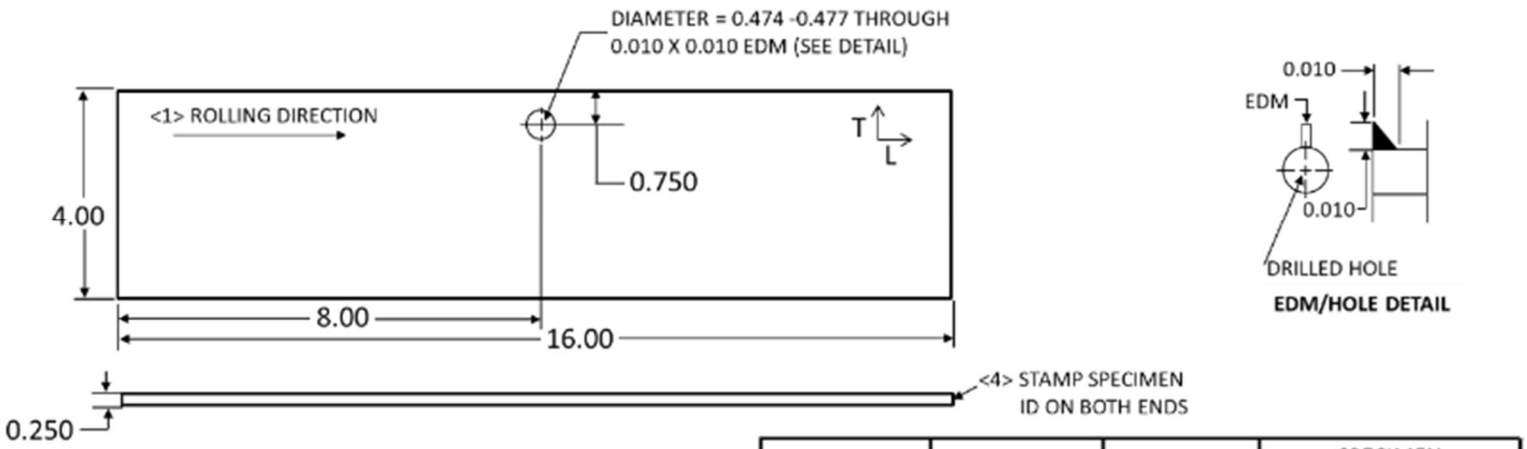

MATERIAL	QUANTITY	THICKNESS	SPECIMEN IDENTIFICATION
2024-T351	2	0.250	NCX150ED-X (1 TO 2)

<1> ROLLING DIRECTION IS CRITICAL FOR ALL SPECIMENS
<2> ALL SPECIMENS SHOULD COME FROM THE SAME PLATE
<3> DEBURR AND POLISH EDGES OF SPECIMEN. DO NOT CHAMFER OR RADIUS EDGE OF HOLE. POLISH AREA AROUND HOLE.
<4> STEEL STAMP SPECIMEN ID ON BOTH ENDS IN A VISIBLE LOCATION
<5> MATERIAL CERTIFICATIONS ARE REQUIRED

	NAME	DATE			
DRAWN	DALLEN ANDREW	2/22/2012	TITLE : NON COLD EXPANDED E/D =1.5 SPECIMEN		
MATERIAL	SEE TABLE				
QTY. REQD	SEE TABLE				
FINISH	64 RMS		SIZE	DWG. NO.	REV
UNLESS OTHERWISE SPECIFIED: DIMENSIONS ARE IN INCHES TOLERANCES: X.XX = ±0.01 X.XXX = ±0.001					
				WEIGHT:	SHEET 1 OF 1

Figure B.3: Specimen drawing for NCX 150ED-1,-2 specimens.

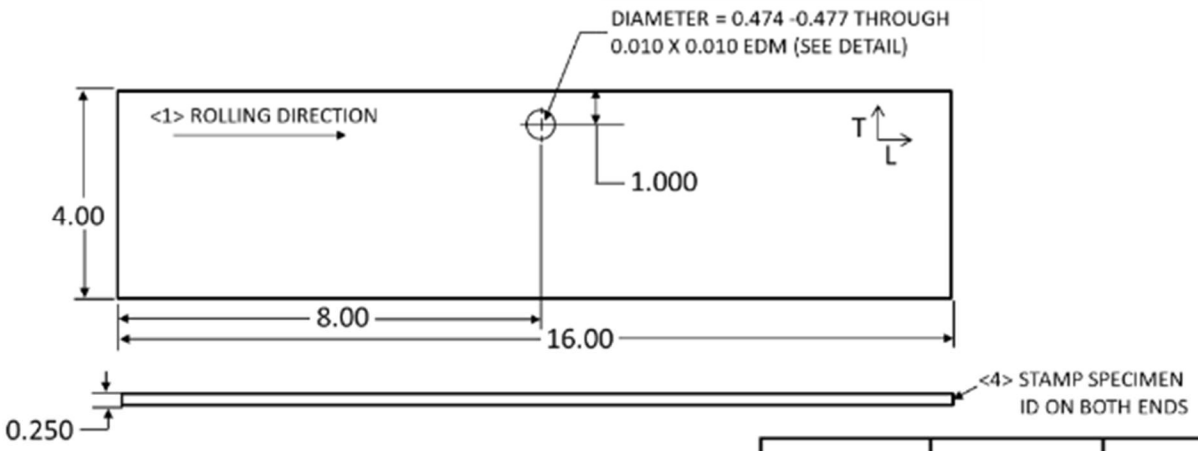

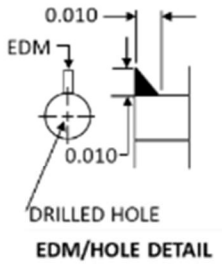

MATERIAL	QUANTITY	THICKNESS	SPECIMEN IDENTIFICATION
2024-T351	2	0.250	NCX200ED-X (1 TO 2)

<1> ROLLING DIRECTION IS CRITICAL FOR ALL SPECIMENS
<2> ALL SPECIMENS SHOULD COME FROM THE SAME PLATE
<3> DEBURR AND POLISH EDGES OF SPECIMEN. DO NOT CHAMFER OR RADIUS EDGE OF HOLE. POLISH AREA AROUND HOLE.
<4> STEEL STAMP SPECIMEN ID ON BOTH ENDS IN A VISIBLE LOCATION
<5> MATERIAL CERTIFICATIONS ARE REQUIRED

	NAME	DATE			
DRAWN	DALLEN ANDREW	2/22/2012	TITLE : NON COLD EXPANDED E/D =2.0 SPECIMEN		
MATERIAL	SEE TABLE				
QTY. REQD	SEE TABLE				
FINISH	64 RMS		SIZE	DWG. NO.	REV
UNLESS OTHERWISE SPECIFIED: DIMENSIONS ARE IN INCHES TOLERANCES: X.XX = ±0.01 X.XXX = ±0.001					
				WEIGHT:	SHEET 1 OF 1

Figure B.4: Specimen drawing for NCX200ED-1,-2 specimens.

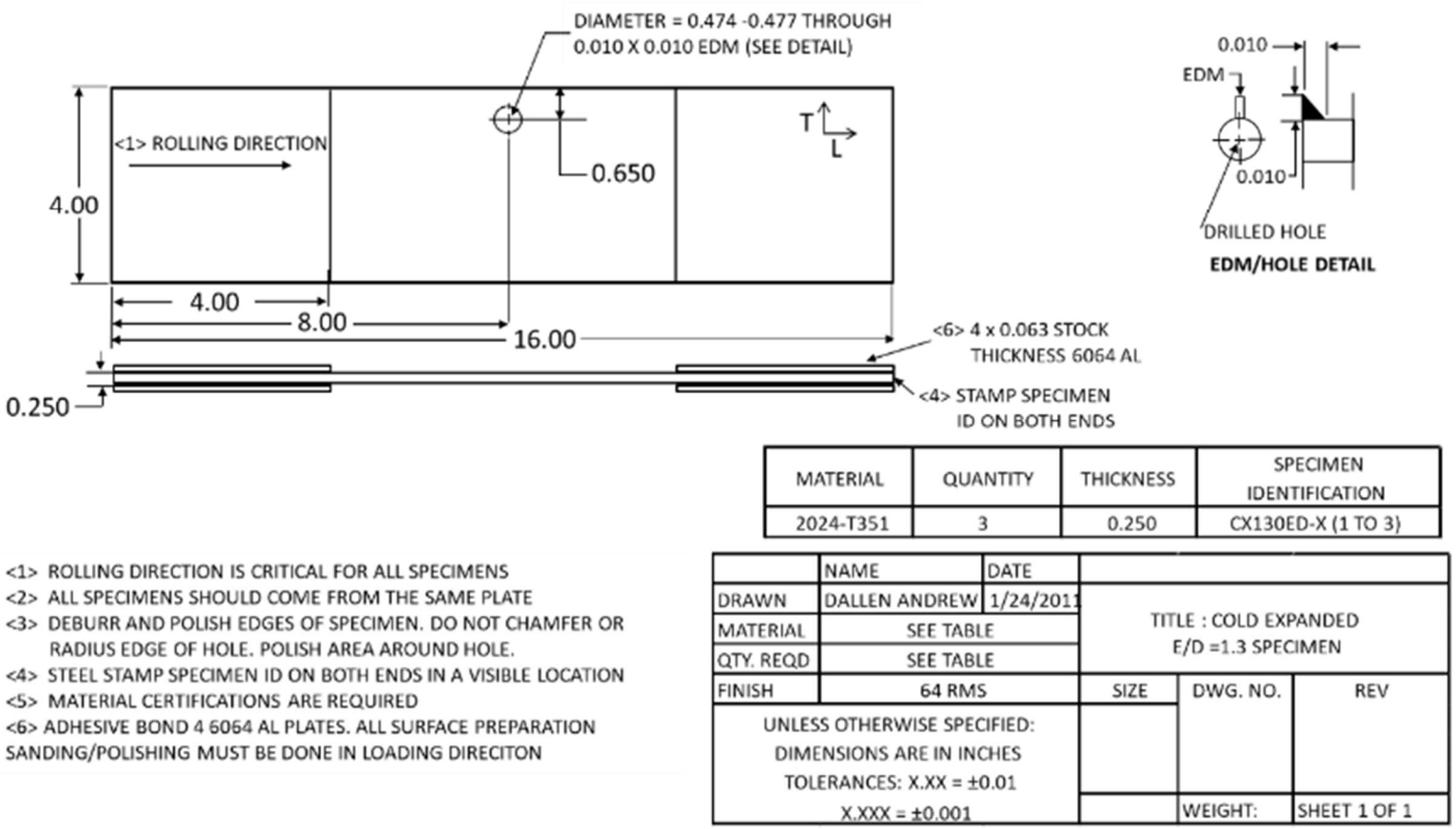

MATERIAL	QUANTITY	THICKNESS	SPECIMEN IDENTIFICATION
2024-T351	3	0.250	CX130ED-X (1 TO 3)

<1> ROLLING DIRECTION IS CRITICAL FOR ALL SPECIMENS
<2> ALL SPECIMENS SHOULD COME FROM THE SAME PLATE
<3> DEBURR AND POLISH EDGES OF SPECIMEN. DO NOT CHAMFER OR RADIUS EDGE OF HOLE. POLISH AREA AROUND HOLE.
<4> STEEL STAMP SPECIMEN ID ON BOTH ENDS IN A VISIBLE LOCATION
<5> MATERIAL CERTIFICATIONS ARE REQUIRED
<6> ADHESIVE BOND 4 6064 AL PLATES. ALL SURFACE PREPARATION SANDING/POLISHING MUST BE DONE IN LOADING DIRECITON

	NAME	DATE			
DRAWN	DALLEN ANDREW	1/24/2011	TITLE : COLD EXPANDED E/D =1.3 SPECIMEN		
MATERIAL	SEE TABLE				
QTY. REQD	SEE TABLE				
FINISH	64 RMS		SIZE	DWG. NO.	REV
UNLESS OTHERWISE SPECIFIED: DIMENSIONS ARE IN INCHES TOLERANCES: X.XX = ±0.01 X.XXX = ±0.001				WEIGHT:	SHEET 1 OF 1

Figure B.5: Specimen drawing for CX130ED-1,-2,-3 specimens.

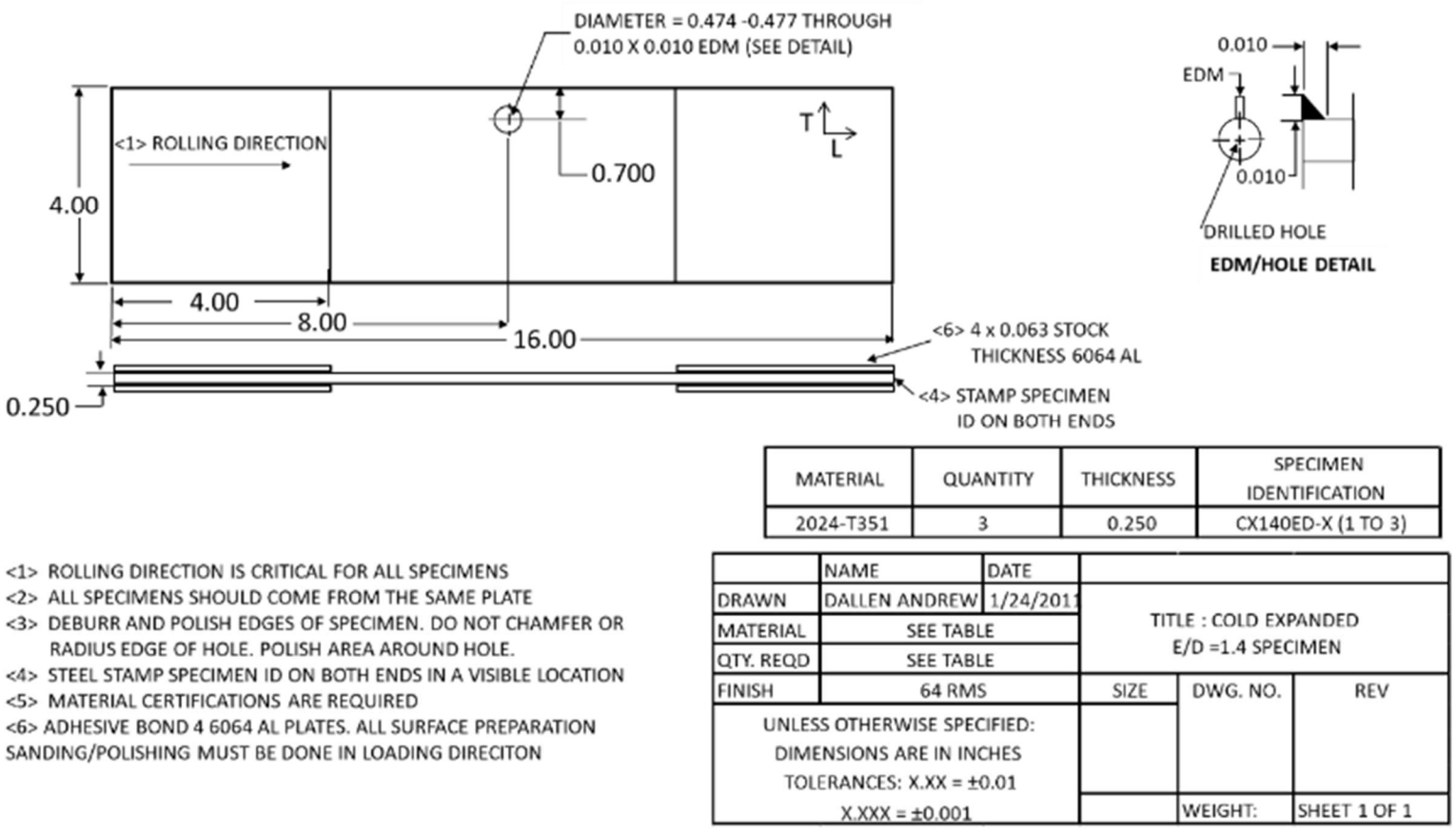

MATERIAL	QUANTITY	THICKNESS	SPECIMEN IDENTIFICATION
2024-T351	3	0.250	CX140ED-X (1 TO 3)

<1> ROLLING DIRECTION IS CRITICAL FOR ALL SPECIMENS
<2> ALL SPECIMENS SHOULD COME FROM THE SAME PLATE
<3> DEBURR AND POLISH EDGES OF SPECIMEN. DO NOT CHAMFER OR RADIUS EDGE OF HOLE. POLISH AREA AROUND HOLE.
<4> STEEL STAMP SPECIMEN ID ON BOTH ENDS IN A VISIBLE LOCATION
<5> MATERIAL CERTIFICATIONS ARE REQUIRED
<6> ADHESIVE BOND 4 6064 AL PLATES. ALL SURFACE PREPARATION SANDING/POLISHING MUST BE DONE IN LOADING DIRECITON

	NAME	DATE	
DRAWN	DALLEN ANDREW	1/24/2011	TITLE : COLD EXPANDED E/D =1.4 SPECIMEN
MATERIAL	SEE TABLE		
QTY. REQD	SEE TABLE		
FINISH	64 RMS	SIZE	DWG. NO. / REV
UNLESS OTHERWISE SPECIFIED: DIMENSIONS ARE IN INCHES TOLERANCES: X.XX = ±0.01 X.XXX = ±0.001			WEIGHT: / SHEET 1 OF 1

Figure B.6: Specimen drawing for CX140ED-1,-2,-3 specimens.

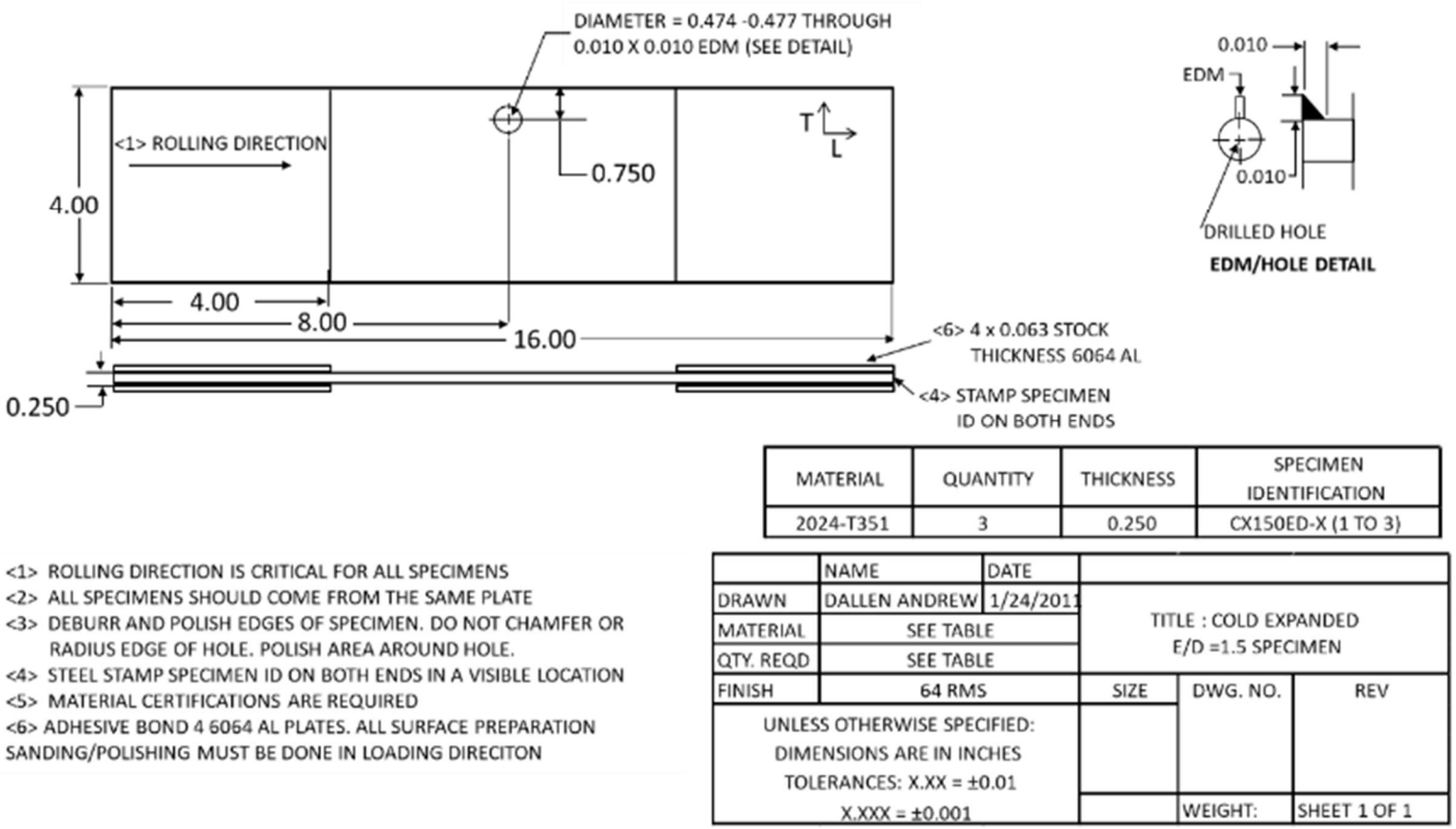

MATERIAL	QUANTITY	THICKNESS	SPECIMEN IDENTIFICATION
2024-T351	3	0.250	CX150ED-X (1 TO 3)

<1> ROLLING DIRECTION IS CRITICAL FOR ALL SPECIMENS
<2> ALL SPECIMENS SHOULD COME FROM THE SAME PLATE
<3> DEBURR AND POLISH EDGES OF SPECIMEN. DO NOT CHAMFER OR RADIUS EDGE OF HOLE. POLISH AREA AROUND HOLE.
<4> STEEL STAMP SPECIMEN ID ON BOTH ENDS IN A VISIBLE LOCATION
<5> MATERIAL CERTIFICATIONS ARE REQUIRED
<6> ADHESIVE BOND 4 6064 AL PLATES. ALL SURFACE PREPARATION SANDING/POLISHING MUST BE DONE IN LOADING DIRECITON

	NAME	DATE			
DRAWN	DALLEN ANDREW	1/24/2011	TITLE : COLD EXPANDED E/D =1.5 SPECIMEN		
MATERIAL	SEE TABLE				
QTY. REQD	SEE TABLE				
FINISH	64 RMS		SIZE	DWG. NO.	REV
UNLESS OTHERWISE SPECIFIED: DIMENSIONS ARE IN INCHES TOLERANCES: X.XX = ±0.01 X.XXX = ±0.001					
				WEIGHT:	SHEET 1 OF 1

Figure B.7: Specimen drawing for CX150ED-1,-2,-3 specimens.

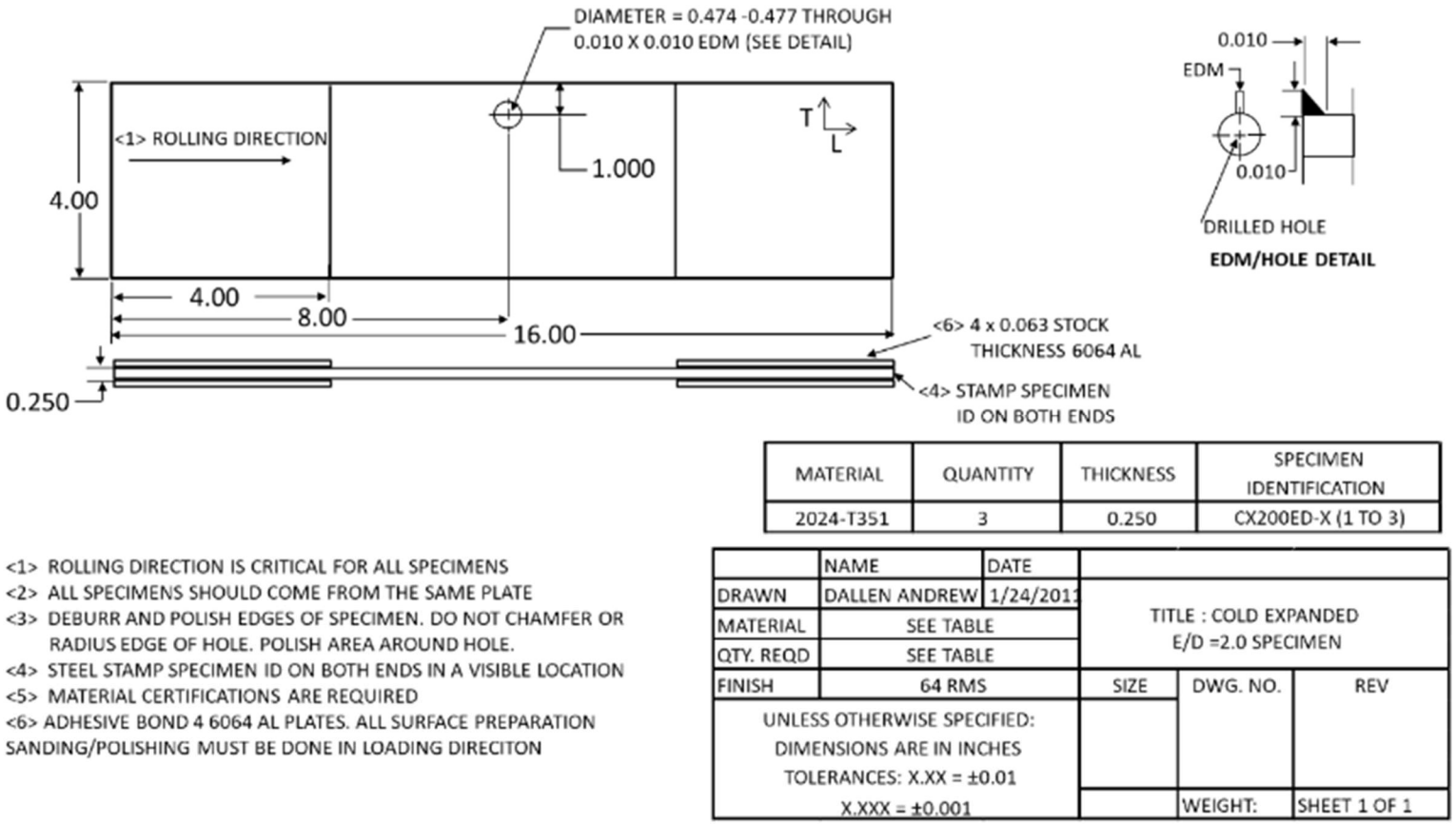

MATERIAL	QUANTITY	THICKNESS	SPECIMEN IDENTIFICATION
2024-T351	3	0.250	CX200ED-X (1 TO 3)

<1> ROLLING DIRECTION IS CRITICAL FOR ALL SPECIMENS
<2> ALL SPECIMENS SHOULD COME FROM THE SAME PLATE
<3> DEBURR AND POLISH EDGES OF SPECIMEN. DO NOT CHAMFER OR RADIUS EDGE OF HOLE. POLISH AREA AROUND HOLE.
<4> STEEL STAMP SPECIMEN ID ON BOTH ENDS IN A VISIBLE LOCATION
<5> MATERIAL CERTIFICATIONS ARE REQUIRED
<6> ADHESIVE BOND 4 6064 AL PLATES. ALL SURFACE PREPARATION SANDING/POLISHING MUST BE DONE IN LOADING DIRECITON

	NAME	DATE			
DRAWN	DALLEN ANDREW	1/24/201	TITLE : COLD EXPANDED E/D =2.0 SPECIMEN		
MATERIAL	SEE TABLE				
QTY. REQD	SEE TABLE				
FINISH	64 RMS		SIZE	DWG. NO.	REV
UNLESS OTHERWISE SPECIFIED: DIMENSIONS ARE IN INCHES TOLERANCES: X.XX = ±0.01 X.XXX = ±0.001					
				WEIGHT:	SHEET 1 OF 1

Figure B.8: Specimen drawing for CX200ED-1,-2,-3 specimens.

APPENDIX C

MACHINE CALIBRATION CERTIFICATION

CERTIFICATE OF CALIBRATION

ISSUED BY: INSTRON CALIBRATION LABORATORY

DATE OF ISSUE: 23-Feb-2019

CERTIFICATE NUMBER: **026021919085905**

NVLAP CALIBRATION
NVLAP Lab Code 200301-0

ILAC-MRA

INSTRON®

Instron
825 University Avenue
Norwood, MA 02062-2643
Telephone: (800) 473-7838
Fax: (781) 575-5750
Email: service_requests@instron.com

APPROVED SIGNATORY

Type of Calibration: Force
Relevant Standard: ASTM E4-16
Date of Calibration: 19-Feb-2019

Customer Requested Due Date: 19-Feb-2020

Customer

Name: US Air Force - Hill Air Force Base
Address: 00 ACL/MADLM
7278 4th Street; Bldg 100, bay D
Hill AFB, UT 84056
bryce.jolley@us.af.mil
P.O./Contract No.:
Contact: Bryce Jolley

Machine

Manufacturer: MTS
Serial Number: 370.25/10471022 (M457750)
System ID: 370.25/10471022 (M457750)
Range Type: Single

Transducer

Manufacturer: MTS
Transducer ID: 661.22H-01/10423926D (M385871)
Capacity: 56202.24 lbf
Type: Tension/Compression

Classification

Indicator 1. - Digital Readout - PASSED**

Certification Statement

This certifies that the forces verified with machine indicator(s) (listed above) that are identified as "PASSED" are WITHIN ±1% accuracy, 1% repeatability, and zero return tolerance. All machine indicators were verified on-site at customer location by Instron in accordance with ASTM E4-16. The Simple Acceptance decision rule has been agreed to and employed in the determination of conformance to the identified metrological specification. The certification is based on runs 1 and 2 only. A third run is taken to satisfy uncertainty requirements according to ISO 17025 specifications.

The calibration and equipment used conform to a controlled Quality Assurance program which meets the specifications outlined in ANSI/NCSL Z540.1-1994, ISO 10012:2003, ISO 9001:2015 and ISO/IEC 17025:2017.

**** within ±0.5% accuracy and 0.5% repeatability.**

Method

The testing machine was verified in the 'As Found' condition with no adjustments or repairs carried out. This is also the 'As Left' condition.

Instron CalproCR Version 3.40

Figure C.1: Calibration certification of force readings for servo-hydraulic fatigue machine used in experiments.

APPENDIX D

FATIGUE CRACK GROWTH DATASHEETS

NCX130ED-1 Crack Growth Datasheet				
Test Date: 12/26/2018 10:10:47 AM		**Width (in): 4.0025**		
Max Stress (ksi): 33		**Thickness (in): 0.2529**		
Loading Rate (kip/sec): 165		**Area (in^2): 1.012**		
Hole Diameter (in): 0.5047		**Ligament Length (in): 0.3963**		
Flight Hours	**Crack Length (inches)**			**Comments**
	Front Surface	**Back Surface**	**Bore**	
0	0.04170		0.05594	
240	0.05876		0.07130	
480	0.06672		0.08383	
960	0.08210		0.11264	
1450	0.10276		0.13511	
1930	0.12724		0.17129	
2180	0.15302		0.19594	
2420	0.17576	0.00000	0.23117	
2540	0.18912	0.02812	0.25290	Through Thickness
2660	0.20858	0.07588		
2900	0.24472	0.15762		
3029	0.28386	0.23168		
3149	0.35930	0.31262		
3163	0.39630	0.39630		Ligament Failure

Figure D.1: NCX130ED-1 fatigue crack growth datasheet.

NCX130ED-2 Crack Growth Datasheet				
Test Date: 1/14/2019 10:31:39 AM		**Width (in): 4.0025**		
Max Stress (ksi): 33		**Thickness (in): 0.252**		
Loading Rate (kip/sec): 165		**Area (in^2): 1.009**		
Hole Diameter (in): 0.5010		**Ligament Length (in): 0.3992**		
Flight Hours	**Crack Length (inches)**			**Comments**
	Front Surface	**Back Surface**	**Bore**	
0	0.04296		0.04566	
60	0.04670		0.04704	
120	0.04716		0.05216	
420	0.05606		0.05809	
900	0.06812		0.08166	
910	0.06982		0.08523	
1390	0.08244		0.11035	
1870	0.09558		0.13464	
1880	0.09798		0.13248	
2360	0.11846		0.15551	
2840	0.14426		0.19349	
2849	0.15062		0.19837	
2969	0.16266		0.21439	
3029	0.16758		0.22204	
3089	0.17558	0.00000	0.23219	
3209	0.18606	0.02756	0.25200	Through Thickness
3329	0.20306	0.07722		
3569	0.24078	0.15512		
3689	0.25550	0.18054		
3749	0.27018	0.20586		
3809	0.28344	0.22606		
3869	0.29102	0.23152		
3929	0.31160	0.26204		
3989	0.34094	0.32474		
4018	0.39920	0.38240		
4022	0.39920	0.39920		Ligament Failure

Figure D.2: NCX130ED-2 fatigue crack growth datasheet.

NCX140ED-1 Crack Growth Datasheet				
Test Date: 12/19/2018 9:10:43 AM		**Width (in): 4.0018**		
Max Stress (ksi): 33		**Thickness (in): 0.253**		
Loading Rate (kip/sec): 165		**Area (in^2): 1.012**		
Hole Diameter (in): 0.5003		**Ligament Length (in): 0.4481**		
Flight Hours	**Crack Length (inches)**			**Comments**
	Front Surface	**Back Surface**	**Bore**	
0	0.03592		0.04394	
480	0.05742		0.07368	
960	0.07094		0.09093	
1450	0.08564		0.11228	
1930	0.10084		0.13476	
2420	0.12320		0.16315	
2900	0.14672		0.19462	
3149	0.17038	0.00000	0.22304	
3389	0.19068	0.04192	0.25300	Through Thickness
3629	0.21996	0.11124		
3869	0.25780	0.17550		
4119	0.32602	0.28398		
4179	0.34022	0.30062		
4218	0.44810	0.44810		Ligament Failure

Figure D.3: NCX140ED-1 fatigue crack growth datasheet.

NCX140ED-2 Crack Growth Datasheet				
Test Date: 1/11/2019 12:33:07 PM		**Width (in): 4.0016**		
Max Stress (ksi): 33		**Thickness (in): 0.2526**		
Loading Rate (kip/sec): 165		**Area (in^2): 1.011**		
Hole Diameter (in): 0.5015		**Ligament Length (in): 0.4498**		
Flight Hours	**Crack Length (inches)**			**Comments**
	Front Surface	**Back Surface**	**Bore**	
0	0.03934		0.05021	
60	0.04432		0.05897	
120	0.04732		0.06212	
180	0.04926		0.06340	
480	0.05968		0.07706	
960	0.07376		0.09779	
970	0.07502		0.09907	
1450	0.08796		0.11816	
1930	0.10196		0.13641	
1940	0.10322		0.14072	
2420	0.12392		0.16965	
2900	0.15120		0.20137	
2909	0.15436	0.00000	0.20530	
3389	0.19884	0.06108	0.25260	Through Thickness
3869	0.26290	0.18658		
3879	0.27220	0.21098		
4288	0.44980	0.44980		Ligament Failure

Figure D.4: NCX140ED-2 fatigue crack growth datasheet.

NCX150ED-1 Crack Growth Datasheet				
Test Date: 12/17/2018 1:50:36 PM		**Width (in): 4.0021**		
Max Stress (ksi): 33		**Thickness (in): 0.2523**		
Loading Rate (kip/sec): 165		**Area (in^2): 1.010**		
Hole Diameter (in): 0.5016		**Ligament Length (in): 0.4968**		
Flight Hours	**Crack Length (inches)**			**Comments**
	Front Surface	**Back Surface**	**Bore**	
0	0.04084		0.05278	
240	0.05386		0.06433	
720	0.06856		0.08692	
1210	0.08016		0.10428	
1690	0.09294		0.12897	
2180	0.11340		0.15337	
2660	0.13164		0.18531	
3149	0.16426		0.21876	
3389	0.17736	0.00000	0.23486	
3629	0.19622	0.05106	0.25230	Through Thickness
3869	0.22194	0.10784		
4119	0.26384	0.18524		
4359	0.30042	0.24222		
4599	0.35194	0.32336		
4659	0.36504	0.34206		
4769	0.49680	0.49680		Ligament Failure

Figure D.5: NCX150ED-1 fatigue crack growth datasheet.

NCX150ED-2 Crack Growth Datasheet				
Test Date: 1/8/2019 3:48:11 PM		**Width (in): 4.0025**		
Max Stress (ksi): 33		**Thickness (in): 0.2526**		
Loading Rate (kip/sec): 165		**Area (in^2): 1.011**		
Hole Diameter (in): 0.5023		**Ligament Length (in): 0.4968**		
Flight Hours	**Crack Length (inches)**			**Comments**
	Front Surface	**Back Surface**	**Bore**	
0	0.03684		0.05508	
480	0.06098		0.07849	
960	0.07300		0.09603	
970	0.07300		0.09873	
1450	0.08614		0.11265	
1930	0.09886		0.12695	
1940	0.10062		0.13119	
2420	0.11716		0.15097	
2900	0.13298		0.17105	
2909	0.13688		0.17783	
3389	0.15932		0.20716	
3629	0.17024	0.00000	0.22212	
3869	0.18620	0.02110	0.25260	Through Thickness
3879	0.19068	0.03828		
4359	0.23936	0.13300		
4839	0.30604	0.23366		
4849	0.31736	0.25690		
4909	0.32986	0.27630		
4969	0.33940	0.29644		
5029	0.36104	0.32788		
5089	0.37686	0.34892		
5149	0.39404	0.36388		
5209	0.49710	0.49710		Ligament Failure

Figure D.6: NCX150ED-2 fatigue crack growth datasheet.

NCX200ED-1 Crack Growth Datasheet				
Test Date: 12/6/2018 12:56:50 PM		**Width (in): 4.0024**		
Max Stress (ksi): 33		**Thickness (in): 0.2527**		
Loading Rate (kip/sec): 165		**Area (in^2): 1.011**		
Hole Diameter (in): 0.5025		**Ligament Length (in): 0.7506**		
Flight Hours	**Crack Length (inches)**			**Comments**
	Front Surface	**Back Surface**	**Bore**	
0	0.04440		0.04106	
247	0.04790		0.06268	
487	0.05390		0.06806	
737	0.05798		0.08285	
977	0.06344		0.07829	
1217	0.07004		0.09739	
1457	0.07156		0.10059	
1697	0.07610		0.09811	
1947	0.08284		0.11357	
2187	0.08782		0.11489	
2427	0.09194		0.11802	
2667	0.09608		0.12762	
2917	0.10498		0.13811	
3157	0.10974		0.14464	
3397	0.11662		0.15292	
3637	0.12372		0.17326	
3886	0.13598		0.17910	
4126	0.14370		0.19087	
4366	0.15822		0.19805	
4486	0.15838		0.20486	
4606	0.16502		0.21325	
4736	0.17626		0.22772	
4856	0.18428	0.00000	0.23881	
4976	0.18934	0.01530	0.25270	Through Thickness
5096	0.19792	0.03902		
5336	0.21088	0.07016		
5576	0.22526	0.10116		
5826	0.24682	0.14340		
6066	0.26508	0.17482		
6306	0.28438	0.19922		
6546	0.30648	0.22712		
6676	0.32484	0.25606		
6736	0.33190	0.26454		
6796	0.33844	0.26892		
6856	0.34244	0.27370		
6916	0.35346	0.28952		
6976	0.36314	0.30008		
7036	0.37398	0.31044		
7096	0.37974	0.31774		
7156	0.38864	0.33804		
7216	0.40302	0.35304		
7276	0.41594	0.36926		
7336	0.42404	0.38126		
7396	0.43742	0.39590		
7456	0.45684	0.42952		
7516	0.47338	0.44638		
7576	0.48480	0.46172		
7636	0.56266	0.56916		
7683	0.75060	0.75060		Ligament Failure

Figure D.7: NCX200ED-1 fatigue crack growth datasheet.

NCX200ED-2 Crack Growth Datasheet				
Test Date: 12/27/2018 9:02:24 AM		**Width (in): 4.0024**		
Max Stress (ksi): 33		**Thickness (in): 0.2519**		
Loading Rate (kip/sec): 165		**Area (in^2): 1.008**		
Hole Diameter (in): 0.5020		**Ligament Length (in): 0.7481**		
Flight Hours	**Crack Length (inches)**			**Comments**
	Front Surface	**Back Surface**	**Bore**	
0	0.03930		0.05704	
480	0.05688		0.07560	
960	0.06666		0.08730	
1450	0.07924		0.10155	
1930	0.08714		0.11966	
2420	0.10188		0.13790	
2900	0.11282		0.14985	
3389	0.13276		0.17025	
3869	0.14976		0.19280	
4359	0.17304	0.00000	0.22002	
4839	0.19856	0.03164	0.25190	Through Thickness
5329	0.23382	0.11318		
5809	0.26496	0.16472		
5819	0.26830	0.17600		
6059	0.28892	0.20576		
6299	0.30858	0.22826		
6779	0.35606	0.28794		
6789	0.36248	0.29516		
7269	0.44764	0.39670		
7389	0.46986	0.42316		
7509	0.50702	0.46792		
7569	0.51838	0.48240		
7629	0.54968	0.52046		
7678	0.74810	0.74810		Ligament Failure

Figure D.8: NCX200ED-2 fatigue crack growth datasheet.

CX130ED-1 Crack Growth Datasheet				
Test Date: 2/9/2019 11:57:08 AM		**Width (in): 4.0012**		
Max Stress (ksi): 33		**Thickness (in): 0.2517**		
Loading Rate (kip/sec): 165		**Area (in^2): 1.007**		
Hole Diameter (in): 0.5028		**Ligament Length (in): 0.3969**		
Flight Hours	**Crack Length (inches)**			**Comments**
	Front Surface	**Back Surface**	**Bore**	
0	0.04616		0.04971	
1200	0.06482		0.07507	
4810	0.08734		0.11818	
8419	0.11748		0.16748	
10099	0.16060	0.00000	0.20971	
10699	0.19490	0.01624	0.25170	Through Thickness
10819	0.20608	0.04574		
10889	0.21920	0.07576		
11069	0.24568	0.12088		
11189	0.25794	0.15060		
11309	0.28012	0.18706		
11549	0.33168	0.26176		
11609	0.35324	0.28976		
11648	0.39690	0.39690		Ligament Failure

Figure D.9: CX130ED-1 fatigue crack growth datasheet.

CX130ED-2 Crack Growth Datasheet				
Test Date: 3/8/2019 1:28:21 PM		**Width (in): 4.0024**		
Max Stress (ksi): 33		**Thickness (in): 0.2528**		
Loading Rate (kip/sec): 165		**Area (in^2): 1.012**		
Hole Diameter (in): 0.5030		**Ligament Length (in): 0.3983**		
Flight Hours	**Crack Length (inches)**			**Comments**
	Front Surface	**Back Surface**	**Bore**	
0	0.04582		0.05015	
1200	0.06696		0.07438	
6010	0.09514		0.13403	
7220	0.10264		0.14470	
9620	0.12634		0.18124	
10829	0.16116	0.00000	0.21340	
11549	0.20582	0.01924	0.25280	Through Thickness
11789	0.23360	0.09208		
11849	0.23704	0.10300		
11909	0.24400	0.12184		
11969	0.25220	0.13790		
12029	0.26152	0.15192		
12089	0.26872	0.15996		
12149	0.27648	0.17510		
12209	0.28938	0.19284		
12269	0.30172	0.21382		
12329	0.31026	0.22464		
12389	0.33034	0.25662		
12449	0.38562	0.32010		
12460	0.39830	0.39830		Ligament Failure

Figure D.10: CX130ED-2 fatigue crack growth datasheet.

CX130ED-3 Crack Growth Datasheet				
Test Date: 3/27/2019 12:29:23 PM			**Width (in): 4.0024**	
Max Stress (ksi): 33			**Thickness (in): 0.2539**	
Loading Rate (kip/sec): 165			**Area (in^2): 1.016**	
Hole Diameter (in): 0.5026			**Ligament Length (in): 0.3992**	
Flight Hours	**Crack Length (inches)**			**Comments**
	Front Surface	**Back Surface**	**Bore**	
0	0.04838		0.05179	
480	0.06628		0.13610	
1680	0.07374		0.14316	
4810	0.09174		0.16978	
7220	0.10500		0.18962	
9620	0.12636		0.21811	
10829	0.14884	0.00000	0.25245	
11369	0.16964	0.05544	0.25390	Through Thickness
12029	0.21410	0.10744		
12509	0.26040	0.16836		
12749	0.29736	0.22090		
12809	0.30614	0.22894		
12929	0.35750	0.29838		
12971	0.39526	0.34448		
12987	0.39920	0.39920		Ligament Failure

Figure D.11: CX130ED-3 fatigue crack growth datasheet.

CX140ED-1 Crack Growth Datasheet				
Test Date: 2/6/2019 3:35:09 PM		**Width (in): 4.0015**		
Max Stress (ksi): 33		**Thickness (in): 0.2525**		
Loading Rate (kip/sec): 165		**Area (in^2): 1.010**		
Hole Diameter (in): 0.5017		**Ligament Length (in): 0.4498**		
Flight Hours	**Crack Length (inches)**			**Comments**
	Front Surface	**Back Surface**	**Bore**	
0	0.04298		0.04718	
480	0.05762		0.06037	
2400	0.06678		0.07988	
4810	0.07662		0.09945	
9620	0.09018		0.13603	
14439	0.11382		0.19021	
16839	0.13046	0.00000	0.21485	
19249	0.19858	0.06796	0.25250	Through Thickness
19789	0.24002	0.13552		
19969	0.26042	0.16660		
20209	0.28620	0.20858		
20329	0.30250	0.23188		
20449	0.32578	0.27032		
20569	0.35036	0.31710		
20653	0.44980	0.44980		Ligament Failure

Figure D.12: CX140ED-1 fatigue crack growth datasheet.

CX140ED-2 Crack Growth Datasheet				
Test Date: 3/4/2019 11:05:50 AM		**Width (in): 4.0006**		
Max Stress (ksi): 33		**Thickness (in): 0.2529**		
Loading Rate (kip/sec): 165		**Area (in^2): 1.012**		
Hole Diameter (in): 0.5026		**Ligament Length (in): 0.4467**		
Flight Hours	**Crack Length (inches)**			**Comments**
	Front Surface	**Back Surface**	**Bore**	
0	0.04452		0.03957	
480	0.05594		0.06181	
4810	0.07704		0.09854	
7220	0.08666		0.12494	
9620	0.09776		0.15120	
12029	0.11406		0.17187	
14439	0.13984	0.00000	0.20648	
16839	0.25910	0.15930	0.25290	Through Thickness
16959	0.26916	0.18144		
17079	0.28768	0.21208		
17199	0.30548	0.23444		
17319	0.32750	0.27568		
17379	0.34166	0.28736		
17439	0.36422	0.32108		
17489	0.44670	0.44670		Ligament Failure

Figure D.13: CX140ED-2 fatigue crack growth datasheet.

CX140ED-3 Crack Growth Datasheet				
Test Date: 3/25/2019 8:43:32 PM		**Width (in): 4.0016**		
Max Stress (ksi): 33		**Thickness (in): 0.2531**		
Loading Rate (kip/sec): 165		**Area (in^2): 1.013**		
Hole Diameter (in): 0.5028		**Ligament Length (in): 0.4496**		
Flight Hours	**Crack Length (inches)**			**Comments**
	Front Surface	**Back Surface**	**Bore**	
0	0.04438		0.04847	
480	0.05660		0.06430	
4810	0.07964		0.12876	
9620	0.10096		0.20274	
12029	0.11860		0.21104	
14439	0.15304	0.00000	0.23915	
15639	0.21770	0.08838	0.25310	Through Thickness
16119	0.26540	0.15658		
16359	0.29288	0.20112		
16479	0.30900	0.22644		
16599	0.33384	0.27746		
16659	0.34302	0.28438		
16719	0.36160	0.31890		
16768	0.37764	0.34234		
16769	0.44960	0.44960		Ligament Failure

Figure D.14: CX140ED-2 fatigue crack growth datasheet.

CX150ED-1 Crack Growth Datasheet				
Test Date: 1/31/2019 5:31:10 PM		**Width (in): 4.0029**		
Max Stress (ksi): 33		**Thickness (in): 0.252**		
Loading Rate (kip/sec): 165		**Area (in^2): 1.009**		
Hole Diameter (in): 0.5039		**Ligament Length (in): 0.5011**		
Flight Hours	**Crack Length (inches)**			**Comments**
	Front Surface	**Back Surface**	**Bore**	
0	0.04630		0.05646	
4810	0.08188		0.10754	
9619	0.09792		0.14660	
14438	0.11372		0.18235	
19248	0.15340	0.00000	0.23277	
20447	0.18264	0.05610	0.25200	Through Thickness
21287	0.22934	0.12384		
21647	0.26302	0.17098		
21897	0.29790	0.22352		
22017	0.31056	0.24306		
22137	0.33142	0.28174		
22257	0.35066	0.31102		
22317	0.36564	0.33160		
22377	0.38460	0.35858		
22477	0.50110	0.50110		Ligament Failure

Figure D.15: CX150ED-1 fatigue crack growth datasheet.

CX150ED-2 Crack Growth Datasheet				
Test Date: 2/25/2019 12:14:58 PM		**Width (in): 4.0017**		
Max Stress (ksi): 33		**Thickness (in): 0.2524**		
Loading Rate (kip/sec): 165		**Area (in^2): 1.010**		
Hole Diameter (in): 0.5011		**Ligament Length (in): 0.5026**		
Flight Hours	**Crack Length (inches)**			**Comments**
	Front Surface	**Back Surface**	**Bore**	
0	0.04328		0.05667	
1200	0.06512		0.07687	
3610	0.07618		0.09748	
6010	0.08272		0.12453	
9620	0.09596		0.16030	
12029	0.10644		0.19115	
13229	0.11364		0.20743	
15639	0.12750		0.23189	
16119	0.13062	0.00000	0.23242	
16599	0.13350	0.00610	0.25240	Through Thickness
18049	0.14638	0.04314		
18529	0.15458	0.05236		
19009	0.16282	0.06428		
19489	0.17204	0.07620		
20209	0.19660	0.10504		
20449	0.20688	0.11838		
20689	0.22272	0.13190		
20929	0.23972	0.15166		
21169	0.25916	0.16698		
21409	0.27974	0.20660		
21659	0.31466	0.26380		
21779	0.33390	0.29200		
21899	0.36068	0.32870		
21959	0.37076	0.34640		
22019	0.38756	0.37658		
22069	0.50260	0.50260		Ligament Failure

Figure D.16: CX150ED-2 fatigue crack growth datasheet.

CX150ED-3 Crack Growth Datasheet				
Test Date: 3/23/2019 9:11:18 PM		**Width (in): 4.0021**		
Max Stress (ksi): 33		**Thickness (in): 0.2528**		
Loading Rate (kip/sec): 165		**Area (in^2): 1.012**		
Hole Diameter (in): 0.5018		**Ligament Length (in): 0.4986**		
Flight Hours	**Crack Length (inches)**			**Comments**
	Front Surface	**Back Surface**	**Bore**	
0	0.04780		0.06788	
480	0.06018		0.07727	
7220	0.08858		0.16487	
10829	0.10212		0.18320	
14439	0.12048	0.00000	0.22310	
16839	0.13754	0.00902	0.25280	Through Thickness
19249	0.19646	0.10472		
20449	0.28452	0.21450		
20689	0.31550	0.24884		
20809	0.33322	0.27008		
20929	0.36100	0.30892		
21049	0.38908	0.34274		
21135	0.49860	0.49860		Ligament Failure

Figure D.17: CX150ED-3 fatigue crack growth datasheet.

CX200ED-1 Crack Growth Datasheet				
Test Date: 1/18/2019 10:35:46 AM		**Width (in): 4.0023**		
Max Stress (ksi): 33		**Thickness (in): 0.2528**		
Loading Rate (kip/sec): 165		**Area (in^2): 1.012**		
Hole Diameter (in): 0.5016		**Ligament Length (in): 0.7509**		
Flight Hours	**Crack Length (inches)**			**Comments**
	Front Surface	**Back Surface**	**Bore**	
0	0.04790		0.05428	
540	0.05866		0.06140	
1030	0.06232		0.06739	
1510	0.06392		0.07214	
1990	0.06576		0.07277	
2959	0.06876		0.07595	
3919	0.07092		0.08437	
4889	0.07320		0.08779	
5859	0.07552		0.09212	
6819	0.07664		0.09584	
7789	0.07778		0.09818	
9229	0.08094		0.10303	
10678	0.08450		0.11175	
13088	0.08956		0.19477	
14048	0.09168		0.19952	
16948	0.09674		0.20653	
18388	0.10152		0.21184	
19837	0.10432		0.22170	
22727	0.10990		0.22873	
25616	0.11550	0.00000	0.24398	
30436	0.12542	0.04900	0.25280	Through Thickness
31886	0.13180	0.05466		
33325	0.13312	0.06176		
36225	0.14254	0.07298		
39354	0.15288	0.08914		
40554	0.15800	0.09428		
42004	0.16384	0.09872		
42964	0.16598	0.10098		
45373	0.17886	0.11442		
49233	0.21348	0.14498		
50682	0.23902	0.17426		
51642	0.26404	0.19822		
52122	0.28454	0.22242		
52362	0.30212	0.23812		
52602	0.31784	0.25860		
52842	0.33724	0.28444		
53322	0.38550	0.34034		
53802	0.46892	0.44624		
53911	0.75090	0.75090		Ligament Failure

Figure D.18: CX200ED-1 fatigue crack growth datasheet.

CX200ED-2 Crack Growth Datasheet				
Test Date: 1/25/2019 1:58:44 PM		**Width (in): 4.0024**		
Max Stress (ksi): 33		**Thickness (in): 0.2531**		
Loading Rate (kip/sec): 165		**Area (in^2): 1.013**		
Hole Diameter (in): 0.5022		**Ligament Length (in): 0.7504**		
Flight Hours	**Crack Length (inches)**			**Comments**
	Front Surface	**Back Surface**	**Bore**	
0	0.04318		0.04746	
4810	0.06546		0.07751	
9619	0.07202		0.09736	
14439	0.08502		0.11527	
21658	0.09242		0.14232	
28877	0.10480		0.17814	
31276	0.10884		0.18778	
38496	0.12292		0.20160	
45714	0.13688	0.00000	0.23088	
50534	0.15128	0.03188	0.25310	Through Thickness
52933	0.15856	0.05562		
55343	0.16694	0.07548		
56303	0.17382	0.07974		
57263	0.17874	0.08890		
57993	0.18618	0.09672		
59193	0.19224	0.10644		
60393	0.20354	0.11804		
61602	0.21588	0.13942		
62802	0.23572	0.16236		
64002	0.27170	0.20190		
64482	0.29872	0.23154		
64962	0.33616	0.27456		
65202	0.35802	0.30826		
65692	0.43216	0.40282		
65752	0.44158	0.40994		
65812	0.45378	0.42332		
65872	0.47092	0.45182		
65932	0.48752	0.47812		
65992	0.50100	0.48900		
66052	0.56002	0.55990		
66101	0.75040	0.75040		Ligament Failure

Figure D.19: CX200ED-2 fatigue crack growth datasheet.

CX200ED-3 Crack Growth Datasheet				
Test Date: 3/18/2019 6:55:30 PM		**Width (in): 4.0017**		
Max Stress (ksi): 33		**Thickness (in): 0.2527**		
Loading Rate (kip/sec): 165		**Area (in^2): 1.011**		
Hole Diameter (in): 0.5025		**Ligament Length (in): 0.7502**		
Flight Hours	**Crack Length (inches)**			**Comments**
	Front Surface	**Back Surface**	**Bore**	
0	0.04294		0.05523	
1200	0.05738		0.06662	
7220	0.07234		0.08944	
12029	0.07860		0.10846	
18049	0.09076		0.12287	
26468	0.10276		0.16431	
33688	0.11452		0.18311	
40668	0.12824		0.22238	
43068	0.13346		0.22584	
44277	0.13514		0.24406	
45477	0.13768	0.00000	0.25270	Through Thickness
46677	0.14064	0.01052		
49087	0.14550	0.03212		
51497	0.15130	0.04676		
53897	0.15862	0.05388		
56307	0.16662	0.06690		
59916	0.18370	0.08594		
62326	0.20044	0.10424		
63526	0.20876	0.11728		
65936	0.24052	0.15416		
67616	0.28170	0.20300		
68336	0.32924	0.25608		
68586	0.35516	0.29664		
68826	0.38174	0.32470		
69066	0.41574	0.36836		
69306	0.48448	0.45104		
69366	0.50022	0.47570		
69404	0.75020	0.75020		Ligament Failure

Figure D.20: CX200ED-3 fatigue crack growth datasheet.

APPENDIX E

CRACK CLOSURE IMAGES

Figure E.1: Specimen CX130ED-2 under zero applied stress. Crack is approximately 0.103 inches in length and appears to be closed.

Figure E.2: Specimen CX130ED-2 under 3.3 ksi applied stress. Crack is approximately 0.103 inches in length and appears to be closed.

Figure E.3: Specimen CX130ED-2 under 6.6 ksi applied stress. Crack is approximately 0.103 inches in length and appears to be closed.

Figure E.4: Specimen CX130ED-2 under 9.9 ksi applied stress. Crack is approximately 0.103 inches in length and appears to be closed.

Figure E.5: Specimen CX130ED-2 under 13.2 ksi applied stress. Crack is approximately 0.103 inches in length and appears to be closed.

Figure E.6: Specimen CX130ED-2 under 16.5 ksi applied stress. Crack is approximately 0.103 inches in length and appears to be open.

Figure E.7: Specimen CX130ED-2 under 19.8 ksi applied stress. Crack is approximately 0.103 inches in length and appears to be open.

Figure E.8: Specimen CX130ED-2 under 23.1 ksi applied stress. Crack is approximately 0.103 inches in length and appears to be open.

Figure E.9: Specimen CX130ED-2 under 26.4 ksi applied stress. Crack is approximately 0.103 inches in length and appears to be open.

Figure E.10: Specimen CX130ED-2 under 29.7 ksi applied stress. Crack is approximately 0.103 inches in length and appears to be open.

Figure E.11: Specimen CX130ED-2 under 33 ksi applied stress. Crack is approximately 0.103 inches in length and appears to be open.

Figure E.12: Specimen CX140ED-2 under zero applied stress. Crack is approximately 0.140 inches in length and appears to be closed.

Figure E.13: Specimen CX140ED-2 under 3.3 ksi applied stress. Crack is approximately 0.140 inches in length and appears to be closed.

Figure E.14: Specimen CX140ED-2 under 6.6 ksi applied stress. Crack is approximately 0.140 inches in length and appears to be closed.

Figure E.15: Specimen CX140ED-2 under 9.9 ksi applied stress. Crack is approximately 0.140 inches in length and appears to be closed.

Figure E.16: Specimen CX140ED-2 under 13.2 ksi applied stress. Crack is approximately 0.140 inches in length and appears to be open.

Figure E.17: Specimen CX140ED-2 under 16.5 ksi applied stress. Crack is approximately 0.140 inches in length and appears to be open.

Figure E.18: Specimen CX140ED-2 under 19.8 ksi applied stress. Crack is approximately 0.140 inches in length and appears to be open.

Figure E.19: Specimen CX140ED-2 under 23.1 ksi applied stress. Crack is approximately 0.140 inches in length and appears to be open.

Figure E.20: Specimen CX140ED-2 under 26.4 ksi applied stress. Crack is approximately 0.140 inches in length and appears to be open.

Figure E.21: Specimen CX140ED-2 under 29.7 ksi applied stress. Crack is approximately 0.140 inches in length and appears to be open.

Figure E.22: Specimen CX140ED-2 under 33 ksi applied stress. Crack is approximately 0.140 inches in length and appears to be open.

Figure E.23: Specimen CX150ED-3 under zero applied stress. Crack is approximately 0.102 inches in length and appears to be closed.

Figure E.24: Specimen CX150ED-3 under 3.3 ksi applied stress. Crack is approximately 0.102 inches in length and appears to be closed.

Figure E.25: Specimen CX150ED-3 under 6.6 ksi applied stress. Crack is approximately 0.102 inches in length and appears to be closed.

Figure E.26: Specimen CX150ED-3 under 9.9 ksi applied stress. Crack is approximately 0.102 inches in length and appears to be closed.

Figure E.27: Specimen CX150ED-3 under 13.2 ksi applied stress. Crack is approximately 0.102 inches in length and appears to be closed.

Figure E.28: Specimen CX150ED-3 under 16.5 ksi applied stress. Crack is approximately 0.102 inches in length and appears to be open.

Figure E.29: Specimen CX150ED-3 under 19.8 ksi applied stress. Crack is approximately 0.102 inches in length and appears to be open.

Figure E.30: Specimen CX150ED-3 under 23.1 ksi applied stress. Crack is approximately 0.102 inches in length and appears to be open.

Figure E.31: Specimen CX150ED-3 under 26.4 ksi applied stress. Crack is approximately 0.102 inches in length and appears to be open.

Figure E.32: Specimen CX150ED-3 under 29.7 ksi applied stress. Crack is approximately 0.102 inches in length and appears to be open.

Figure E.33: Specimen CX150ED-3 under 33 ksi applied stress. Crack is approximately 0.102 inches in length and appears to be open.

Figure E.34: Specimen CX200ED-3 under zero applied stress. Crack is approximately 0.107 inches in length and appears to be closed.

Figure E.35: Specimen CX200ED-3 under 3.3 ksi applied stress. Crack is approximately 0.107 inches in length and appears to be closed.

Figure E.36: Specimen CX200ED-3 under 6.6 ksi applied stress. Crack is approximately 0.107 inches in length and appears to be closed.

Figure E.37 : Specimen CX200ED-3 under 9.9 ksi applied stress. Crack is approximately 0.107 inches in length and appears to be closed.

Figure E.38: Specimen CX200ED-3 under 13.2 ksi applied stress. Crack is approximately 0.107 inches in length and appears to be closed.

Figure E.39: Specimen CX200ED-3 under 16.5 ksi applied stress. Crack is approximately 0.107 inches in length and appears to be closed.

Figure E.40: Specimen CX200ED-3 under 19.8 ksi applied stress. Crack is approximately 0.107 inches in length and appears to be open.

Figure E.41: Specimen CX200ED-3 under 23.1 ksi applied stress. Crack is approximately 0.107 inches in length and appears to be open.

Figure E.42: Specimen CX200ED-3 under 26.4 ksi applied stress. Crack is approximately 0.107 inches in length and appears to be open.

Figure E.43: Specimen CX200ED-3 under 29.7 ksi applied stress. Crack is approximately 0.107 inches in length and appears to be open.

Figure E.44: Specimen CX200ED-3 under 33 ksi applied stress. Crack is approximately 0.107 inches in length and appears to be open.

REFERENCES

[1] W. A. J. Albert, "Über Treibseile am Harz," *Archive für Mineralogie Geognosie Bergbau und Hüttenkunde,* vol. 10, pp. 215-234, 1838.

[2] Ministry of Transport and Civil Aviation, "Report of the Court of Inquiry into the Accidents to Comet G-ALYP on 10th January, 1954 and Comet G-ALYY on 8th April, 1954," Her Majesty's Stationery Office, London, 1955.

[3] The National Transportation Safety Board, "LAX02GA201," 23 April 2004. [Online]. Available: https://www.ntsb.gov/about/employment/_layouts/ntsb.aviation/brief.aspx?ev_id=20020621X00954&key=1. [Accessed 28 March 2019].

[4] ASM International Handbook Committee, ASM Handbook Volume 11: Failure Analysis and Prevention, Materials Park: ASM International, 2002.

[5] Aerospace Structures Information and Analysis Center, "The History of the Aircraft Structural Integrity Program," Flight Dynamics Laboratory, Wright-Patterson AFB, 1980.

[6] J. W. Lincoln, "Effect of Aircraft Failures on USAF Structural Requirements," United States Air Force, 2000.

[7] Department of Defense, "Aircraft Structural Integrity Program (MIL STD 1530D Change 1)," Department of Defense Standard Practice, United States Air Force, 2016.

[8] A. A. Griffith, "The Phenomena of Rupture and Flow in Solids," *Philos. Trans. of the Roy. Soc. of London,* vol. A 221, pp. 163-198, 1921.

[9] G. R. Irwin, "Structural Aspects of Brittle Fracture," *App. Mat. Res.,* vol. 3, pp. 65-81, 1964.

[10] M. L. Williams and G. A. Ellinger, "Investigation of Structural Failures of Welded Ships," *Welding Journal,* no. 32, pp. 498s-527s, 1953.

[11] ASM International Handbook Committee, ASM Handbook Volume 19: Fatigue and Fracture, Materials Park: ASM International, 1996.

[12] Air Force Structures, Structures Bulletin EN-SB-08-012, Revision D - In-Service Inspection Crack Size Assumptions for Metallic Structures, Wright-Patterson AFB: USAF, 2018.

[13] American Society for Testing and Materials (ASTM), Standard Test Method for Measurement of Fatigue Crack Growth Rates (E 647), West Conshohocken: American Society for Testing and Materials, 2000.

[14] LexTech Inc., "AFGROW Fracture Mechanics and Fatigue Crack Growth Analysis Software, Version 5.03.03.23," 2019.

[15] Department of Defense, DoD Joint Service Specification Guide, Wright-Patterson AFB: United States Air Force, 2006.

[16] ASM International Handbook Committee, ASM Handbook Volume 5: Surface Engineering, Materials Park: ASM International, 1994.

[17] Fatigue Technologies Inc., "FTI process specification 8101D cold expansion of holes using the standard split sleeve system and countersink cold expansion (CsCx™)," Fatigue Technologies Inc., Seattle, 2002.

[18] R. A. Pell, P. W. Beaver, J. Y. Mann and J. G. Sparrow, "Fatigue of Thick-Section Cold-Expanded Holes With and Without Cracks," *Fat. and Frac. of Eng. Mat. and Struct.,* vol. 12, no. 6, pp. 553-567, 1989.

[19] D. L. Ball and D. R. Lowry, "Experimental Investigation on the Effects of Cold Expansion of Fastener Holes," *Fat. and Frac. of Eng. Mat. and Struct.,* vol. 21, no. 1, pp. 17-34, 1998.

[20] S. Carlson, "Experimantally Derived Beta Corrections to Accurately Model the Fatigue Crack Growth Behavior at Cold-Expanded Holes in 2024-T351 Aluminum Alloys," M.S. thesis, Dept. Mech. Eng., Univ. Utah, Salt Lake City, 2008.

[21] R. Pilarczyk, "Experimentally Derived Beta Corrections to Predict Fatigue Crack Growth at Cold-Expanded Holes in 7075-T651 Aluminum Alloy," M.S. thesis, Dept. Mech. Eng., Univ. Utah, Salt Lake City, 2008.

[22] O. Buxbaum and H. Huth, "Expansion of Cracked Fastener Holes as a Measure for Extension of Lifetime to Repair," *Eng. Frac. Mech.,* vol. 28, pp. 689-698, 1987.

[23] G. L. Petrak and R. P. Stewart, "Retardation of Cracks Emanating From Fastener Holes," *Eng. Frac. Mech.,* vol. 6, pp. 275-282, 1974.

[24] N. Chandawanich and W. N. Sharpe Jr., "An Experimenatal Study of Fatigue Crack Initiation and Growth from Cold Expanded Holes in Aluminum Alloys," *Int. J. Fatig.,* vol. 22, pp. 189-203, 1999.

[25] V. Lacarac, D. J. Smith, M. J. Pavier and M. Priest, "Fatigue Crack Growth From Plain and Cold Expanded Holes in Aluminum Alloys," *Int. J. Fatig.,* vol. 22, no. 3, pp. 189-203, 1999.

[26] X. Zhang and Z. Wang, "Fatigue Life Improvement in Fatigue-Aged Fastener Holes Using the Cold Expansion Technique," *Int. J. Fatig.,* vol. 25, no. 9-11, pp. 1249-1257, 2003.

[27] A. Buch and A. Berkovits, "Effect of Cold-Working by hole expansion on Fatigue Life of 7075-T351 and 7475-T651 Aluminum Lugs With and Without Initial Flaws Under Maneuver Loading Spectrum," *Materialwissenschaft und Werkstofftechnik,* vol. 18, no. 3, 1987.

[28] J. J. Warner, "Cold Expansion Effects on Cracked Fastener Holes Under Constant amplitude and Spectrum Loading in the 2024-T351 Aluminum Alloy," M.S. thesis, Dept. Mech. Eng., Univ. Utah, Salt Lake City, 2012.

[29] A. Brot and A. Nathan, "Increasing Fatigue and crack Growth Lives of Short Edge Margin Holes," in *13th Symposium of the International Committee on Aeronautical Fatigue*, Pisa, 1985.

[30] M. R. Ayatollahi and M. A. Nik, "Edge Distance Effects on Residual Stress Distribution Around a Cold-Expanded Hole in Al 2024 Alloy," *Comp. Mat. Sci.,* vol. 45, pp. 1134-1141, 2009.

[31] D. L. Andrew, "Investigation of Cold Expansion of Short Edge Margin Holes With Preexisting Cracks in 2024-T351 Aluminum Alloy," M.S. thesis, Dept. Mech. Eng., Univ. Utah, Salt Lake City, 2011.

[32] D. L. Andrew, P. N. Clark and D. W. Hoeppner, "Investigation of cold expansion of short edge margin holes with pre-existing cracks in 2024-T351 aluminum alloy," *Fat. and Frac. of Eng. Mat. and Struct.,* no. 37, pp. 406-416, 2013.

[33] Hill Engineering, LLC, "NG-0144-A10-00030008-13-RPT-A," Department of the Air Force, 538 Aircraft Sustainment Wing, Hill AFB, 2013.

[34] J. Warner, Interviewee, *A-10 Aircraft Structural Integrity Program Lead.* [Interview]. 22 February 2019.

[35] S. A. Fawaz, "Fatigue Crack Growth in Riveted Joints," Ph.D. dissertation, Dept. Aero. Eng., Delft Univ. of Tech., The Netherlands, 1997.

[36] Engineering Software Research and Development (ESRD), Inc., "StressCheck(R) Version 10.4," ESRD, inc., St. Louis, 2018.

[37] "Broad Application for Modeling Failure (BAMF) Version 6.0," Hill Engineering, LLC, Rancho Cordova, 2019.

[38] S. S. Carlson, "Quantifying the Effect of a Fatigue Crack on the Residual Stress Field Induced by the Split Sleeve Cold Expansion Process in 2024-T351 and 7075-T651 Aluminum Alloys," Ph.D. dissertation, Dept. Mech. Eng., Univ. Utah, Salt Lake City, 2018.